# Investigating the role of ERK signalling dynamics in the regulation of stem cell heterogeneity

Deathridge, Julia Rose

*Awarding institution:*
King's College London

# Investigating the role of ERK signalling dynamics in the regulation of stem cell heterogeneity

*Julia Deathridge*

A dissertation submitted in partial fulfillment

of the requirements for the degree of

**Doctor of Philosophy**

of

**King's College London**.

Faculty of Life Sciences and Medicine

King's College London

January 25, 2019

I, Julia Deathridge, confirm that the work presented in this thesis is my own. Where information has been derived from other sources, I confirm that this has been indicated in the work.

# Abstract

Stimulation of the ERK/MAPK pathway is required for the exit from pluripotency and onset of differentiation in mouse embryonic stem (ES) cells. Many markers of pluripotency show heterogeneous expression under standard ES cell culture conditions, reflecting varying tendencies for either pluripotency and being primed for differentiation. Inhibition of the ERK/MAPK pathway causes much of this heterogeneity to be lost, driving cells into a more pluripotent state. However, immunofluorescence revealed only a weak relationship with levels of pERK and pluripotency markers at the single cell level, implying the magnitude of ERK signalling may only have a weak input into cell state. The aim of this work was to gain insight into the relationship between ERK activity dynamics and ES cell differentiation. To enable this I implemented a FRET-based biosensor to monitor ERK signalling dynamics in single living cells. I found that ERK activity was highly heterogeneous, with considerable variability in ERK signalling between single cells within ES cell colonies. Surprisingly, the magnitude and dynamics of ERK signalling were not strongly coupled to the loss of pluripotency marker expression, implying the normal dynamic range of ERK signalling is not rate-limiting in single cells during differentiation. Using custom-built image analysis software, I demonstrated that ERK signalling dynamics were sensitive to the degree of cell crowding, and were similar in neighbouring cells. By imaging cell lineages, I showed that sister cells from a mitotic division were highly correlated in their ERK activity, an effect that was apparent whether cells remained adjacent or moved apart after division, suggesting cell autonomous inheritance of cell signalling state.

Overall, these data imply a combination of cell lineage and niche contributes to the absolute level of ERK signalling in mouse ES cells.

# Acknowledgements

Firstly, I would like to thank both my supervisors, Jonathan Chubb and Maddy Parsons. Jonathan, for all his ideas and astonishing levels of scientific knowledge that I can only hope to have at least partially absorbed over the last few years. His constant understanding of my many experimental failures, providing me with the confidence and support I needed to keep the project moving forward, and for helping me see the positivity in my results when all I could see was the negative. I would also like to thank Maddy Parsons, for making my progression through the PhD programme such a seamless experience, and her unwavering confidence that one day we would get the FRET to work, which without her knowledge and guidance, I don't think would have been possible.

I thank my lab, past and present, for all their excellent ideas, brilliant lab meeting discussions, and for all the enjoyable birthday lunches. I would like to give particular thanks to Vlatka Antolovic, for helping me immeasurable amounts with all my data analysis and for teaching me something that I never thought possible - how to write MATLAB code! I thank my friends here at the LMCB for allowing me to drag them away from their work for endless chattering in the corridor, lengthy tea breaks, and some very memorable pub trips. I would like to extend extra gratitude to the lunch time crew who never failed to make me laugh and for always being up for an intense, but highly enjoyable, political debates.

I want to acknowledge my ‘non-science’ friends for being an excellent source of fun and escapism from the lab, and for always taking a very keen interest in how my cells were doing. Special thanks goes to Victoria Hellon, for being a brilliant housemate and for cooking about 90% of my work lunches; I would be a much poorer student without her. Finally, I want to thank my parents for not only letting me come invade them for some intense weeks of thesis writing, but for all the encouragement, advice, and infinite support that they have given me over the years.

# Contents

# List of Figures

# List of Tables

# List of Abbreviations

| | |
|---|---|
| ICM | Inner Cell Mass |
| TE | Trophoectoderm |
| PrE | Primitive Endoderm |
| EPI | Epiblast |
| ES cells | Mouse embryonic stem cells |
| LIF | Leukaemia Inhibitory Factor |
| MAPK | Mitogen-activated protein kinase |
| MEK | Mitogen-activated protein kinase kinase |
| ERK | Extra-cellular regulated kinase |
| GSK3 | Glycogen synthase kinase 3 |
| RTK | Receptor tyrosine kinase |
| Grb2 | Growth factor receptor bound protein |
| SOS | Son of Sevenless |
| IEGs | Immediate early response genes |
| DUSPs | Dual specificity phosphatases |

| | |
|---|---|
| PC-12 | Rat adrenal pheochromocytoma |
| PKC | Protein kinase C |
| FRET | Forster resonance energy transfer |
| FGF | Fibroblast growth factor |
| DMSO | Dimethyl sulfoxide |
| EDTA | Ethylenediaminetetraacetic acid |
| FBS | Fetal bovine serum |
| PFA | Paraformaldehyde |
| LUT | Look-up table |
| FOV | Field of view |
| ROI | Region of interest |
| PD | MEK inhibitor PD0325901 |
| OD | Okadaic Acid |
| NLS | Nuclear localisation signal |
| NES | Nuclear export signal |
| CV | Co-efficient of variation |
| r | Pearson's correlation |
| $R^2$ | Co-efficient of determination |
| KS-test | KolmogorovSmirnov test |

# Chapter 1

# Introduction

## 1.1 Maintenance of pluripotency in mouse embryonic cells

### 1.1.1 Formation of the blastocyst

Following fertilization mammalian ooctyes undergo a number of cleavage divisions to generate a cluster of cells known as the morula (Selwood and Johnson, 2006). In murine development, cells of the blastocyst first become defined at the 8-cell stage following specification towards the trophoectoderm (TE) or inner cell mass (ICM). Cells at the outer edge of the morula will adopt a TE fate (Tarkowski and Wróblewska, 1967) and will up-regulate the marker Cdx2, whilst cells in the centre will down-regulate Cdx2 and maintain the expression of Oct4 and Sox2, defining them to the ICM (Niwa et al., 2005; Strumpf, 2005). A combination of mechanisms have been implicated to be involved in the fate specification of the TE, including compaction mediated cell polarity (Johnson and Ziomek, 1981; Johnson and McConnell, 2004), differential contractility between inner and outer cells (Maître et al., 2016), cell position dependant signalling (Nishioka et al., 2009; Hirate et al., 2012), and stochastic gene expression (Goolam et al., 2016).

As development continues, cells of the ICM become restricted to either an Epiblast (EPI) or Primitive endoderm (PrE) fate, which give rise to the embryo proper and extra-embryonic tissues respectively. Precursors of the EPI (Nanog) and PrE (Gata6) fate are initially expressed in a 'salt and pepper' distribution within the ICM resulting from the mutual antagonism between these two markers (Plusa et al., 2008; Chazaud et al., 2006). PrE and EPI progenitor cells become physically segregated into two distinct layers by the late blastocyst stage (E4.5) coinciding with reinforcement of their fate identity (Plusa et al., 2008; Chazaud et al., 2006; Grabarek et al., 2012). Following implantation, cells of the epiblast become epithelized and expression of lineage specific markers begin to emerge as cells become irreversibly specified towards a cell fate (Osorno et al., 2012).

During these early stages of development, prior to implantation at E4.5, cells of the ICM have been shown to demonstrate a high degree of plasticity; retaining a capacity to contribute to all three lineages following transplantation into a host, irrespective of previous lineage bias (Grabarek et al., 2012). The broad potential of these cells highlights the regulative nature of embryo development as cells are able to respond and adapt to changing external cues (Martinez Arias et al., 2013). However, how is this transient development potential established? And what causes a single cell to exit this highly pluripotent state and adopt a cell fate trajectory? Investigating these questions *in vivo* comes with many experimental challenges, such as small cell numbers and limited accessibility. Consequently, much of our understanding of how pluripotency evolves and the molecular mechanisms driving cell fate transitions have come from *in vitro* studies of cell lines derived from the embryo.

### 1.1.2 Capturing pluripotency *in vitro*

Mouse embryonic stem (ES) cells are derived from the ICM of the pre-implantation blastocyst and can give rise to all embryonic lineages (Evans and Kaufman, 1981). The pluripotency capacity of these cells is characterized by their ability to contribute to the progeny of all different cell types following injection into the blastocyst

(Bradley et al., 1984). Since the first immortalization of ES cells in culture, the ability to derive and propagate cells indefinitely has progressed significantly over the last 30 years.

ES cells were initially derived and maintained by culturing on a bed of feeder cells. It later became apparent that feeder cells could be replaced by culturing ES cells under defined conditions in the presence of Leukaemia Inhibitory Factor (LIF) (Smith et al., 1988), which sustains ES cells in a state of self-renewal through activation of the JAK/STAT3 pathway (Niwa et al., 1998). Culturing with LIF, together with serum (hereafter called serum/LIF), subsequently became the standard protocol for deriving and maintaining ES cells. Under these conditions ES cells can be propagated indefinitely whilst maintaining their pluripotency potential.The LIF induced self-renewal capacity of ES cells is thought to reflect epiblast cells during diapause, when reduced oestrogen levels halt development at the pre-implantation stage, which incidentally was the initial state from which ES cells were derived (Smith, 2001).

Although derivation of ES cells from the epiblast was improved by the addition of LIF and BMP, survival efficiency of ES cells was still low and restricted to the 129 mouse strain (Nichols et al., 1990; Ying et al., 2003). Inhibition of the MAPK (mitogen activated protein kinase)/ ERK (extra-cellular regulated kinase) pathway was found to promote self-renewal and increase the lifetime of primary explants during ES cell derivation (Buehr and Smith, 2003). These findings led to the advent of a new culture condition referred to as 2i, which is comprised of an inhibitor of the MAPK pathway and an inhibitor of glycogen synthase kinase-3 (GSK3) (Ying et al., 2008). GSK3 was initially introduced to rescue the viability of ES cells following inhibition of the MAPK pathway (Ying et al., 2008). However, it has been found to have an additional role in enhancing the self-renewal state by blocking the repressive function of Tcf3 on the core pluripotency network (Wray et al., 2011). Under 2i culture conditions ES cells display a molecular profile more similar to the pre-implantation epiblast cells of the embryo, as well as an increased propensity

for self-renewal (Nichols et al., 2009; Boroviak and Nichols, 2014; Boroviak et al., 2015). Furthermore, use of this culture system has greatly enhanced the efficiency of ES cell derivation and has been successfully applied to the derivation of ES cells from other mice strains and rodent species (Nichols et al., 2009; Buehr et al., 2008; Li et al., 2008).

### 1.1.3 Naïve and primed state of pluripotency

Mouse embryonic development relies on the dynamic progression through different pluripotent states that are characterized by a series of molecular and morphological features. Cells of the pre-implantation epiblast are commonly described as existing in a naïve state of pluripotency, due to their ability to contribute to all somatic, germ line and extra-embryonic lineages (Nichols et al., 2009). The self-renewal capacity of ES cells, and their retained ability to differentiate into all cell lineages following incorporation into the blastocyst, is thought to reflect the pluripotency characteristics of this naïve epiblast state (Nichols et al., 2009), with ES cells exhibiting a similar epigenomic and molecular profile to cells of the pre-implantation epiblast. Discovery of the 2i culture condition showed pluripotency could be further restricted to what is referred to as the ground state (Ying et al., 2008; Silva and Smith, 2008; Marks et al., 2012). Under these conditions cells exhibit a more uniform expression pattern of pluripotency-associated genes, implying a more stable pluripotent state has been reached that is shielded from external signalling cues (Wray et al., 2010; Marks et al., 2012).

Following implantation potency becomes restricted as cells enter defined lineage trajectories, representative of a more primed pluripotent state (Boroviak and Nichols, 2014). Embryonic cells derived from the post-implantation epiblast (EpiSCs) are thought to reflect the molecular characteristics of this primed state, illustrated by the loss of naïve factors, a more closed chromatin structure, and expression of lineage specific genes (Nichols and Smith, 2009; Tesar et al., 2007; Brons et al., 2007). As well as exhibiting a differing epigenomic and molecular

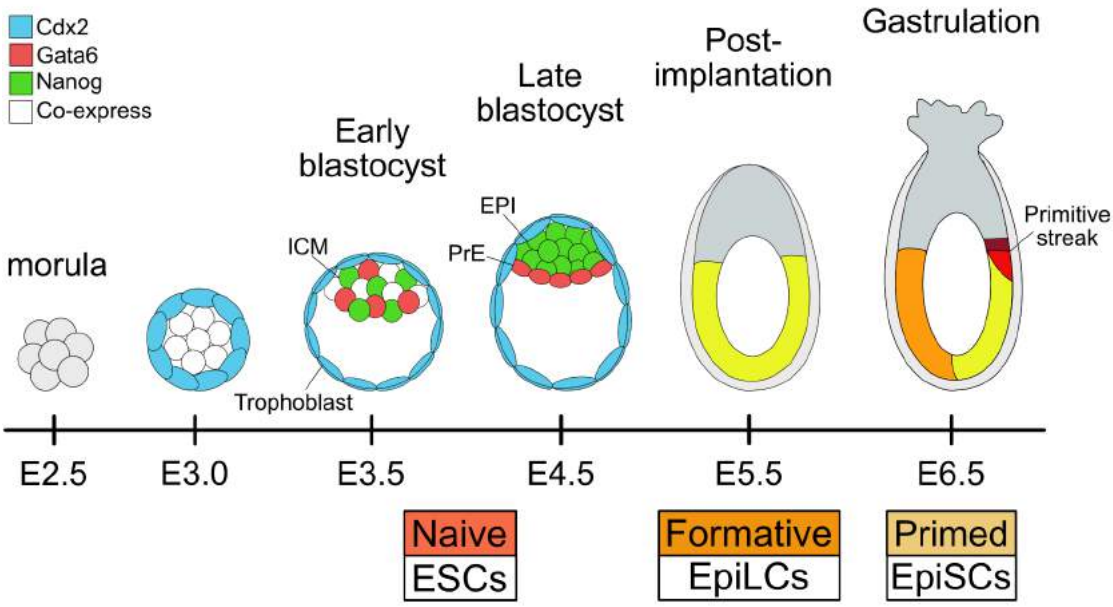


**Figure 1.1: Developmental progression of the early embryo and its corresponding pluripotent states** A series of cell cleavages results in the formation of the morula at E2.5. Following compaction, cells become polarised to form the outer trophoectoderm (TE) and inner cell mass (ICM). At E3.5 precursors of the epiblast (EPI) (Nanog) and primitive endoderm (PrE) (Gata6) begin to emerge in a mutually exclusive 'salt and pepper' fashion with Nanog and Gata6 expressing cells becoming physically segregated into two distinct layers by E4.5. Following implantation the epiblast expands to form a cup like shape and differentiation signals will initiate the onset of gastrulation and the formation of the primitive streak. The boxes below the time line depict the pluriptotent states associated with each of these developmental stages and the embryo derived cells that best encapsulate the epigenetic and molecular profile of each state

profile to ES cells, EpiSCs are also developmentally and functionally distinct from the naïve state of ES cells, demonstrated by their inability to contribute to the ICM following injection into the blastocyst (Tesar et al., 2007). It is interesting to note that EpiSCs can be converted, albeit at a low efficiency, to the naïve state of the epiblast (Bao et al., 2009; Hayashi and Surani, 2009), suggesting that EpiSCs still retain a high degree of plasticity within their pluripotent state.

Convergence from an ESC to EpiSC fate can be achieved following long term culture in EpiSC media conditions (Najm et al., 2011). However, the temporal gap between the loss of naïve pluripotency and the establishment of a lineage primed state has led to the proposal of an interim third state, termed the formative state

(Kalkan et al., 2017; Smith, 2017). ES cells cultured in EpiSC media over a long duration generate an embryonic like epiblast cell (EpiLC) that may be representative of this state (Hayashi et al., 2011). However, the full pluripotent potential of these cells and their ability to contribute to the pre-implantation embryo has not been fully characterized (Morgani et al., 2017).

## 1.2 Single cell heterogeneity

Over the last 15 years it has become increasingly apparent that population averages do not adequately reflect the behaviour of individual cells (Balázsi et al., 2011; Eldar and Elowitz, 2010; Raj et al., 2010). Pioneering work by Elowitz et al. (2002) and Ozbudak et al. (2002) demonstrated a large amount of cell-cell variability in gene expression arising either from 'intrinsic' random variability between copies of a gene or 'extrinsic' variability in other components leading to different single cell responses. Since then heterogeneity in gene expression has been identified in a number of organisms, ranging from bacteria to mammalian cells. Intrinsic variation manifests from transcriptional bursting caused by the inherent property of genes to stochastically switch between 'on' and 'off' states (Elowitz et al., 2002) with differences in the frequency and duration of these bursts setting the mean level of gene expression (Raj et al., 2006). External influences of fluctuations in gene expression include, cell cycle position, heterogeneous culture environment, cell size and variability in upstream components (Eldar and Elowitz, 2010; Symmons and Raj, 2016).

An example of spontaneous expression variability playing a functional role can be seen in the cell fate decisions of the bacterium *Bacillius subtillis*. At any given time a fraction of *Bacillius subtillus* cells will be in a state of genetic competence that allows them to take up DNA from their surrounding environment as a source of food or for incorporation into their own genome (Süel et al., 2007). Development of the competent state is controlled by the master regulator ComK, which is able to directly regulate its own expression and the expression of factors involved in the

maintenance of the competent state. If fluctuations in the expression of ComK go above a certain threshold, ComK becomes able to up-regulate its own expression, generating a pulse in activation that will enforce a transition into the competent state (Süel et al., 2007). Expression variability is crucial to the initiation of the competent state, and loss of this variability leads to a reduced fraction of competent cells and an impaired ability to enter the competent state (Süel et al., 2007; Maamar et al., 2007).

Gene expression variability has also been shown to be of particular prevalence in the developing cells of the embryo, where stem cells are able to spontaneously differentiate into many cell types in an apparently unchanging external environment. An example of this can be seen in the decision between EPI and PrE fate in the early embryo, where the initial emergence of these fates occurs in an 'apparently random' pattern irrespective of their position within the ICM (Dietrich and Hiiragi, 2007; Plusa et al., 2008). Further demonstration of stochastic variation is shown in culturing of ES cells that are able to adopt multiple lineage fates despite exposure to the same external signalling cues (Graf and Stadtfeld, 2008). Advancements in single cell analysis and quantitative studies have demonstrated a high degree of variability within the stem cell state. Addressing the functional significance of cell-cell variability in ES cells has largely come from studies of the pluripotency factor Nanog, which exhibits a highly varied expression pattern under serum/LIF culture conditions.

### 1.2.1 Transcriptional heterogeneity in ES cells

Nanog has been identified to be a key regulator of self-renewal, due to its ability to sustain self-renewal when overexpressed in the absence of LIF (Chambers et al., 2003; Yamaguchi et al., 2005). Use of fluorescent reporters identified Nanog expression to be bimodally distributed with cells existing in either a 'Nanog Low' or 'Nanog High' expression state (Chambers et al., 2007; Singh et al., 2007; Kalmar et al., 2009; Abranches et al., 2014). Functional studies have shown 'Nanog Low' cells to display an increased propensity for differentiation,

whilst ‘Nanog High’ cells remain in a state of self-renewal unable to respond to differentiation cues (Chambers et al., 2007; Abranches et al., 2014; Filipczyk et al., 2013). Purification of these sub-populations by fluorescence activated cell sorting (FACS) demonstrated that each of these expression states were able to recapitulate heterogeneous distribution of expression following 1-2 weeks of culture (Chambers et al., 2007; Kalmar et al., 2009; Abranches et al., 2014). This led to the idea that Nanog expression dynamically fluctuates within ES cells, converting cells between a state of self-renewal and being primed for differentiation (Chambers et al., 2007; Kalmar et al., 2009; Abranches et al., 2014).

Various different mechanisms have been proposed to regulate this heterogeneous expression pattern. At the intrinsic level auto-repression and transcriptional bursting have both been implicated in modulating the expression levels of Nanog (Navarro et al., 2012; Singer et al., 2014; Ochiai et al., 2014a). Singer et al. (2014) further showed that fluctuations in Nanog expression were correlated with dynamic changes in the epigenome of individual cells, with DNA methylation maintaining ES cells in either the low or high expressing state. Another theory, presented by Miyanari and Torres-Padilla (2012), is that monoallelic expression of Nanog in the early epiblast causes an initially variable expression pattern of Nanog. They propose that as the epiblast develops Nanog expression switches to become biallelicly regulated resulting in a more homogeneous expression state. However, further investigation using allelic specific reporter cell lines were unable to replicate this finding (Filipczyk et al., 2013; Faddah et al., 2013; Hansen and van Oudenaarden, 2013). Heterogeneity in cell cycle length, environmental influences and cell density have also been proposed to regulate the expression of Nanog (Cannon et al., 2015; Singer et al., 2014). External signalling factors have also been shown to influence the expression of Nanog, demonstrated by the loss in heterogeneity and more uniform expression pattern of Nanog exhibited by cells following inhibition of the MAPK pathway and GSK3 under 2i culture conditions (Ying et al., 2008). However, how external signal factors are able to modulate the expression of Nanog still remains an open question.

### 1.2.2 Functional significance of dynamic heterogeneity

Other transcription factors of the pluripotency network have also been shown to display varied expression under serum/LIF culture conditions, including naïve factors Stella and Rex1 (Hayashi et al., 2008; Toyooka et al., 2008), PrE marker Hex1 (Canham et al., 2010), and the transcription factor Hes1 (Kobayashi et al., 2009). Intriguingly, reversible state transitions have also been observed for the pluripotency factors Stella and Rex1, as well as Nanog. This dynamic heterogeneity in expression is proposed to reflect a metastable pluripotent state where cells are able to interconvert between a state of self-renewal and being poised for differentiation (Hayashi et al., 2008; Silva and Smith, 2008).

It has been suggested that the increased propensity of cells expressing low levels of pluripotency factors towards differentiation results from an altered ability to respond to signalling cues (Semrau et al., 2017). Thus a situation may arise in which noisy gene expression alters the transcription profile of individual cells, which can be amplified by external signals, allowing cells to become restricted towards a cell fate (Martinez Arias et al., 2013). This process has been referred to as multi-lineage priming, previously alluded to in the development of haemtopoeitic progenitor cells, where varied low expression of multiple lineage markers act to intrinsically prime cells towards various different fates (Hu et al., 1997). In this view, fluctuations in expression may allow ES cells to explore their multi-lineage options before being committed to a fate (Enver et al., 2009; Martinez Arias and Brickman, 2011).

The maintenance of the metastable pluripotent state has also been attributed to the competing lineage specification actions of pluripotency factors (Loh and Lim, 2011). This idea largely derived from the discovery that Oct4 and Sox2 are differentially expressed following mesoderm and neural ectoderm lineage specification in ES cells (Thomson et al., 2011). Overexpression of each of these markers, rather than continuing the maintenance of pluripotency will promote differentiation, with Oct4 overexpression resulting in mesodermal (Niwa et al., 2000) and Sox2 inducing a neuroectodermal fate (Kopp et al., 2008). Furthermore,

other factors of the pluripotency network have also been shown to induce a specific lineage trajectory when overexpressed (Ivanova et al., 2006). Each of these factors are proposed to counteract each others lineage specifying functions, and a carefully controlled balance in their expression acts to sustain cells in an undifferentiated state (Loh and Lim, 2011). If these factors become spontaneously up or down regulated the balance will be disrupted, allowing the lineage specifying actions of a factor to become dominant and direct the differentiation of a cell towards a particular fate (Loh and Lim, 2011). Consequently, the competing actions of pluripotency factors provides ES cells with the opportunity to be continuously primed for commitment to different lineage fates.

This initial view of Nanog expression acting as a switch between a highly pluripotent and lineage primed state has however been challenged by longer time-scale studies of Nanog expression using different fluorescent reporters (Cannon et al., 2015; Filipczyk et al., 2013; Singer et al., 2014). These studies have shown Nanog fluctuations to occur over much longer time-scales, with ES cells existing in relatively stable state of high and low expression for multiple cell cycles (Cannon et al., 2015; Singer et al., 2014; Kumar et al., 2014; Filipczyk et al., 2013). Discrepancies in Nanog behaviour have been attributed to the gene targeting strategies used to make reporter cell lines. A report by Faddah et al. (2013) suggests the heterozygous expression, induced by the insertion of the GFP reporter used for the initial studies on Nanog expression, could be perturbing Nanog regulation causing a dynamic variation in expression across the populations. However, it is of note that differences in Nanog expression were reported using feeder cell culture conditions, and heterogeneity in the expression of Nanog has been identified in feeder free serum/LIF culture conditions using other Nanog reporter lines (Abranches et al., 2014; Filipczyk et al., 2013). Nevertheless, a lot of the contention has surrounded the ability of these reporters to accurately reflect endogenous Nanog protein levels leading many to speculate over the biological relevance of these dynamics fluctuations (Smith, 2013).

In agreement with the above, there is currently no evidence for fluctuating Nanog expression states *in vivo* during development. Although heterogeneities in Nanog expression have been observed *in vivo* during the cell fate EPI/PrE lineage specification (Plusa et al., 2008; Dietrich and Hiiragi, 2007; Guo et al., 2010; Ohnishi et al., 2014), conversion between fates has found to be extremely rare with transitions only being observed in the direction of PrE to EPI fate (Xenopoulos et al., 2015). It is possible, however, that rapid uni-directional transitions between developmental states *in vivo* prevents the possibility of reversions (Xenopoulos et al., 2015). Fluctuations in expression *in vitro* may result from the culture induced self-renewal potential of ES cells, and prolonging the pluripotent state *in vivo*, as in the case of diapause, could provoke a similar dynamic response (Morgani et al., 2017). A counter argument for the existence of Nanog heterogeneity, is that the dual function of LIF as both a promoter of self-renewal and a driver of differentiation, through partial activation of the MAPK pathway, generates a heterogeneous population of self-renewing and differentiated cells (Niwa et al., 2009). This is further illustrated by single cell transcriptomic study that identified two populations of ES cells that reflected the epiblast at different stages of development (Papatsenko et al., 2015).

## 1.3 Transition from the naïve pluripotent state

The naïve pluripotent state is characterized by the expression of a network of transcription factors (Niwa, 2007; Dunn et al., 2014; Boroviak and Nichols, 2014). At the heart of this network are the core pluripotency factors Oct4 and Sox2 that have been shown to be central to maintenance of the pluripotent state (Nichols et al., 1998; Niwa et al., 2000; Avilion et al., 2003; Niwa, 2007). Nanog has also been shown to be a key component in the maintenance of the pluripotency (Chambers et al., 2003; Yamaguchi et al., 2005). However, although critical for the formation of the epiblast, Nanog expression is not required to maintain the pluripotent state of ES cells (Chambers et al., 2007). Nevertheless, these three factors are commonly referred to as the ‘master regulators’ of pluripotency, as they generate a network of

positive feedback in their own expression as well as regulating the expression of other factors in the pluripotency gene network (Loh et al., 2006).

The naïve network is also supported by the expression of the additional factors Klf2/4, Tfcp2l1, Tbx3, Esrrb (Hall et al., 2009; Bourillot et al., 2009; Martello et al., 2013; Niwa et al., 2009; van den Berg et al., 2008; Zhang et al., 2008). These factors are expressed in the naïve epiblast cells of the ICM and become down-regulated following implantation, indicating a transition from the naïve to the primed state (Boroviak and Nichols, 2014). The naïve state of ES cells also relies on the expression of this additional set of factors, as they contribute towards the network of interactions required to control the self-renewal state of ES cells (Dunn et al., 2014). Exit from the naïve state, *in vitro*, is mediated by the removal of 2i or LIF from culture conditions. Naïve factors, as observed in the embryo, become gradually down-regulated as ES cells exit the naïve state, with their expression becoming lost 25h post 2i/LIF removal (Kalkan et al., 2017). Exit from the naïve state, *in vitro* and *in vivo*, is also marked by the upregulation of early post-implantation factors, Otx2, Tcf15, Fgf5 and Oct6 (Acampora et al., 2013; Davies et al., 2013; Boroviak and Nichols, 2014; Kalkan et al., 2017). Monitoring the expression of these factors, by RT-qPCR, has shown naïve factors and post-implantation markers to display differing down-regulation and up-regulation kinetics (Kalkan et al., 2017). Furthermore, exit from the pluripotent state has been shown to occur in a non-synchronous manner, indicative of a varing single cell response to an apparent identical external signalling cue (Semrau et al., 2017; Kalkan et al., 2017).

The naïve pluripotent state can also be defined by epigenetic features that influence the transcriptional output of ES cells. The epigenetic landscape of ES cells is characterized by hypomethylation, histone acetylation and bivalent domains containing histone modifications that repress (H3K27me3) and activate (H3K4me3) the genome (Niwa, 2007; Meissner et al., 2008; Bernstein et al., 2006). These bivalent domains are thought to silence lineage specification genes whilst also poising them for up-regulation by external differentiation cues (Bernstein et al.,

2006). Culturing in 2i leads to a more hypomethylated genome, reduction in the repressive modification H3K27me3, and reduced prevalence of bivalent domains, which is more reminiscent of the permissive open chromatin context of naïve epiblast cells (Marks et al., 2012; Boroviak and Nichols, 2014). In addition, increased DNA methylation and polycomb mediated deposition of H3K27me3 has also been observed during this transition from the naïve state, signifying increased condensation of the chromatin structure as lineage specification begins to occur (Ficz et al., 2013; Leitch et al., 2013; Habibi et al., 2013), consistent with the idea that repression follows or underlies cell type separation (Antolović et al., 2017).

The mechanisms driving changes in the gene regulatory network during the exit from pluripotency are still relatively unknown and are an ongoing area of research. Various different mechanisms have been proposed including, up-regulation of transcriptional repressors of naïve factors, epigenetic silencing by polycomb repressive complexes, and reduced mRNA stability (Kalkan and Smith, 2014). A genome wide knock down showed components of the FGF/ERK signalling pathway to be a required for sufficient exit from the naïve state (Yang et al., 2012; Leeb et al., 2014). Moreover, as many of these transcriptomic and epigenomic changes can occur without the addition of exogenous factors, this would suggest that paracrine signalling that was blocked by 2i could be the major driver of these changes.

## 1.4 ERK signalling dynamics and cell fate choices

As the embryo develops and cells adopt new fates, the transcriptional profile of embryonic cells will be continuously modified by external stimuli. External stimuli are able to influence the transcription network through activation of a series of signal transduction pathways. These pathways will transmit a signal from the cell surface to a target protein that will ultimately activate the molecular program required to change the cell. In the traditional view, external stimuli activate a linear cascade of events resulting in an external output that correlates with the level of external

stimuli. However, it has become increasingly apparent that not just absolute levels but the dynamic differences within signalling pathways play an important role in determining the transcriptional output and subsequent fate of a cell (Purvis and Lahav, 2013). One of the first examples of dynamic changes in activity leading to different cellular outcomes was found in the MAPK/ERK signalling pathway, which I shall describe in detail below.

### 1.4.1 MAPK/ERK pathway

The MAPK pathway is a highly conserved evolutionary pathway found in most eukaryotic cells. Receptor tyrosine kinase (RTK) mediated activation of the MAPK pathway allows for signals to be transmitted from the cell surface to intracellular targets that will instigate an appropriate cellular response (McKay and Morrison, 2007). Signals are relayed through activation of a kinase cascade comprised of Raf, MEK and ERK. Transmission of this signal is stimulated by soluble growth factor ligands that bind to membrane bound receptor tyrosine kinases at the cell surface. RTKs dimerize following binding to the ligand, inducing their activation and allowing for the auto-phosphorylation of tyrosine residues within their intracellular domains. Docking protein Grb2 (Growth factor receptor-bound protein 2) is then able to bind to these auto-phosphorylated sites leading to the recruitment and activation of SOS (Son of Sevenless), which promotes the exchange of GDP to GTP from the GTPase Ras (Figure 1.2).

Ras GTPase is the critical link between RTKs and ERK, as activated Ras is able to interact with and trigger initiation of the Raf/MEK/ERK kinase cascade. Once activated, ERK is able to phosphorylate a multitude of different targets that are associated with range of biological processes, including embryonic development, oncogenesis, and synaptic plasticity (McKay and Morrison, 2007). It is of note that RTK-mediated activation of ERK, described here, is only one of many possible interaction networks involved in the activation of ERK. Other signalling networks, such as those mediated by G-protein coupled receptors, are also known to regulate activation of the Raf/MEK/ERK kinase cascade (Koch et al., 1994). In addition,

further studies of the MAPK/ERK pathway continue to demonstrate increasing levels of complexity within this network involving a vast number of interconnected proteins, beyond this traditional view of sequentially activated events.

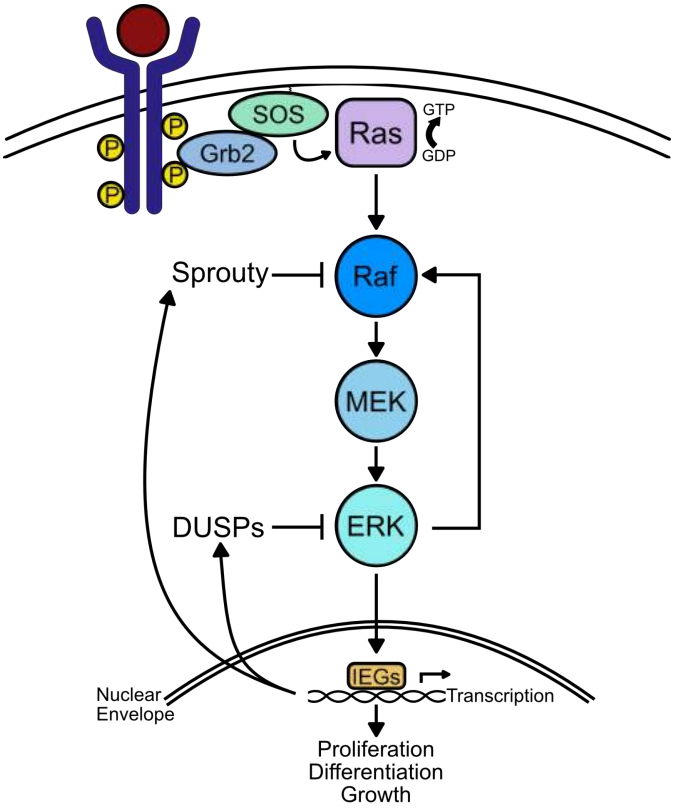


**Figure 1.2: Schematic representation of the MAPK/ERK signalling pathway** Receptor tyrosine kinases become dimerised following ligand binding, and autophosphorylate tyrosine residues within their intracellular domains. This creates a docking site for the adaptor protein Grb2 allowing the recruitment and activation of SOS, which in turn will activate the GTPase Ras. Active Ras will subsequently instigate a kinase cascade ultimately leading to the activation of ERK, which is translocated into the nucleus to rapidly induce the transcription of immediate early genes (IEGs). ERK can also regulate the transcription of multiple other genes including, DUSPs and Sprouty which, in turn, are able to negatively regulate the ERK activity response.

MAPK/ERK signalling can be modulated at multiple levels within its pathway to alter the strength and duration of ERK activity. At the receptor level, ERK activation can be modulated by increased receptor availability, facilitated ligand-RTK binding, and receptor internalization. Intracellularly, negative and positive feedback mechanisms are able to fine-tune the cascade. Negative modulators include SPRED (Sprouty-related proteins with EVH1 domains), Sprouty, and Erbin, which interfere

with protein interactions of the cascade inducing a rapid dampening in activity (Huang et al., 2003; Hanafusa et al., 2002; Sasaki et al., 2003). Conversely, de-phosphorylation of ERK by dual specificity phosphatases (DUSPs) negatively regulates ERK activity over a much longer time scale (Patterson et al., 2009). ERK is also able to negatively regulate its own activity by inhibiting the phosphorylation of SOS (Langlois et al., 1995), Raf (Brummer et al., 2003), or MEK (Pages et al., 1994). In addition, many of these proteins can be transcriptionally regulated by ERK activity allowing for continued adaptation of the signalling response. As well as inhibiting the function of Raf, ERK can also act to stimulate the phosphorylation of Raf as part of a positive feedback mechanism (Higgs and Peterson, 2005). Other ERK induced positive feedback mechanisms include phosphorylation and activation of RKIP (Shin et al., 2009), and degradation of the phosphatase MKP-3 (Marchetti et al., 2005). By influencing the kinetics of ERK activity these auxillary factors and signalling modulators are able to regulate the vast range of cellular responses induced by external stimuli.

### 1.4.2 ERK activity dynamics as a determinant of cell fate

Early studies investigating ERK activity in Rat adrenal pheochromocytoma (PC-12) cells identified that different growth factor stimuli of the RTK/ERK pathway were able to induce differential biological responses; NGF treatment resulted in differentiation whilst EGF treatment led cells to proliferate (Cowley et al., 1994; Marshall, 1995). Further investigation showed that these responses were caused by growth factor dependent differences in ERK activation, with NGF triggering sustained activation and EGF triggering a more transient response. Differences in dynamics induced by upstream stimuli have also been identified in other systems such as the stress response in yeast, the mammalian inflammatory response, and in the entraining of transcriptional bursts by oscillatory signals in *Dictyostelium* (Hao and O'Shea, 2012; Tay et al., 2010; Corrigan and Chubb, 2014), indicating dynamically-controlled cellular outcomes to be a conserved feature of biological signalling.

Targeted perturbation within the ERK signalling pathway revealed positive feedback and negative feedback mechanisms to be regulating these distinct stimuli induced dynamic responses (Santos et al., 2007). Specifically, a molecular response analysis tool (Kholodenko et al., 2002) was used to investigate topological differences in the MAPK pathway of NGF and EGF stimulated cells, showing NGF stimulation to mediate a positive regulatory feedback between ERK and Raf (Santos et al., 2007). They further showed that stimulation and inhibition of protein kinase C (PKC), an activator of this feedback mechanism, resulted in sustained ERK activity in response to EGF and transient activity in response to NGF. Furthermore, rewiring of this feedback mechanism with inhibitor treatment could reverse the response of the two growth factors, resulting in EGF-activated differentiation and NGF-induced proliferation

Another proposed mechanism for encoding differences in dynamics between these two growth factors is through the activation of small GTPases (Sasagawa et al., 2005). Using *in silico* modelling, researchers showed that kinetic variation in Rap1 and Ras1 activity was able to act as a functional read-out for differences in the temporal behaviour and concentration rate of NGF and EGF respectively. Additional complexity is also brought into these dynamics by cross interaction with other signalling pathways. Consequently, the transcriptional program incited by a signal will be related to a complex series of dynamics within its own and additional pathways. An example of this has been shown in PC-12 cell fate determination, as the decision between proliferation and differentiation was found not only to be dependent on pERK levels but also comparative levels of pAKT (Chen et al., 2012). However, the mechanisms involved in decoding this dynamic information to generate the desired response remain unclear.

Differences in ERK activity dynamics are primarily relayed through IEGs that are able to selectively respond to changes in the behaviour of ERK. IEGs such as c-fos, egr-1 and fra, are rapidly transcribed following activation of ERK allowing for an instantaneous response to changes in the temporal and spatial regulation of ERK

activity (Murphy et al., 2002). An example of this can be seen in the differential behaviour of c-fos following transient and sustained ERK responses (Murphy et al., 2002). Specifically, phosphorylation of c-fos by sustained ERK activity stabilises c-fos in the nucleus allowing for activation of the target proteins required to instruct the differentiation fate. In contrast, more recent work has shown regulation of IEGS by ERK dynamics to be mediated at the transcriptional level (Wilson et al., 2017). They showed that frequent pulses of ERK activity were able to incite multiple rounds of transcription whilst sustained ERK, or infrequent pulses, caused a reduction in transcription levels. Furthermore, transcriptional outputs were found to be gene specific, with IEG transcripts accumulating at differing levels despite exposure to the same dynamic stimuli (Wilson et al., 2017). Many of these IEGs control the expression of transcription factors associated with cell fate choices, indicating the significant role ERK dynamics play in the regulatory mechanisms driving cell fate changes (Purvis and Lahav, 2013).

## 1.5 The role of MAPK/ERK signalling in the embryo and ES cells

### 1.5.1 FGF4/ERK signalling regulates lineage specification in the ICM

RTK mediated activation of the ERK signalling pathway by fibroblast growth factor (FGF) has been shown to play a critical role in embryo development. FGF ligand and receptor subtypes are expressed differentially throughout development, with each combination having a distinct function in the patterning of the embryo (Lanner and Rossant, 2010). In the early mouse embryo activation of the ERK pathway is predominantly mediated by the ligand FGF4, which is transcriptionally activated by the direct binding of the Oct4/Sox2 complex to its enhancer region (Yuan et al., 1995). FGF4 is initially expressed in all cells of the morula and 16-cell stage embryo, eventually becoming restricted to the epiblast cells of the ICM (Yuan et al., 1995). Formation of the pre-implantation embryo is highly dependent on activation of the FGF4/ERK signalling pathway and genetic perturbation of

components within this pathway result in an embryonic lethal effect (Feldman et al., 1995; Chazaud et al., 2006).

The second lineage specification in the mammalian embryo is the commitment of ICM cells towards a primitive endoderm (PrE) or epiblast (EPI) fate. Distinction between these two fates is marked by the expression of the transcription factors Nanog and Gata6, which define the EPI and PrE respectively (Chazaud et al., 2006). Cells of the ICM initially co-express both of these factors, however an exclusive 'salt and pepper' pattern of expression begins to emerge as cells become specified towards a fate (Chazaud et al., 2006; Plusa et al., 2008). Several experiments have shown that pharmacological inhibition or genetic perturbation of the FGF4/ERK pathway results in ubiquitous expression of Nanog across the ICM, and a loss of PrE fate (Yamanaka et al., 2010; Nichols et al., 2009; Xenopoulos et al., 2015). Accordingly, activation of the FGF4/ERK pathway by the addition of exogenous FGF4 causes all cells to adopt a PrE cell fate, and Nanog expression within the ICM can no longer be detected (Yamanaka et al., 2010). Taken together these findings indicate the significant role FGF4/ERK signalling plays in lineage specification of the early mouse embryo.

More recent work has shown that changing the timing, duration and level of ERK signalling is able to alter the proportion of EPI and PrE fates within a population (Krawchuk et al., 2013; Schröter et al., 2015; Bessonnard et al., 2014; Nissen et al., 2017). Schröter et al. (2015) demonstrated, by a combined computational and experimental approach, that FGF/ERK signalling was able to regulate the proportion of PrE cells by setting a threshold of Gata expression to act as a switch between these two fates. This mechanism of dosage setting by the ERK pathway could be of consequence in other cell fate choices influenced by changing ERK dynamics (Schröter et al., 2015).

### 1.5.2 FGF4/ERK signalling in ES cells

Early studies of the intercellular signalling networks of ES cells identified the ERK signalling pathway to act as a promoter of differentiation, perhaps reflecting its

*in vivo* role (Burdon et al., 2002; Cheng et al., 1998). Further work showed that autocrine released FGF4 from ES cells was acting as a driver for differentiation, and that inhibition of FGF4/ERK signalling, by genetic perturbation, blocked the neuronal specification of ES cells (Kunath et al., 2007; Stavridis et al., 2007). This phenotype could not be rescued by the addition of other FGF ligands, demonstrating the ligand specificity of the response (Kunath et al., 2007). The generation of the culture condition 2i, discussed previously, further highlighted the significant role ERK signalling plays in the maintenance of pluripotency, as suppression of this pathway was found to be critical to the establishment of the ground pluripotent state (Ying et al., 2008).

Genome-wide studies have shown components of the FGF4/ERK signalling pathway to be critical regulators of the transition from the naïve state (Betschinger et al., 2013; Leeb et al., 2014; Yang et al., 2012). This is supported by genetic perturbation studies revealing activation of ERK to be required for a proficient exit from self-renewal and subsequent lineage specification towards the PrE fate (Findlay et al., 2013; Hamilton et al., 2013; Molotkov et al., 2017). In addition, ERK activity has been associated with the up and down regulation of multiple factors involved in the transition from the naïve state, such as lineage priming factor Tcf15 (Davies et al., 2013), pluripotency factors Nanog and Klf4 (Hamazaki et al., 2006; Dhaliwal et al., 2018). Many of the epigenomic changes that occur during differentiation have also been strongly linked with increased ERK activation levels following the loss of 2i (Ficz et al., 2013). Indeed, activation of ERK has been shown to poise RNAII polymerase at the loci sites of lineage specific genes, allowing ES cells to become primed for lineage commitment (Tee et al., 2014).

Another feature of the 2i culture condition is its ability to disrupt the heterogeneous expression pattern of pluripotency factors observed under serum/LIF culture conditions (Nichols et al., 2009; Silva et al., 2009; Ying et al., 2008). Consequently, ERK signalling is frequently proposed to be a key mechanism in the establishment of this heterogeneous state. Mathematical modelling has shown the heterogeneous

distribution of Nanog and Rex1 expression can be recapitulated in a simple model comprising of a negative feedback loop between FGF4/ERK signalling and Nanog (Herberg et al., 2014). Furthermore, the negative interaction between Nanog and FGF4/ERK signalling, combined with stochastic transcriptional noise, was able to generate switch like behaviour in Nanog expression between a high and low state, reminiscent of what has been observed *in vitro* (Herberg et al., 2014). Although ERK activity has been shown to negatively regulate Nanog expression at the population level (Hamazaki et al., 2006; Santostefano et al., 2012), support of this idea has largely been derived from computational approaches. An investigation into how ERK activity relates to Nanog expression at the single cell level could further our understanding of how molecular heterogeneity is established.

Modulations in ERK activity levels by negative feedback loops have also been implicated in the heterogeneous expression of Nanog. This was initially reported by Lanner and Rossant (2010) who identified a reduction in the expression of the negative regulators DUSP1, DUSP6 and Spred in ES cells with reduced FGF4/ERK signalling. They proposed that negative feedback in the FGF4/ERK signalling network could be driving ES cells back to the un-primed state generating a heterogeneous population. Further work showed that DUSPs act to set a threshold of ERK activity, creating a heterogeneous population of both self-renewing and lineage committed cells (Yang et al., 2012; Hamilton et al., 2013). In addition, negative feedback within the ERK signalling pathway has also been shown to influence the rate of progression from the naïve state (Yang et al., 2012; Nett et al., 2018). Depletion of DUSPs 1/6, or the negative regulator RSK1, results in an altered activation profile of ERK, leading to an accelerated exit from the naïve pluripotent state (Yang et al., 2012; Nett et al., 2018). Progression from the naïve state occurs asynchronously within a population (Semrau et al., 2017; Kalkan et al., 2017). However, how ERK activity relates to the dynamic loss of pluripotency at the single cell level has not been fully explored.

## 1.6 Monitoring ERK activity at the single cell level

Much of the work I have discussed above has relied on population averages. However advancements in single cell technologies have shown signalling dynamics to be highly variable between cells of a population. Variabilities in ERK activity between 'equivalent' cells was initially demonstrated by Ferrell and Machleder (1998) who showed isolated *Xenopus laevis* oocytes to respond in an all-or-nothing manner to progesterone treatment, with ERK being either in a completely 'on' phosphorylated state or completely 'off' dephosphorylated state. This was in contrast to population averages that showed ERK activity levels to increase with increasing increments of progesterone treatment, suggesting that single cell responses in ERK activity are independent from the rest of the population. Since then, the ability to monitor ERK activity at the single cell level has advanced drastically due to the advent of fluorescent protein based reporter systems.

ERK activity dynamics of individual cells were initially monitored by quantifying the nuclear translocation of activated ERK2 that had a fluorescent tag inserted at its endogenous locus (Cohen-Saidon et al., 2009). Quantification of ERK2 levels in nuclei of individual cells demonstrated ERK activity levels to be highly variable within an isogenic population, even prior to growth factor stimulation (Cohen-Saidon et al., 2009). Single cell quantification further showed EGF stimulation to influence the amplitude of ERK activity differentially across the population (Cohen-Saidon et al., 2009). However, using fluorescently tagged ERK as a reporter comes with limitations; it could perturb the functions of ERK and does not consider the cytosolic substrates of the pathway. In addition, more recent work has shown accumulation of ERK levels in the nucleus to be poorly correlated with ERK activity (Wilson et al., 2017; Ahmed et al., 2014).

An alternative system has since arisen for monitoring ERK activity in live cells, employing a genetically encoded FRET-based biosensor known as EKAREV (Harvey et al., 2008; Komatsu et al., 2011). Forster-resonance energy transfer (FRET) is the transfer of energy between a donor and acceptor fluorophore

(Jares-Erijman and Jovin, 2003). CFP and YFP are a commonly used FRET pair due to the spectral overlap of CFP emission with YFP excitation (Figure 1.3A). Activated ERK phosphorylates the substrate sequence of the biosensor allowing it to bind to the phospho-threonine recognition domain FHA1 (Harvey et al., 2008; Komatsu et al., 2011). This conformational change will reduce the distance between the donor (CFP) and acceptor (YFP) fluorophore leading to an increase in FRET efficiency, and an increased level of FRET (Figure 1.3B). A change in FRET ratio therefore correlates with a change in ERK activity, and this can be monitored over-time by live cell imaging.

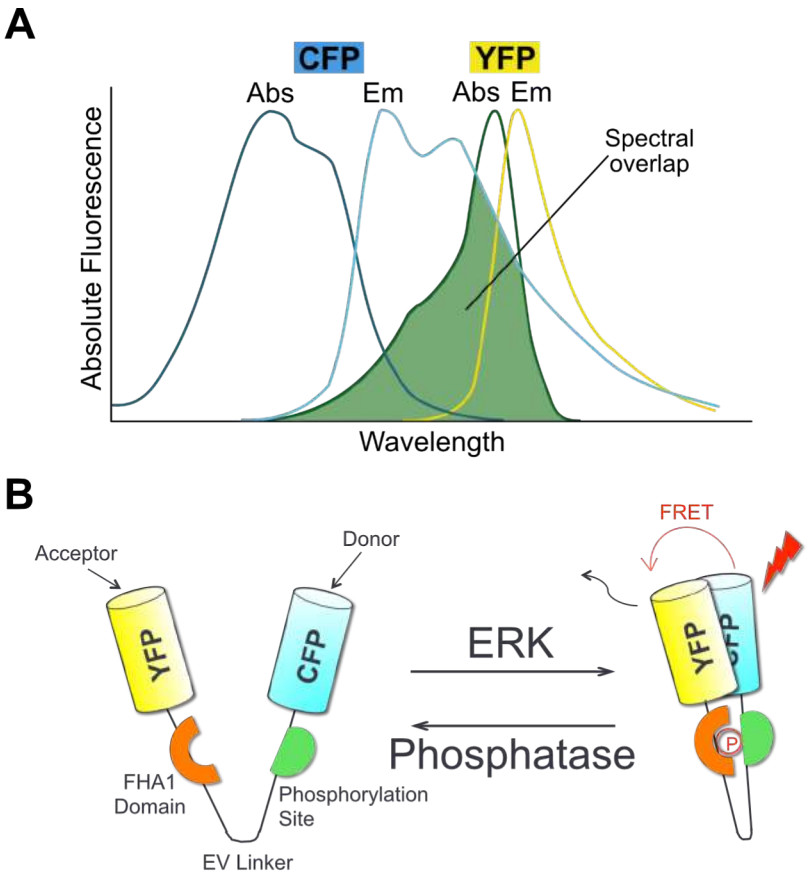


**Figure 1.3: Using a FRET based biosensor to monitor ERK activity as the single cell level** (A) Excitation and emission spectrum of CFP and YFP. Highlighted areas represent spectral overlap. (B) Schematic diagram of the EKAREV FRET biosensor. ERK phosphorylation creates a conformational change in the distance between CFP and YFP causing an increase in FRET.

Using this reporter researchers have found that ERK activity responses to a stimuli vary within a population (Aoki et al., 2013; Albeck et al., 2013; Ryu et al., 2015), in agreement with previous reports (Cohen-Saidon et al., 2009). The increased sensitivity of this reporter has further highlighted the great range of dynamics that the MAPK/ERK pathway can demonstrate, beyond that of the classic sustained and transient response previously observed. Two simultaneous reports utilising the FRET reporter identified ERK activity to occur in a series of stochastic pulses following EGF stimulation, with the frequency and duration of these pulses being correlated to the level of stimulation (Albeck et al., 2013; Aoki et al., 2013). Differences in dynamics of these pulses were found to be receptor dependent, as inhibition of EGFR resulted in altered frequency, whilst inhibition of MEK changed the amplitude of the response. Both studies showed pulses in ERK activation to regulate the rate of proliferation, either by frequency (Aoki et al., 2013) or duration in the on state (Albeck et al., 2013). Other pathways have also been shown to relay information in a pulsatile manner (Purvis and Lahav, 2013), thus frequency-modulated pulses could be a widely used strategy for the transmission and functional determination of extracellular signalling cues (Albeck et al., 2013; Levine et al., 2013). Building on this work Ryu et al. (2015) applied the pulsatile theory to the differentiation of PC-12 cells, once again using the FRET reporter as a single cell read-out of ERK activity. In agreement with previous work (Chen et al., 2012), they identified response to sustained EGF and NGF stimulation to be heterogeneous within a population, with cells displaying a combination of transient and sustained activity under both stimuli. They further showed that pulsatile growth factor stimulation could induce a homogeneous differentiation response irrespective of the stimuli, suggesting that cell fate choices can be encoded in the temporal pattern of ERK activation.

The FRET based biosensor does however come with limitations; primarily the use of two fluorescent proteins making it difficult to image multiple biological outputs alongside dynamics changes in ERK. To over come this barrier, Regot et al. (2014) have developed a kinase translocation reporter (KTR) system that

uses nucleocytoplasmic shuttling as a read-out of kinase activity. The reporter is comprised of both a nuclear localisation signal (NLS) and nuclear export signal (NES). Upon phosphorylation the NES and NLS become positively and negatively regulated respectively, leading to an increase in the export rate of the reporter. The reporter is tagged to a single fluorescent protein and dynamic changes in kinase activity are quantified by measuring the fluorescence ratio between the cytoplasm and nucleus. Development of an ERK specific KTR (ERK-KTR) identified basal fluctuations in ERK activity in agreement with previous reports using the FRET based biosensor system (Regot et al., 2014). Applying the KTR system to additional kinases, such as JNK and P38, further demonstrated these fluctuations in kinase activity to be specific to ERK. However, as with all reporter systems the KTR system does come with limitations, such as a loss in sub-cellular distribution in kinase activity as well requiring the ability to extract fluorescent intensities from both the nucleus and cytosol, which may be challenging in certain cell lines, such as naive ES cells where the structural architecture of cells is primarily dominated by the nuclei.

More recently the ERK-KTR system has been applied *in vivo* to study the vulva system of Caenorhabditis elegans (de la Cova et al., 2017). In this system the EGFR/Ras/ERK signalling network, along with NOTCH and Wnt, coordinate to pattern the fate of the five vulva precursor cells (VPCs). Fate specification is thought to be mediated by a gradient in EGF signal, emitted from the central anchor cell (Schmid and Hajnal, 2015). Using the ERK-KTR reporter de la Cova et al. (2017) showed differences in cell fate to be regulated by the frequency in ERK activity pulses, with primary cells exhibiting an increased frequency compared to tertiary and secondary fated cells. It is possible that frequency modulated differences in ERK activity may be a common feature of developmental ERK signalling (Dessauges and Pertz, 2017) and measuring single cell dynamics of ERK activity in other systems could play a key role in our understanding of cell fate regulation.

## 1.7 Aims of the thesis

1. To investigate the relationship between the levels of pERK and the expression of pluripotent markers at the single cell level.

2. To generate an ES cell line expressing a FRET based biosensor and establish a suitable method for measuring changes in FRET at a single cell resolution.

3. Utilise the FRET based biosensor to explore ERK activity dynamics of individual cells following exit from the naive state, in relation to their pluripotent state, focusing on the expression of the pluripotency factor Nanog.

4. To investigate how the micro-environment of a cell, such as local density and behaviour of neighbouring cells, influences ERK activity and Nanog expression, using custom-built analysis tools.

5. To investigate whether cell lineage is able to influence the ERK activity dynamics of daughter cells.

# Chapter 2

# Materials and Methods

## 2.1 ES Cell Culture

### 2.1.1 Culture Conditions

ES cells were routinely maintained in serum/LIF culture conditions comprised of Glasgows Minimum Essential Medium (GMEM, Gibco) supplemented with 10% Fetal Bovine Serum (FBS), 1mM Penicillin Streptomycin (Gibco), 2mM L-Glutamine, 1mM Sodium Pyruvate, 1mM Non-Essential Amino Acids (Lonza), 7.7ppm $\beta$-mercaptoethanol and 500$\mu$l LIF synthesized in the lab. Cells were cultured in T25 flasks (CellStar) coated with 0.1% gelatin, and incubated at 37°C with 5% CO2.

For splitting, cells were washed with 5ml PBS and incubated in 1.5ml of Accutase (Sigma, A6964) for 5 minutes or until the cells had dissociated from the bottom of the flask. Cells were subsequently transferred to a 15ml centrifuge tube, using 8ml of LIF/Serum media, and were centrifuged for 3 minutes at 300g. Cells were then re-suspended in 8ml of serum/LIF media and transferred to a 0.1% gelatin coated flask, at a ratio of 1:4 or 1:6 depending on confluency. Media was added to reach a final volume of 7ml. Cells were split every other day to ensure confluency did not go above a 70-80%.

Alternative culture condition 2i/LIF was also used to maintain cells in a more pluripotent state (Ying et al., 2008). 2i/LIF media is made up of the same components as serum/LIF culture conditions, supplemented with with CHIR99021 (3$\mu$M, Axon Medchem) and PD0325901 (1$\mu$M, Axon Medchem). Cells cultured in 2i/LIF were split every other day at a ratio of 1:3 and were used where indicated.

For differentiation, ES cells were cultured for a minimum of 2 passages in 2i/LIF conditions, before being plated at 1-1.5 cells/cm$^2$ in 2i/LIF media on 10$\mu$g/ml laminin (Merck, CC095) or 0.1% gelatin coated dishes. Medium was then replaced after 20-24h, or at specified time points, with media free from LIF and 2i.

### 2.1.2 Cryopreservation

Cells were grown to a 70-80% confluency in a T25 or T75 flask and were cyropreserved in 10% DMSO with serum/LIF at -80°C or in liquid nitrogen. Upon thawing, cells were added to 8ml of serum/LIF media and centrifuged for 3 minutes at 300g. Cells were re-suspended in 4ml of media and added to a 6-well plate coated with 0.1% gelatin and growth expanded to a T25 after 2-3 days.

### 2.1.3 Inhibitor Treatment

Cells were treated with MEK inhibitor PD0325901 (Sigma-Aldrich) at 1$\mu$M or 10$\mu$M for time courses stated in Chapter 3. In parallel, where stated (Chapter 3), cells were also treated with phosphatase inhibitor Okadaic Acid (Cell Signaling, 5934) at 20nM as described in (Ahmed et al., 2014), for either 45 or 90 minutes. Cells were subsequently harvested or fixed for use in Western blot or immunofluorescence experiments.

### 2.1.4 Transformation and selection

#### 2.1.4.1 DNA digest

DNA constructs to be transformed were linearised prior to electroporation. 100-150$\mu$g of cDNA plasmid was linearised with 5$\mu$l Sca1 restriction enzyme (New England Biolabs) and incubated overnight at 37°C. 1$\mu$l of digested cDNA was run on a 1% agrose gel (1% molecular biology grade agarose (Eurogentec))

and 300 ng/ml ethidium bromide in Tris acetate buffer (TAE: 40 mM Tris-acetate, 1 mM EDTA) at 100-135V to check digestion and quantity. Digested cDNA was purified by phenol extraction (add equal sample volume of phenol, mix and centrifuge 13,000 rpm for 2 minutes, pipette off top phase, repeat once more). cDNA was precipitate in 2 volumes 100% ethanol and 0.1 volumes 3M NaAc pH 5.2, washed in 70% ethanol and re-suspended in TE (10 mM Trish-HCL, 1mM EDTA) at 1$\mu$g/$\mu$l.

#### 2.1.4.2 Electroporation

Cells were grown to a 60-70% confluency in a T75 flask, washed with PBS and dissociated with Accutase. Cells were collected by centriguation at 300g and washed once in PBS before re-suspension in 800$\mu$l of PBS. This cell suspension was added to approximately 40$\mu$g of linearised DNA, and gently mixed by pipetting. Cells, with cDNA, were transferred to a 4mm cuvette (Molecular Bioproducts) and electroporated with an exponential decay protocol of 240V, 500$\mu$F using a Bio-Rad Gene Pulser XCell system. Following electroporation cells were immediately plated on gelatin coated 145mm petri dishes (ThermoFisher Nunc Cell-Culture Treated), with 80% in one dish and 20% in the other, in serum/LIF culture conditions. Transformants were selected using 5$\mu$g/ml of blasticidin S (Calbiochem), which was applied to cells every 2-3 days over a 10 day period. If transformation was successful cells were either passaged into a T75 for cryofreezing, or subsequently single cell cloned by colony isolation.

For single cell cloning, cells were rinsed in PBS and 30-40 colonies were selected from a single transformant dish, ensuring each colony chosen was detached from the rest of the population. Each selected colony was carefully dislodged using a P20 pipette and transferred, in a 15$\mu$l volume of PBS, to single gelatin coated well of a 96 well plate and re-suspended in 170$\mu$l of serum/LIF media. Selection was added the following day and was maintained over 2-4 day period. Successfully growing colonies were transferred to a 24 well plate and expression levels were checked using a Leica DMIRB inverted microscope. Highly expressing clones were growth

expanded to a T25 or a T75, in the presence of selection, and cryofrozen.

### 2.1.5 Cell lines used

A TNGA line (from Austin Smith) was used to image Nanog levels (Chambers et al., 2007). To image Rex1 expression, OCRG9 cell line (from Hitoshi Niwa) was used (Toyooka et al., 2008). Both cell lines were cultured as above.

For imaging of ERK activity dynamics a ES cell line expressing the NLS tagged and NES tagged EKAREV FRET biosensor (Harvey et al., 2008; Komatsu et al., 2011) were used. Initial E14-EKAREV-NLS line, and EKAREV-NES line, used in this work were constructed by Jonathan Chubb. E14 TG2A ES cells were electroporated with EKAREV-NLS or EKAREV-NES plasmid (both from Michiyuki Matsuda), following linearisation of both plasmids with a Sca1 enzyme, as described above. To establish a more stably expressing EKAREV-NLS cell line a PiggyBAC transposon was employed (Aoki et al., 2012). E14 TG2A ES cells were simultaneously electroporated with 2$\mu$g of EKAREV-NLS plasmid and 2$\mu$g of pCMV-mPBase transposase expression vector (from Allan Bradley) (Ivics et al., 2009) as described. Selection with blasticidin (5$\mu$g/ml) was initiated 36 hours later and single cell cloning was subsequently carried out following 10 days of selection. Successfully transformed clones were cyrofrozen and used for all future FRET assays.

E14-EKAREV-TA cell line was generated by electroporation of E14 TG2A ES cells with EKAREV-TA (from Toru Hiratsuka). Transformants were selected using blasticidin (5$\mu$g/ml) and selection was maintained for 10 days. Single cell colony isolation was then carried out, as described, and successfully transformed clones were cyrofreezed and used for further assays.

E14-SECFP and E14-YFP lines were constructed to generate donor-only and acceptor-only cell lines to control for bleed-through. SECFP and YFP plasmids were constructed by Jonathan Chubb. SECFP and YPet fluorophore sequences of the EKAREV biosensor were amplified by PCR utilising primers containing

restriction endonuclease cut sites for EcoR1 (**GAATTC**GGCATG) and Xho1 (TAA**CTCGAG**). These sequences were cloned into pBlue-script II plasmids and were checked by Sanger sequencing. ppBbsr2-3594nls plasmid was digested with Sal1 and EcoR1, to replace the EKAREV-NLS gene with either the YPet or SECFP fluorophore sequence. E14 TG2A ES cells were electroporated with either the SECFP or YFP plasmid, following linearisation with a Sca1 enzyme, as described above.

## 2.2 Immunofluorescence

For immunofluorescence experiments cells were seeded into a 8-well glass bottom micro-slide (Ibidi), at 1-1.5x$10^4$/$cm^2$ or to reach 60-70% confluency at time of fixation. Cells were washed with PBS, fixed in 4% Para-formaldehyde in PBS (PFA) for 20 minutes at room temperature, and permeabilised with 0.2% TritonX-100 in PBS (Sigma, T8787) for 10 minutes. Following washing in PBS, cells were blocked in 5% BSA PBS for 30 minutes at room temperature and incubated in primary antibody (Table 2.1) in blocking solution overnight at 4°C. After washing in PBS, cells were incubated in secondary antibody (Table 2.2) for 1h at room temperature. To stain the nuclei cells were incubated in DAPI (4$\mu$g/ml, Sigma) for 5 minutes at room temperature, however this was not done for all experiments. Cells were washed with PBS and stored at 4°C or imaged that day.

All pERK staining experiments were carried out using a Tyramide signal amplification kit. Following permeabalization in Triton X-100, 3% $H_2O_2$ in PBS was added for 20 minutes to block endogenous peroxidase activity. Cells were washed in PBS and blocked with 3% BSA in PBS. pERK primary antibody was added and cells were incubated overnight at 4°C. Secondary antibody HRP anti-rabbit (NA934V, GE healthcare) was diluted 1:100 in 3% BSA and added for 1 hour at room temperature. Cells then washed 3 times, for 10 minutes each, in 3% BSA. Tyramide signal amplification reagent (Alexa Fluor 594, T20950, Life

Technologies) was diluted 1:200 in the provided amplification buffer with 0.015% H2O2, and added to cells for 10 minutes in the dark at room temperature. Cells were washed 3 times in PBS and stored at 4°C or imaged that day.

## 2.3 Western Blotting

Cells were harvested in RIPA buffer (Tris-HCl pH7.5 20mM, NaCl 150mM, EDTA 1mM, EGTA 1mM, NP40 1%, NaDoc 1%) containing phosphatase inhibitor cocktails 2 and 3 (1:100, Sigma-Aldrich), and EDTA protease inhibitor (1:10, Roche). Protein concentration was measured using the Pierce BCA Protein Assay kit (ThermoScientific 23227) and equal amounts of protein was loaded onto Nu-PAGE Novex 4-12% Bis-Tris protein gels (Invitrogen). Protein was transferred onto a methanol activated PDVF (Immobilon-P, Merck) membrane by wet transfer.

Membranes were blocked in 5% BSA in TBS-T (Tris.Cl pH 7.6 50mM, NaCl 15mM, Tween-20 0.1%) for 1h at room temperature and incubated in primary antibody (Table 2.1) in 5% BSA TBS-T overnight at 4°C. Following washing in TBS-T, membranes were incubated in secondary HRP antibody (Table 2.2) for 1h at room temperature in 5% BSA TBS-T. Blots were developed with SuperSignal West Pico Chemiluminescent Substrate (ThermoFisher Scientific) and imaged using ImageQuant LAS 4000 (GE healthcare Life Sciences).

Following visualisation of pERK levels, membranes were washed in TBS-T and cut into two sections to be incubated overnight at 4°C with either an ERK primary antibody (Table 2.1) for pERK quantification, or Histone H3 primary antibody (Table 2.1) which was used as a loading control. Membranes were washed in TBS-T, and secondary HRP antibody was added for 1h, as above. HRP was visualised with SuperSignal West Pico Chemiluminescent Substrate (ThermoFisher Scientific) and imaged using ImageQuant LAS 4000 (GE healthcare Life Sciences). Western blots were analysed using Image Studio Lite (LI-COR).

| Company | Protein | Host | Cat no. | Dilution | |
|---|---|---|---|---|---|
| | | | | IF | WB |
| Cell Signalling | pERK | Rb | 9101S | 1:200 | 1:1000 |
| | ERK | Rb | 9102S | | 1:1000 |
| Abcam | H3 | Rb | 1791 | | 1:1000 |
| eBiosciences | Nanog | Rat | 14-5761-80 | 1:200 | |
| | Sox2 | Rat | 14-9811-82 | 1:100 | |
| Perseus Proteomics | Esrrb | Ms | P46705-00 | 1:100 | |

**Table 2.1: Primary antibodies used for this study.** Blank spaces in dilution column indicate the antibody was not used for this study. WB: western blot, IF: immunofluorescence.

| Company | Antibody | Cat no. | Dilution |
|---|---|---|---|
| GE healthcare | Donkey anti-rabbit HRP | NA934V | 1:20000 |
| Jackson ImmunoResearch | Cy3 mouse anti-rat IgG (H+L) | 212-165-168 | 1:200 |
| | Cy3 donkey anti-mouse IgG (H+L) | 715-165-150 | 1:200 |
| Life Technologies (Alexa Fluor) | TSA 594 tyramide | T20950 | 1:200 |

**Table 2.2: Secondary antibodies used for this study.** Dilutions as shown here, unless otherwise stated in the text.

## 2.4 Microscopy

### 2.4.1 Immunofluorescence

TNGA and OCRG9 immuno-stained cells were imaged using the Nikon Ultraview VOX spinning disc confocal microscope (TiE inverted stand, Nikon; CSU-X1 spinning disc scanning head, Yokogawa) with an EMCCD camera (C9100-13, Hamamatsu) and a 60x objective lens. 488nm (15 % power) laser was used to visualise GFP tagged Nanog or Rex1 with 250-700ms exposure, and pERK staining was imaged using a 561m (20% power) laser with a 350-800ms exposure. DAPI was imaged using a 405 nm laser at 3% power with 150-400ms exposure. 5-6 XY positions were located for each experimental condition and a Z-stack with 0.25$\mu$m Z intervals were taken.

E14 TG2A wild-type cells and E14-EKAREV-NLS cells immunostained following differentiation experiments or FRET time series were imaged using a widefield system (Zeiss Axiovert 200) with an EMCCD camera (C9100-13, Hamamastsu).

Images were captured using a GFP/mCherry filter set (Chroma 59022) and 40x1.30 NA objective with 250-400ms exposure, Gain of 3 and sensitivity of 50. For each experimental condition 5-6 XY positions were captured and a 30-50$\mu$m Z-stack with 1$\mu$m Z intervals were taken.

### 2.4.2 Imaging the FRET biosensor

#### 2.4.2.1 Confocal imaging

**SP5**

FRET imaging was carried out at 37°C with a Leica TCS SP5 confocal microscope using a 40x oil objective and HyD hybrid detectors. A 514 nm laser at 8% power and 458nm laser at 25% power was used to excite YFP and CFP respectively, and emission was collected in a 550-600nm or 470-500nm bandpass depending on the image being acquired. For time-lapse imaging a 30$\mu$m Z-stack with 3$\mu$m Z-slices was taken every 15 minutes over a 10 hour period. A YFP channel image (YFPex-YFPem) and FRET channel image (YFPex-CFPem) were acquired at each time-point.

**Olympus**

Cells were imaged on an Olympus FluoView FV1200 microscope using a 60x oil objective and a 4 frame average. A 458nm laser at 10% power was used to excite CFP and emission was collected at a 475-500nm bandpass for CFP channel images and a 540-600nm bandpass for FRET channel images.

**STED**

Images were captured on a Leica gSTED super-resolution system using a 40x oil objective and HyD hybrid detectors. A 405nm diode laser was used to excite CFP and a tunable white light laser (WLL) was used to excite YFP at 514nm. FRET and YFP images were captured at a 540-600nm emission bandpass, whilst CFP images were captured with a bandpass of 475-500nm. A 2 line average and 2 frame average was used for each image.

#### 2.4.2.2 Fluorescent-lifetime imaging (FLIM)

FLIM images were acquired using the following equipment: Laser-scanning microscope (Zeiss, model: LSM510) using a 40x oil objective, detector with single photon sensitivity (Becker and Hickl, model: HPM-100-40), time-correlated single photon counting (TCSPC) electronics (Becker and hickl, model: SPC-830), and pulsed excitation source (two-photon excitation by Ti:sapphire laser at 720nm; Chameleon Ultra, Coherent). Images were acquired using the SPCM software and anlaysed in SPCImage ((Becker et al., 2002)).

#### 2.4.2.3 Wide-field imaging

FRET imaging of EKAREV-E14 cells was carried out at 37°C and 7% CO2 using a wide-field fluorescence system (Zeiss Axiovert 200) with an EMCCD camera (C9100-13, Hamamastsu). Images were acquired using ECFP/EYFP FRET filter set (Chroma 89002) and 40x oil objective. Two images were acquired: YFP channel image (YFPex-YFPem), and FRET channel image (CFPex-YFPem) with a Gain of 3 and sensitivity of 100. Bleed-through was corrected for using E14-SECFP and E14-YFP expressing lines (see 3).

## 2.5 Time-lapse FRET imaging

### 2.5.1 2i removal experiments

EKAREV-E14 cells cultured under 2i/LIF conditions were seeded onto either a 8-well glass bottom micro-slide or a 35mm imaging dish (Ibidi), coated with 10$\mu$g/ml laminin or 0.1% gelatin, to arrive at a final confluency of 60-70% immediately prior to imaging. Cells were imaged using a wide-field system (see above for settings) with 200-380ms and 700-900ms exposure for YFP and FRET channel images respectively. A neutral density (Chroma) filter was further used to attenuate illumination to 10% of the lamp intensity in order to reduce phototoxicity. Once a field of view (FOV) had been established, cells were washed in PBS and media was changed to 2i free media immediately before the first image was

acquired. For each XY position a 40-60$\mu$m Z-stack was taken with 1$\mu$m Z-slices, every 5 mins for 4-5 hours.

### 2.5.2 Imaging of differentiating ES cells in relation to Nanog expression

To measure the FRET dynamics of differentiating ES cells, EKAREV-E14 cells were plated onto 35mm glass-bottomed dish (Ibidi) coated with 10$\mu$g/ml of laminin, in 2i/LIF media supplemented with serum 20-24h prior to the withdrawal of 2i/LIF. Ratiometric FRET imaging was carried out 5 minutes before and 16h after the removal of 2i/LIF using the wide-field system described (Zeiss Axiovert 200). A YFP and FRET channel image were captured every 5 minutes for the first 3 hours and at 10 minutes thereafter, with 380ms and 800ms exposure for each channel. A 20-30$\mu$m z-stack, with 2$\mu$m step size, was acquired at each time point and 5 FOV were collected in parallel using a motorised *xy* stage.

In order to compare FRET dynamics with the expression of Nanog, cells were washed in PBS and fixed with 4% PFA for 20 minutes under the microscope immediately after completion of the FRET time lapse imaging. Location of each FOV was noted prior to immunostaining using the 500$\mu$m cell location grid imprinted on the imaging dish (Ibidi), so the same colonies of cells that were captured for the FRET time series could be re-imaged following immunostaining of Nanog. Immunofluorescence imaging was carried out as previously described employing the same Z-stack size, and z interval distance, used during FRET time-lapse imaging.

## 2.6 Image Analysis

### 2.6.1 Ratiometric Analysis of FRET

Ratiometric analysis was carried out between the YFP and FRET channel images using the imageJ plugin RatioPLUS. 25 pixel rolling background subtraction was applied to both images, as can be seen in Figure 2.1B. A background region of interest (ROI) was selected and measured in both channels. A cell with a signal intensity that represents the majority of the population was selected and its

minimum intensity was measured. An example of the intensity values measured can be seen in Figure 2.1C. The clipping value was calculated for both channels, which along with the background signal, was entered into the RatioPLUS plugin. The same clipping value was used for all the fields of view in the same experiment to make ratiometric images comparable. Following the application of the RatioPLUS plugin a 16-colour look up table (LUT) was applied. Outlier pixel values were removed from the ratio image using the built in imageJ plugin *Remove Outliers* (radius=2, threshold=50) and a *3D median blur* (x=1, y=1, z=1) was applied to smooth the image (Figure 2.1C).

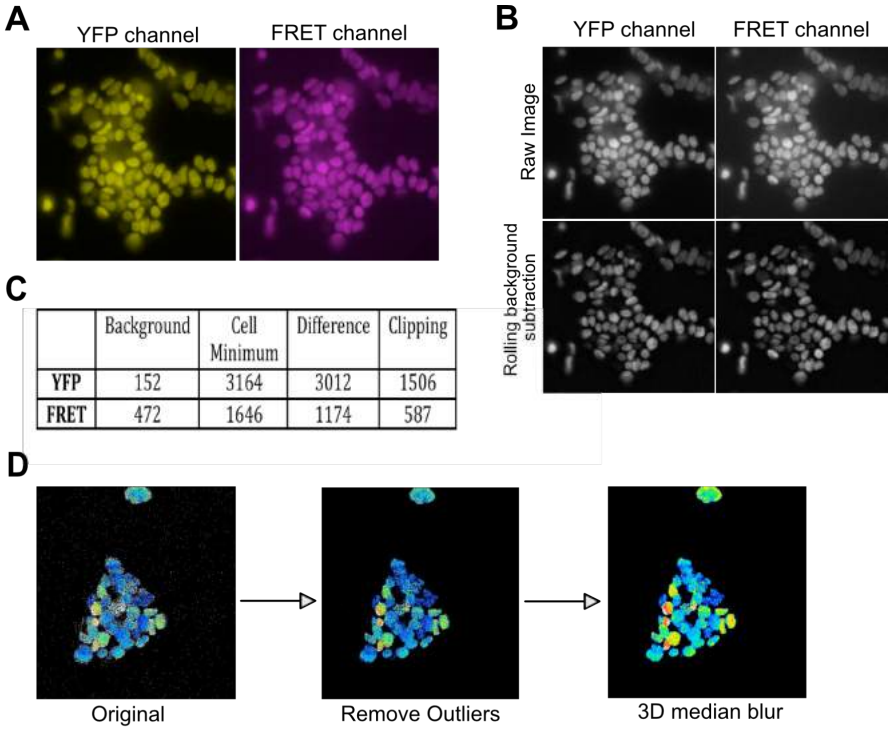


| | Background | Cell Minimum | Difference | Clipping |
|---|---|---|---|---|
| YFP | 152 | 3164 | 3012 | 1506 |
| FRET | 472 | 1646 | 1174 | 587 |

**Figure 2.1: Method for ratiometric analysis.** (A) YFP channel (YFPex-YFPem) and FRET channel image (CFPex-YFPem) of mESCs expressing EKAREV from wide-field microscope. (B) imageJ plugin rolling ball background subtraction (25 pixels) was applied to both images to remove high background levels and blurring around cells. (C) Table of example intensity values measured and used in RatioPLUS plugin. (D) Work-flow of processing applied to ratiometric image. All quantification was carried out on original ratiometric image.

The average Ratiometric FRET value of static cells was quantified using imageJ. Briefly, the YFP channel was used to segment nuclei after applying a 25 pixel rolling background subtraction. A binary mask was then created using a median Gaussian filter and Otsu thresholding. Touching objects were further separated using the Watershed and Fills Holes algorithm. Nuclei were detected using the Analyse Particles function (size=30-infinity pixel) and regions of interest (ROIs) were manually checked. ROIs were applied to the ratiometric FRET image and the mean pixel intensity of each region (nuclei) was measured for a single z-slice. Intensities were taken from the raw ratiometric images and measured over 5 FOV. Values were compiled together for each condition and measurements were represented as a histogram or boxplot using in built MATLAB (mathswork) functions.

### 2.6.2 Single cell FRET tracking

FRET dynamics of single cells over time were quantified by manually tracking cells using a MATLAB graphics interface developed by Adam Corrigan. Cell position was determined by clicking on the centroid of a nuclei for each frame and storing the coordinates of each click into a MATLAB array. All manual tracking was carried out on YFP channel images, due to the strong signal, following the application of 25 pixel rolling background subtraction in imageJ. Imported image arrays were adjusted to discount pixels below the clipping values calculated during the ratiometric analysis. The ratiometric intensity at each mouse clicked coordinate was then calculated using the same formula used in the RatioPLUS plugin. A 2x3 voxel cylinder was applied to each mouse clicked coordinate and the average FRET and YFP intensity of each shape was measured, and a ratio of the two values (FRET/YFP) was calculated and stored in a MATLAB array. FRET tracks were subsequently smoothed, by applying a moving averaging filter with a span of 5, to reduce experimental noise and all subsequent analysis was carried using smoothed tracks, unless stated otherwise. Cells that underwent division were noted down alongside any daughter cells for future analysis.

### 2.6.3 Immunofluorescence Quantification

To measure intensities at the single cell level a similar method used to track FRET dynamics was also applied. Briefly, the coordinates of each cell were manually selected by mouse clicking on the centroid of nuclei. Intensity levels were extracted from the chosen coordinates by calculating the median pixel intensity of 3D shape (5x5x3 voxel) centred over the mouse clicked coordinate. When possible DAPI staining was used to aid manual segmentation of cells.

## 2.7 Quantification Analysis

### 2.7.1 Clustering

FRET tracks of single cells of individual experiments were clustered using the k-means MATLAB (MathWorks) function. Optimal number of clusters within each data set was assigned using silhouette criteria (Rousseeuw, 1987). Cell tracks being clustered must be of equal length. Thus any cells that were not present for the entirety of the time portion being clustered were excluded from the analysis.

A MATLAB script (Vlatka Antolovic) was used to localise the cells of each cluster, using the mouse clicked coordinates recorded during manual tracking. Position of tracked cells were plotted in a 512x512 plot and a colour key was applied to distinguish between clusters.

### 2.7.2 Calculation of cell density

Cell density was determined by assigning a density value to each cell that was calculated using a custom built MATLAB script (Vlatka Antolovic). A maximum projection of the YFP channel, following background subtraction, was imported into MATLAB and converted into a binary imaging using a specified threshold. Cell position coordinates that were recorded during tracking, were applied to the binary image and a circle of radius 50 (pixels) was drawn around each coordinate. Circle areas were defined by creating a 512x512 binary matrix for each cell and measuring the distance of each element from the coordinate of the cell using the Euclidean Squared method. All elements that were a distance of less than 50 pixels

from the coordinate were assigned a value of 1 and all elements with a distance greater than 50 pixels were assigned a value of 0. From these matrices the indices of each circle could be identified and then applied to the binary image.

The sum of pixel intensities within each circle indices was calculated and assigned to its corresponding cell. The greater the number of cells that fall within the circle indices the higher the value. These density values can therefore act as indicator for the population density of a cell's environment. For example a cell at the edge of a population will have a much lower density value than a cell that is in the middle of a population. To test the accuracy of these density values cell positions were plotted and a LUT representing the density value of a cell was applied to each point. Plots were overlayed over the YFP channel image for comparison.

### 2.7.3 Identification of neighbouring cells

Neighbouring cells were identified using a similar method used to calculate cell density. Cell positions, recorded during manual tracking, were used to draw a circle of a specified radius around each cell. The radius of the circle was adjusted to incorporate the cell-cell contacts of each cell, and a radius of 30 pixels was found to be optimal. A grayscale image of all the circles summed together was used to evaluate radius size and ensure that each drawn circle only encompassed directly neighbouring cells.

Circle areas were defined using a binary matrix. All elements within a 25 pixel radius of a coordinate, calculated using the euclidean squared method, were designated the value of 1 and all remaining elements were assigned a value of 0. A binary matrix was developed for each cell using the coordinates recorded from manual tracking. From these matrices the circle indices of each cell could be calculated and compared against one another. This was done by applying the circle indices of a cell to the binary matrices of all other cells in a population and calculating the size of the elements that fell within these indices. If the circle indices of two cells do not overlap the size of all the elements will be equal to zero and the cells are not considered to be neighbours. However, if the two circle indices do

overlap there will be elements with a size greater than zero and the cells will be considered neighbours. This was repeated for all the cells in a population and the neighbours of each cell were recorded in a MATLAB array.

# Chapter 3

# Using a FRET based biosensor to measure ERK activity in ES Cells

## 3.1 Introduction

Suppression of the MAPK pathway is a critical component of the 2i/LIF culture condition that maintains ES cells in a naive pluripotent state (Ying et al., 2008). Activation of ERK signalling by FGF4 promotes the onset of differentiation and perturbation of this pathway by genetic manipulation of chemical inhibitors impedes ES cell differentiation (Kunath et al., 2007; Stavridis et al., 2007; Burdon et al., 2002). As previously mentioned, a network of transcription factors are central to the regulation of pluripotency in ES cells and expression of these factors helps maintain cells in a state of self-renewal. Under serum/LIF conditions these factors are heterogeneously expressed but under 2i their expression becomes more uniform (Ying et al., 2008; Niwa et al., 2009). Perturbation of the FGF/ERK signalling pathway has been shown to modulate the expression and behaviour of various components of this pluripotency network (Hamazaki et al., 2006; Yeo et al., 2014; Davies et al., 2013; Yang et al., 2012). However, how the ERK signalling pathway directly feeds into the transcriptional regulation of pluripotency and triggers the onset of differentiation remains unclear.

Previous studies examining ERK activity in ES cells have primarily relied on biochemical methods making it difficult to explore temporal changes and any cell-cell variation that could be occurring. However, it has become increasingly apparent that signalling dynamics can vary widely within a population and lead to multiple different cellular outcomes (Purvis and Lahav, 2013). This has been shown to be of particular prevalence in the MAPK/ERK pathway, where differences in the frequency and level of ERK can determine the fate of a cell (Marshall, 1995; Santos et al., 2007; Albeck et al., 2013; Aoki et al., 2013). Thus ERK activity dynamics could be an essential mechanism in regulating the transcriptional network of pluripotency in ES cells.

In this chapter I have used single cell quantification tools to explore the relationship between the expression of pluripotency factors and pERK levels. Using these tools I have also explored how pERK levels change following the removal of LIF and subsequent entry into lineage commitment. Here I will also discuss how I am using a FRET based biosensor to follow changes in ERK activity at the single cell level. I will describe how FRET image acquisition settings were established and demonstrate the suitability of the FRET based biosensor for monitoring ERK activity in ES cells.

## 3.2 Comparing levels of pERK with the expression of pluripotent markers at the single cell level

To monitor the transcriptional regulation of Nanog, I employed an ES cell line known as TNGA, which has a GFP inserted directly after the Nanog start codon (Chambers et al., 2007). Cells were cultured in standard serum/LIF conditions, then fixed and immunostained for pERK. Figure 3.1A shows a small proportion of ES cells exhibiting high levels of pERK when cultured in the presence of LIF (+LIF) suggesting that ERK activity levels are not uniform within a cell population. Additionally, these high pERK levels could no longer be detected when cells were treated with a MEK inhibitor, confirming the specificity of the immunostaining

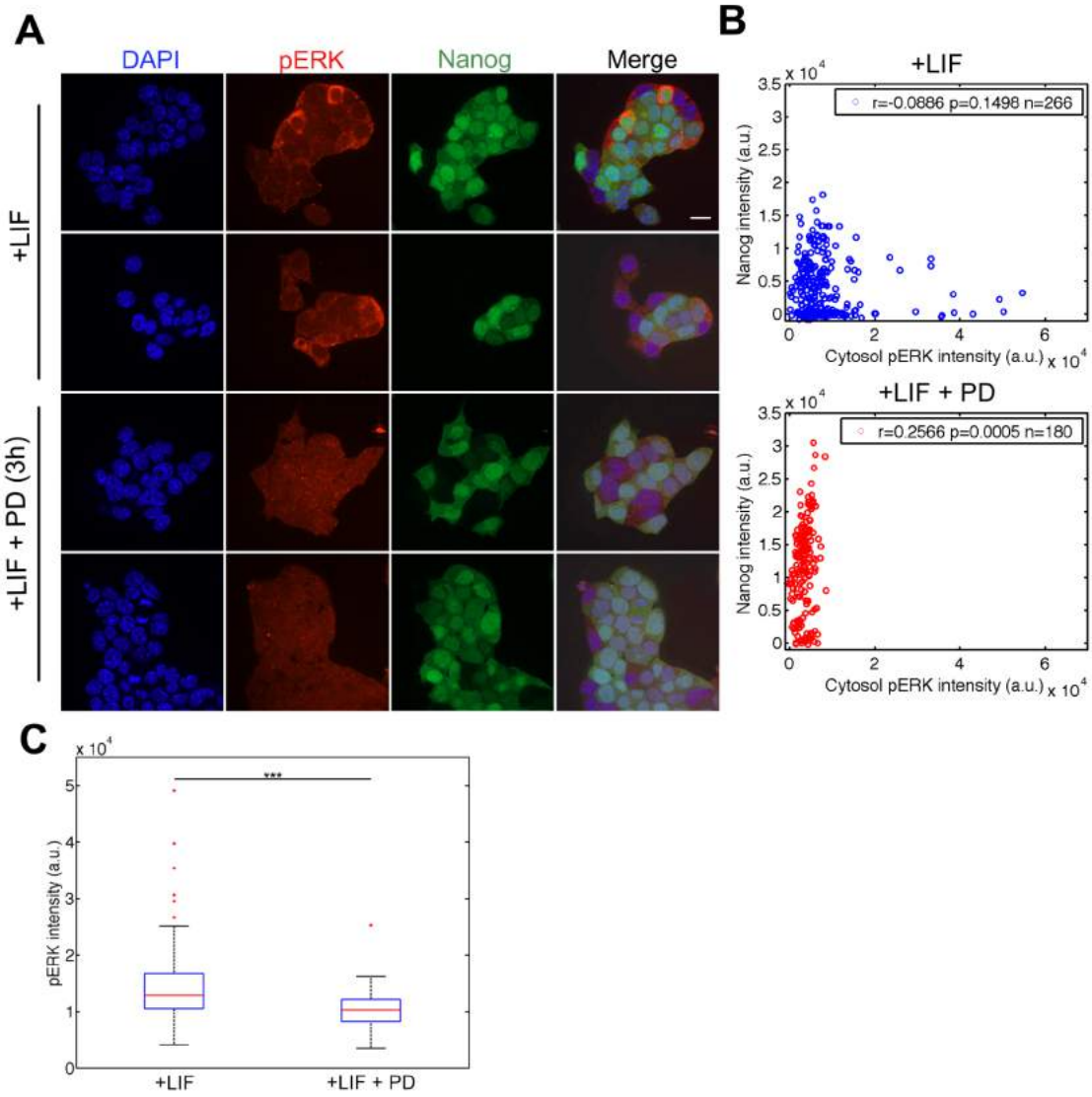


**Figure 3.1: Relationship between pERK and the expression of Nanog** (A) Immunofluorescence of ES cells expressing GFP reporter for Nanog immunostained for pERK (red). Cells were also stained for DAPI to facilitate identification of individual cells. +LIF represents standard ES culture conditions. Cells were also treated with the MEK inhibitor PD0325901 (PD) (1$\mu$M) 3h prior to fixation as a negative control. Scale bar = 20$\mu$m (B) Expression of Nanog reporter in the nucleus of each cell was plotted against its corresponding cytosolic pERK level and Pearson correlation coefficient was calculated. ES cells in +LIF are shown in blue (r=-0.0886, p=0.1498, n=266). ES cells treated with PD are shown in red (n=180, r=0.256, p=0.0005). (C) Boxplot of pERK levels measured in +LIF and +LIF + PD conditions and pERK levels were found to be significantly different using an unpaired Student's t-test. *** signifies p$\leq$0.001

(Figure 3.1A and C). An increased expression in the GFP reporter for Nanog could also be detected following the inhibition of MEK, with cells exhibiting a more homogeneous expression pattern. To measure intensities at the single cell level a point was manually selected within each cell to generate a coordinates. Intensities were extracted from the DAPI, pERK and GFP channels by calculating the mean pixel intensity in boxes of 5x5x3 voxels centred on each coordinate. This was carried out on every cell over 5-6 fields of view (FOVs) to generate a large dataset which could then be used for further analysis. Due to the antibody and the immunofluorescence protocol used I was only able to detect pERK in the cytosol of the cell. Thus two coordinates were generated per cell, one for the nucleus and one for the cytosol.

GFP levels in the nucleus should reflect the transcriptional activity of Nanog (Chambers et al., 2007). Therefore, the GFP nuclear signal intensity of each cell was plotted against its corresponding cytosolic pERK intensity to determine the relationship between Nanog expression levels and ERK activity (Figure 3.1B). Pearson correlation coefficients were then calculated to measure the linear strength between these two variables identifying Nanog expression and pERK levels to be weakly negatively correlated (r=-0.089, p=0.1498, n=266) (Figure 3.1B). Moreover, averaging of correlation values between experimental repeats resulted in a weak negative correlation (r=-0.096) implying that Nanog reporter expression is not simply related to instantaneous activation of ERK. However, it is important to note that a disparity between GFP and the expression of endogenous Nanog protein has been observed in the TNGA line (Faddah et al., 2013; Cannon et al., 2015), which could be masking a correlation between pERK levels and expression of Nanog.

Another pluripotency factor that is heterogeneously expressed in ES cells is Rex1 (Toyooka et al., 2008). To investigate whether Rex1 behaved comparably to Nanog in relation to ERK activity I utilised the ES cell line OCRG9, which has GFP inserted into the Rex1 coding sequence (Toyooka et al., 2008). Cells were cultured in standard ES conditions (serum/LIF), then fixed and immunostained for pERK as

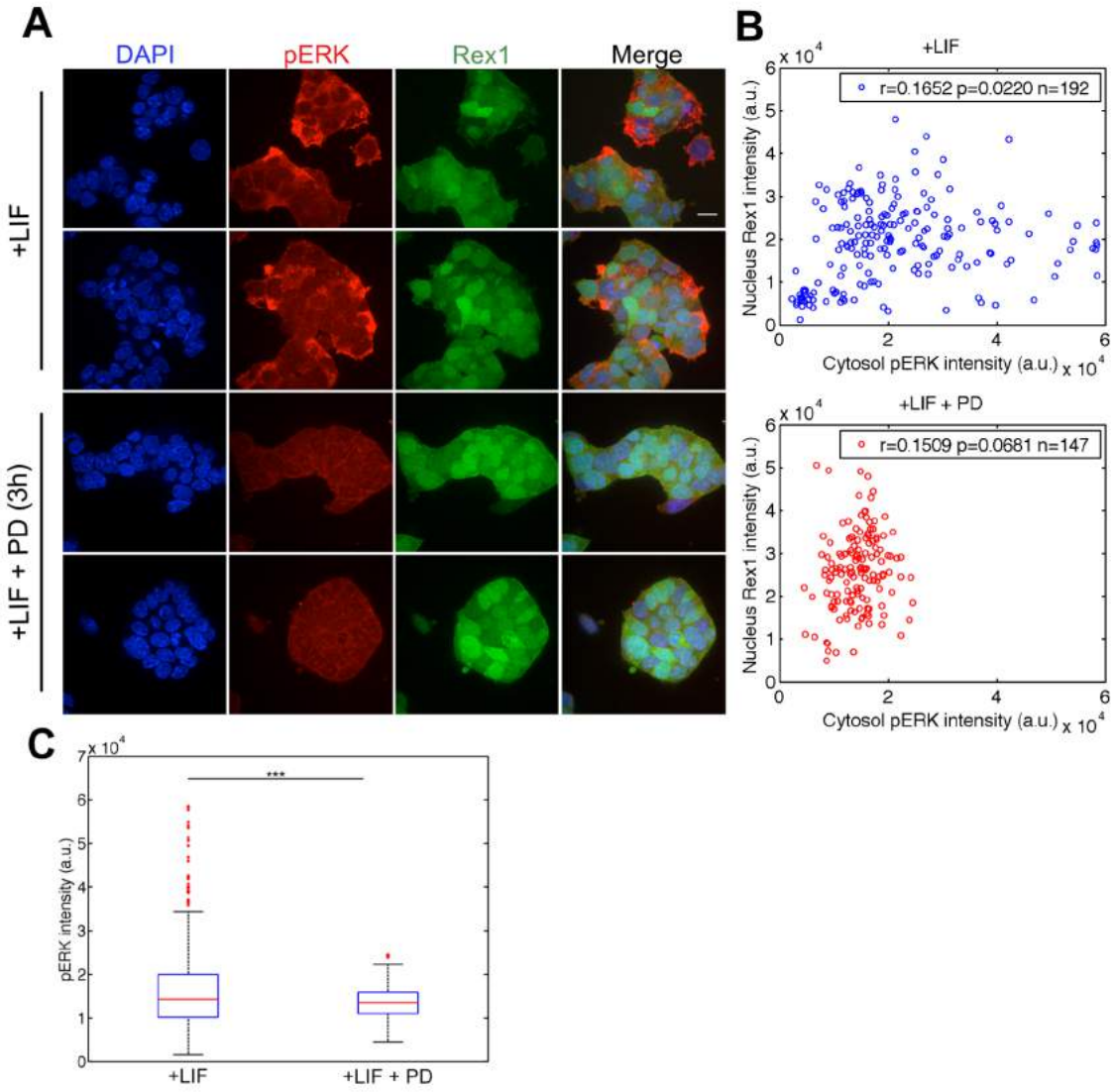


**Figure 3.2: Relationship between pERK and the expression of Rex1** (A) Immunofluorescence of ES cells expressing GFP reporter for Rex1 immunostained for pERK (red). Cells were also stained for DAPI to facilitate identification of individual cells. +LIF represents standard ES culture conditions. Cells were also treated with the MEK inhibitor PD0325901 (PD) (1$\mu$M) 3h prior to fixation as a negative control. Scale bar = 20$\mu$m (B) Expression of Rex1 reporter in the nucleus of each cell was plotted against its corresponding cytosolic pERK level and Pearsons correlation coefficient was calculated. ES cells in +LIF are shown in blue (n=192) and a weak positive correlation was observed (r=0.1652, p=0.0220). Correlations with $p \leq 0.05$ are considered significant. ES cells treated with PD are shown in red (n=147, r=0.1509, p=0.0681). (C) Boxplot of pERK levels measured in +LIF and +LIF + PD conditions and pERK levels were found to be significantly different using an unpaired Student's t-test. *** signifies $p \leq 0.001$

before (Figure 3.2A). Signal intensities were extracted from the cytosol coordinates of the pERK channel and plotted against nucleus GFP levels of the same cell. Conversely, Pearsons correlation coefficient revealed a positive linear correlation between cytosolic pERK and nuclear Rex1 levels (r=0.1652, p=0.022, n=192), suggesting a disparity in behaviour between the two reporters (Figure 3.2B). Averaging of correlation values between three experimental replicates showed Rex1 expression and pERK levels to be poorly correlated (r=0.0887). I was therefore unable to identify any clear relationship for either Rex1 or Nanog in relation to ERK activity. Figure 3.1 and 3.2 shows a large proportion of signal detected in the pERK channel under serum/LIF conditions could also be detected following treatment with a MEK inhibitor (+LIF+PD), which is likely to be the result of background staining. Inclusion of these pERK intensities could be precluding a relationship between the reporter and pERK levels. Additionally, I was only able to measure the pERK levels of the cytosol, and pERK levels of the nuclei could be more strongly correlated with Rex1 and Nanog expression.

## 3.3 Inducing differentiation reduces pERK levels

ES cells can be maintained in a state of self-renewal under culture conditions in the presence of the cytokine LIF (Smith et al., 1988). LIF primarily functions through the JAK/STAT3 pathway and in the absence of STAT3, LIF is no longer able to inhibit differentiation and support the self-renewal of ES cells (Niwa et al., 1998; Matsuda et al., 1999). MAPK pathway and PI3K pathway are also activated by LIF, and along with JAK/STAT3 these 2 pathways can regulate the expression levels of Nanog, Tbx3 and Klf4, which when individually overexpressed can support the self-renewal of ES cells independently of LIF (Niwa et al., 2009). Removal of LIF from culture conditions causes induction of differentiation (Burdon et al., 2002). I was therefore interested to see what would happen to ERK activity when LIF was removed and ES cells began entering the differentiation pathway.

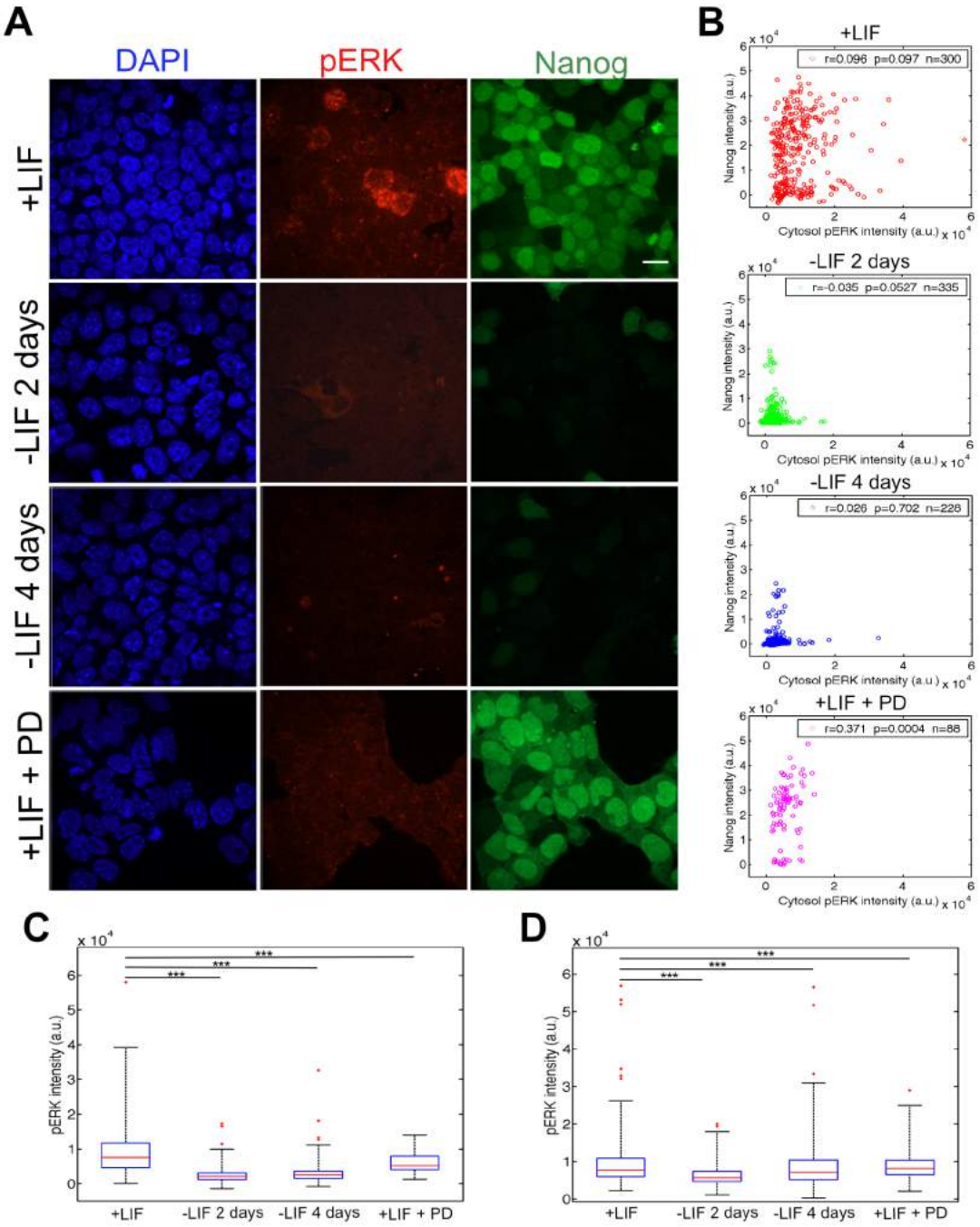


**Figure 3.3: Removal of LIF from TNGA cells causes a change in ERK activity** (A) Immunofluorescence for pERK (red) in the TNGA ES cell line following culture in LIF (+LIF), 2 days without LIF (-LIF 2 days), 4 days without LIF (-LIF 4 days), 4 days with LIF and a MEK inhibitor (1$\mu$M) (+LIF +PD). Cells were stained with DAPI to facilitate identification of individual cells. Scale bar = 20$\mu$m (B) Expression of Nanog reporter was plotted against pERK intensity of each cell and Pearsons correlation coefficient was calculated; + LIF (r=0.096, p=0.097, n=300) (red), -LIF 2 day (r=-0.035, p=0.0527, n=335) (green), -LIF 4 days (r=0.026, p=0.702, n=228) (blue), +LIF +PD (r=0.371, p=0.004, n=88) (pink). (C) Distribution of the pERK levels measured for all four conditions in the TNGA line. (D) Distribution of the pERK levels measured for all four conditions in the OCRG9 Rex1 reporter line. pERK levels were compared against +LIF using a unpaired Student's t-test. *** signifies p$\leq$0.001. Data typical of three independent replicates

To investigate the affect of LIF on ERK activity, TNGA cells (Chambers et al., 2007) were cultured over 4 days either in the presence of LIF, without LIF for all 4 days, without LIF for 2 days, or with LIF and a MEK inhibitor. Cells were fixed and immunostained for pERK, and images were analysed using MATLAB to measure the intensity in each of the channels at the selected coordinates, as before. Removal of LIF caused a decrease in pERK following 2 days and 4 days of LIF removal (Figure 3.3A). Quantification revealed the majority of cells were exhibiting both low pERK levels and low Nanog levels (Figure 3.3B). The low Nanog expression levels detected indicates that the removal of LIF has induced differentiation, as low expression of pluripotent markers is associated with ES cells being primed for differentiation (Chambers et al., 2007). Boxplots of the pERK intensities highlights the significance of the decrease in pERK activity with the average level of pERK, following 4 days of LIF removal, appearing even lower than in inhibitor treated cells (Figure 3.3C). These results were surprising as I had expected pERK levels to increase following LIF removal due to the requirement of FGF/ERK signalling for the induction of differentiation (Kunath et al., 2007; Stavridis et al., 2007).

The experiment was subsequently repeated using the OCRG9 Rex1 reporter cell line to determine if a similar affect could be observed. Figure 3.3D shows a significant decrease in pERK levels following the removal of LIF for 2 days, similar to what was observed in the TNGA line. However, pERK levels do appear to be slightly higher following 4 days of culture in the absence of LIF compared to levels detected in the TNGA ES cells, which is likely to result from experimental variations or cell line differences (Figure 3.3C). Nevertheless, these results show a significant decrease in pERK levels following the absence of LIF for 2 and 4 days in both cell lines, suggesting that this response is comparable between different ES cell lines.

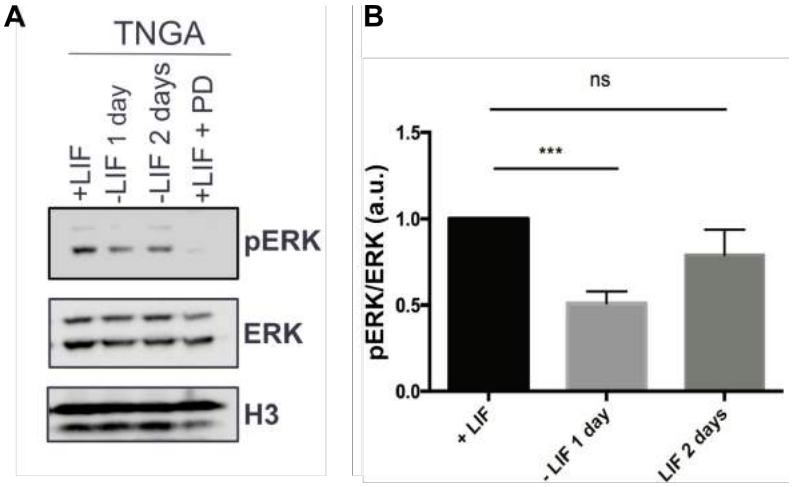


**Figure 3.4: Western blots corroborate our finding that removal of LIF causes a decrease in pERK.** (A) TNGA ES cells were cultured in LIF (+LIF), without LIF for 1 day (-LIF 1 day), without LIF for 2 days (-LIF 2 days), and with LIF and PD0325901 at 1$\mu$M (+LIF +PD). Western blots were performed with anti-phospho-ERK, anti-ERK and anti-H3 antibodies (n=3) (B) Active ERK levels were determined by the ratio of pERK/ERK at the indicated times following the removal of LIF. Data are presented relative to +LIF control levels as means $\pm$ SEM. pERK/ERK levels were compared against control (+LIF) using an unpaired Student's t-test. **ns** = $p>0.05$, *** = $p\leq 0.001$

Following on from these results, I decided to see if a similar effect could be seen by western blot using the same TNGA ES cell line. Cells were cultured either in the presence of LIF, absence of LIF for 1 day, absence of LIF for 2 days, or in the presence of LIF supplemented with a MEK inhibitor for 2 days. A decrease in pERK levels was detected in cells cultured in the absence of LIF for 1 day compared to cells cultured in standard serum/LIF conditions (Figure 3.4). However, an increase in pERK levels could be observed following 2 days of culture in the absence of LIF (Figure 3.4). These findings are in slight disagreement with the immunofluorescence data, which showed a significant decrease in pERK levels at 2 days following the removal of LIF. This disparity may arise from the inclusion of nuclear pERK levels, as well as cytosolic, from the western blot analysis, which could not be quantified from the immunofluorescence data. Despite this slight variation in response, a decrease in ERK activity following the removal of LIF could be identified, providing further support to the immunofluorescence observed response.

These findings are potentially at odds with the known role of ERK signalling in the induction of differentiation. However, it is highly probable that by looking at single snap shots in time we are missing important dynamic information and need to be looking at a much greater time resolution. Moreover, the pERK levels, detected by immunofluorescence, imply that ERK activity is likely to be heterogeneous within an ES cell population. To address this I wanted to identify a method for measuring ERK activity dynamics at a single cell resolution and find a way to compare these to the expression of pluripotency markers.

## 3.4 Using a FRET based biosensor to measure ERK activity at the single cell level

A FRET based biosensor known as EKAREV has successfully been used to monitor ERK signalling dynamics in a range of different cell types, and its use has led to the identification of distinct ERK activity patterns (Aoki et al., 2013; Albeck et al., 2013; Hiratsuka et al., 2014; Sparta et al., 2015). I therefore wanted to see if the EKAREV FRET biosensor could be used to monitor the ERK signalling dynamics of ES cells.

The EKAREV biosensor is comprised of a YPet and SECFP FRET pair tagged with either a nuclear localisation signal (NLS) or nuclear export signal (NES) to monitor nuclear or cytosolic ERK activity respectively (Komatsu et al., 2011; Harvey et al., 2008). To establish a stable cell line, ES cells were transformed with either an NLS tagged or NES tagged EKAREV, as described in Materials and Methods. The ES cell line expressing the NLS tagged biosensor was used initially due to the nuclei of ES cells taking up a large proportion of cellular space making it easier to image and quantify than the NES tagged EKAREV expressing line. However, expression levels of the NLS EKAREV tagged biosensor were highly variant between cells causing difficulties with dynamic range during image acquisition. Consequently, I decided to employ a piggyBAC transposon system, which has been used previously to stably express EKAREV in a HeLa cell line (Aoki et al., 2012). ES cells were

co-transformed with the mouse codon optimised piggyBAC transposase (Cadiñanos and Bradley, 2007), which recognises the transposon recognition sequence flanking EKAREV, and the biosensor at a ratio of 1:1. Using the piggyBAC system generated a cell line with more uniform expression of the biosensor and this cell line was used for all subsequent FRET experiments.

### 3.4.1 Optimisation of instrument for FRET analysis

Intensity based ratiometric methods are commonly used for FRET time-lapse imaging due to the speed of acquisition, which can report on rapid changes in dynamics, using easily available conventional wide-field and confocal microscope systems (Pietraszewska-Bogiel and Gadella, 2011). FRET read-outs are highly dependent on the microscopy method used and how images are processed to calculate FRET ratio values (Spiering et al., 2013). An optimum protocol for imaging the EKAREV-NLS expressing ES cell line therefore had to be established, which required the trialling of different fluorescent microscopes.

The EKAREV biosensor is comprised of a SECFP donor and YFP acceptor fluorophore. When ERK is active the sensor will become phosphorylated generating a conformational change reducing the distance between the two fluorophores allowing for a transfer of energy and an increase in the level of FRET. FRET levels are measured by exciting the donor fluorophore (SECFP) at the appropriate wavelength, and detecting the level of light emitted from the acceptor fluorophore (YFP). The YFP and CFP fluorophore will be of equal concentration and distribution in biosensor expressing cells, and a ratio of FRET levels against YFP or SECFP can be used to quantify the level of FRET within individual cells. Ratiometric measurements require the acquisition of donor or acceptor channel images alongside the imaging of FRET. For this work, YFP images were primarily used due to the longer exposure times required for imaging of the SECFP fluorophore. A FRET channel and YFP channel image were acquired for the majority of the microscopes trialled, and a imageJ plugin was used to calculate the ratio between these two images. A 16 colour Look-up Table (LUT) was

subsequently applied in order to visualise the spread of ratio values across each image.

Multiple different confocal microscopes were trialled in order to identify the optimum protocol for imaging of the EKAREV-NLS expressing ES cell line. Testing FRET imaging protocols on different imaging systems. We used a Leica TCS SP5 with 40x objective, Olympus FluoView FV1200 using 60x objective, a Leica gSTD super-resolution system (SP8) (40x) and a wide-field system (see Materials and Methods). Except for the Olympus system, images show a single field-of-view with the corresponding FRET/YFP ratio image. A CFP channel image was captured with the Olympus due to the absence of an appropriate YFP excitation laser and the corresponding FRET/CFP image is shown. Scale bars = 20m

The first system to be trialled was the Leica SP5 confocal system as it was already equipped with the appropriate lasers for imaging of the EKAREV biosensor (Figure 3.5A). Despite being able to detect a signal in both the YFP and FRET channel, Table 3.1 shows that the pixel intensities measured from the 8-bit FRET channel image were extremely low, providing a small dynamic range in which to monitor changes in FRET signal. Additional confocal systems, Leica SP8 and FV1200 Olympus, were subsequently trialled to see if a greater level of signal could be detected (Figure 3.5B and C). The HyD detectors of the SP8 microscopes can detect lower levels of light than the PMT detectors of the SP5 owing to their increased sensitivity, potentially providing a greater dynamic range to monitor changes in FRET. However, the SP8 system available was not equipped with an appropriate laser for excitation of the SECFP fluorophore. As a result, FRET images had to be acquired using a 405nm diode laser which is unable to fully excite the SECFP fluorophore, leading to a loss in available transferable energy to the YFP fluorophore, and an overall reduction in the level of FRET signal that can be detected. The mean pixel intensity of the FRET channel (Table 3.1), which is the average of all cells in the FOV shown in Figure 3.5B, was higher than the mean pixel intensity of the FRET channel image acquired with the SP5. However,

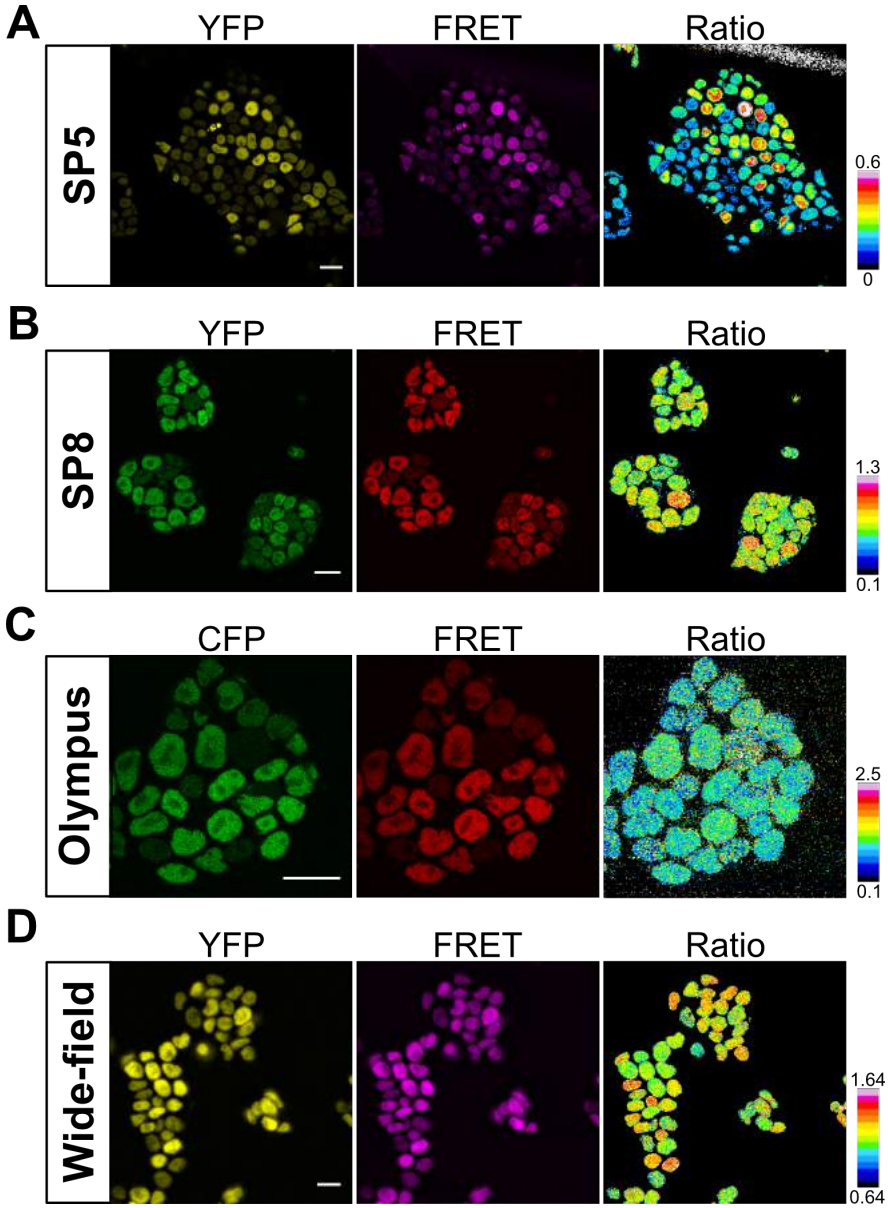


**Figure 3.5: Trialling of alternative microscopes for ratiometric FRET analysis.** For each microscope (A) Leica TCS SP5 confocal with 40x objective (B) Leica gSTED super-resolution system (SP8) (40x) (C) Olympus FluoView FV1200 microscope (60x) and (D) Zeiss Axiovert widefield 200 wide-field system (Wide-field). Except for the Olympus system, images show a single FOV of a YFP and FRET channel image of ES cells expressing EKAREV-NLS under serum/LIF culture conditions. A CFP channel image was captured with the Olympus due to the absence of an appropriate YFP excitation laser and the corresponding FRET/CFP image is shown. Scale bars = 20m

the mean pixel intensity measured is still relatively low offering a limited dynamic range to detect changes in FRET, and image acquisition times were slow, which could result in the loss of important dynamic information.

Ratiometric FRET images were also acquired with an FV1200 Olympus confocal microscope, as it is configured for FRET imaging and has two high-sensitivity gas gallium phosphide (GaAsP) detectors, which can be used to image very dim samples (Figure 3.5C). The average pixel intensity of the FRET channel, calculated from all cells in the FOV shown, was 584.1 (Table 3.1) with a mean background intensity of 355.1a.u.. The Olympus produces 16-bit images, therefore 584.1a.u. is still in the lower range of potential pixel intensities. Furthermore, ratiometric analysis showed FRET ratio levels to be uniform within a population (Figure 3.5C) which is inconsistent with ratiometric images obtained using alternative microscope systems (Figure 3.5A, B and D). High background intensities can greatly reduce the signal to noise ratio (Aoki and Matsuda, 2009) and this could be causing variation in FRET signal between cells to be lost.

| | **YFP** | | | **FRET** | | |
|---|---|---|---|---|---|---|
| **Microscope** | mean (a.u.) | min (a.u.) | background (a.u.) | mean (a.u.) | min (a.u.) | background (a.u.) |
| SP5 | 59.3 | 19.3 | 0.65 | 15.5 | 3.6 | 3.23 |
| SP8 | 58.5 | 9.8 | 2.08 | 42.9 | 9.0 | 2.98 |
| Olympus* | 742.5 | 125.3 | 603.5 | 584.1 | 91.0 | 355.3 |
| Wide-field | 11662 | 9107 | 3533 | 14788 | 12068 | 6872 |

**Table 3.1: Table of pixel intensities of the YFP and FRET channel images captured**. The mean and minimum (min) pixel intensity was quantified for each cell in the FOV shown in figure 3.5 using imageJ as described in materials. Pixel intensities were measured in the YFP and FRET channel image for every microscope and the minimum and mean intensity of all cells were averaged together to get a final value. For background intensity a mean pixel intensity was calculated over a assigned ROI in which no cells were present.* signifies CFP channel pixel intensity measurement

Previous studies have used a wide-field microscope system to carry out ratiometric imaging of the EKAREV biosensor (Aoki and Matsuda, 2009; Aoki et al., 2013; Albeck et al., 2013). Wide-field systems, although offering increased back-ground fluorescence and optical convolution, have high acquisition rates and can provide reduced phototoxicity to cells (Sanderson et al., 2014). In addition, the increased gain of the EMCCD camera available with the wide-field system used for FRET

imaging allows for the detection of dim fluorescence emission, greatly increasing the range of pixel intensities that can be measured within a population. The mean pixel intensity of the FRET channel acquired from a wide-field system was considerably higher than the signal collected by confocal microscopy (Table 3.1). Moreover, the lower photo-toxicity and faster image acquisition times are advantageous for long course time-lapse imaging. As a result of these benefits, and the greater range of pixel intensities captured, a widefield system was found to be the most appropriate microscope system and was used for all subsequent ratiometric FRET imaging of the EKAREV-NLS ES cell expressing line.

### 3.4.2 Fluorescence lifetime imaging (FLIM) of the EKAREV biosensor

Fluorescence lifetime is the average time a fluorophore spends in the excited state before returning to the ground state. Excited fluorphores return to the ground state by emission of a fluorescence photon, however energy can also be transferred to the environment or converted internally (Swift and Trinkle-Mulcahy, 2004). Every fluorophore has its own intrinisc fluorescence lifetime, which usually ranges between 1-10 nanoseconds (ns) in the case of biologically used fluorophores (Hum et al., 2012). However, if fluorescence is quenched and energy is transferred to the environment the fluorescence lifetime of a fluorophore will decrease, becoming shorter than its characteristic lifetime. The fluorescence lifetime of a fluorophore is measured by applying a short two photon laser pulse to a sample and the number of photons emitted over time is subsequently recorded. This laser pulse is then applied to the sample multiple times and the fluorescence decay time between each pulse are compiled to establish an average life time (Swift and Trinkle-Mulcahy, 2004).

The principles of FLIM can be applied to FRET imaging as quenching of the donor fluorophore by FRET will cause a reduction in the fluorescence lifetime of the donor. A ratio can the be calculated between the fluorescence lifetime of the quenched and non-quenched donor to generate a read out for changing FRET efficiency. FLIM is considered to be a more accurate quantification method than ratiometric FRET as it is not reliant on intensity based measurements (Maryu et al.,

2018). Moreover, FLIM-FRET is not affected by donor or acceptor photobleaching which can introduce artefacts into ratiometric methods (Birtwistle et al., 2011). In light of this, I wanted to investigate whether FLIM measurements could be applied to the imaging of the EKAREV-NLS ES cell line as a possible alternative to the current ratiometric method that had been established.

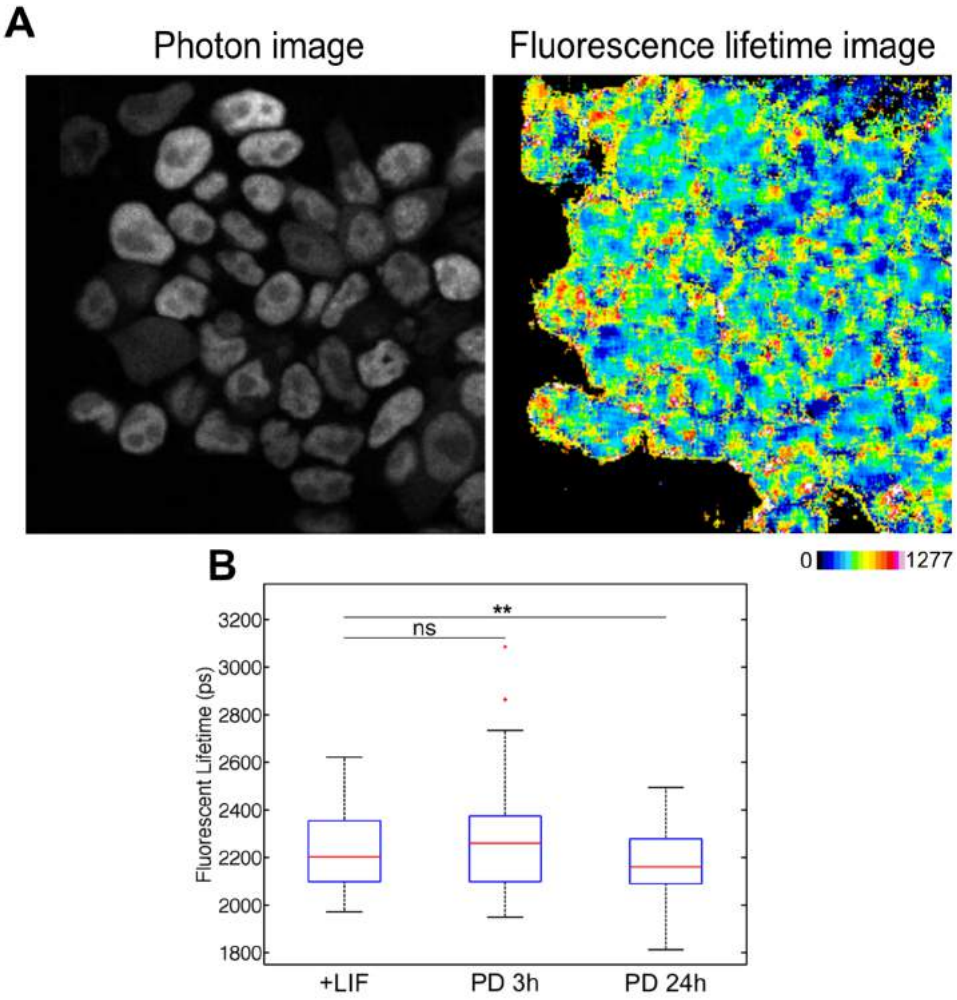


**Figure 3.6: Fluorescent life-time imaging of ES cells expressing the EKAREV biosensor.** (A) Example of images captured by FLIM. A fluorescent emission image was taken to identify cells (Photon image) and an image representing the mean fluorescent life-time of each pixel with a LUT applied. Mean fluorescent life-times in the image shown ranged from 0-1277.46ps. (B) Boxplot of mean fluorescent lifetime values of every cell over 4-5 FOV following treatment with a MEK inhibitor (PD0325901) (10$\mu$M) for 3h (PD 3h) and 24h (PD 24h), and in serum/LIF conditions (+LIF) as a positive control. Fluorescent life-times were compared against control using an unpaired Student's t-test. **ns** = $p>0.05$, ** = $p\leq 0.01$

EKAREV-NLS expressing ES cells were cultured under serum/LIF culture conditions and cells were treated with a MEK inhibitor (PD0325901) for 3 or 24 hours. FLIM images were acquired using a Zeiss LSM510 Laser-scanning microscope and 5 FOV were taken for each condition. Images were analsyed using SPCM software (Becker et al., 2002) and a fluorescent life time value was calculated for each pixel. Two images were created following analysis in the SPCM software: an image of emitted photons and an image of the mean fluorescent life time of every pixel (Figure 3.6A). Cells were segmented using the photon image and a region of interest for each cell was applied to the fluorescent life time image to calculate the mean fluorescent life-time.

Inhibition of the MAPK pathway with a MEK inhibitor should cause a decrease in the FRET efficiency of the EKAREV biosensor resulting in an increased fluorescence lifetime. However, no significant increase (P=0.1925) in the fluorescence lifetime of the SECFP donor fluorophore could be observed following 3 hour treatment with a MEK inhibitor and 24h treatment with a MEK inhibitor resulted in a statistically significant (P=0.0082) decrease in mean fluorescence life-time compared to control (Figure 3.6B). SECFP fluorophore is a brighter version of the ECFP fluorophore (developed by A. Miyawaki) (Komatsu et al., 2011), which has multi-exponential life times (Birtwistle et al., 2011; Duncan et al., 2004). Duncan et al. (2004) identified ECFP to have a long fluorescent lifetime of 2190$\pm$240ps and a short life time of 420$\pm$120ps. This long fluorescent lifetime is in relevant agreement with the fluorescence life-time of our SECFP donor under serum/LIF conditions (Figure 3.6B), however the values detected do seem slightly higher. The multi exponential life-times of the SECFP fluorophore make it difficult to compare quenched donor and non-quenched donor fluorescence lifetimes, which can result in unreliable read outs of FRET efficiency, and could be causing these unexpected fluorescence lifetime measurements that were observed. To investigate the FRET efficiency of our SECFP donor fluorophore further, FLIM imaging of an ES cell line expressing SECFP only should be carried out.

FRET-FLIM imaging offers many technical advantages to ratiometric methods. However, the microscope equipment required is more complex and the currently available system was unable to accommodate long time-course imaging due the absence of a $CO_2$ chamber. Additionally, image acquisition times were slower and an increased image interval rate could cause important dynamic information to be lost. It is also of note that Harvey et al. (2008) have shown that ratiometric FRET imaging of the EKAR biosensor has an improved signal to noise ratio compared to FLIM imaging methods. As a result of these disadvantages, and the two fluorescence lifetimes of our donor SECFP fluorphore, FLIM was not used for any further FRET imaging.

### 3.4.3 Correcting for bleed-through in ratiometric FRET imaging

An alteration in FRET efficiency is caused by the non-radiative exchange of energy from a donor to an acceptor fluorophore. However, some of the apparent FRET signal detected will be the consequence of emission from the donor fluorophore bleeding through into the acceptor emission wavelength (Swift and Trinkle-Mulcahy, 2004). It was therefore important to generate donor-only and acceptor-only control cell lines, to evaluate the contribution bleed-through has on the final FRET signal.

ES cells were transformed with either YFP or SECFP fluorophore to generate YFP-only and CFP-only cell lines. Control lines were cultured under serum/LIF conditions and imaged using the same acquisition settings used to image EKAREV-NLS expressing cells. The amount of signal in the FRET channel of the YFP-only cell line appeared very low, suggesting that bleed-through from the YFP fluorophore has a negligible affect on the overall FRET signal (Figure 3.7A). Imaging of the CFP only expressing cell line however, revealed a relatively strong signal in the FRET channel despite FRET being unable to occur (Figure 3.7A). To determine the amount of FRET signal detected with the CFP only cell line every pixel in the CFP channel image was plotted against every pixel value in the FRET channel for 5 different FOV (Figure 3.7B). A line of best fit was drawn

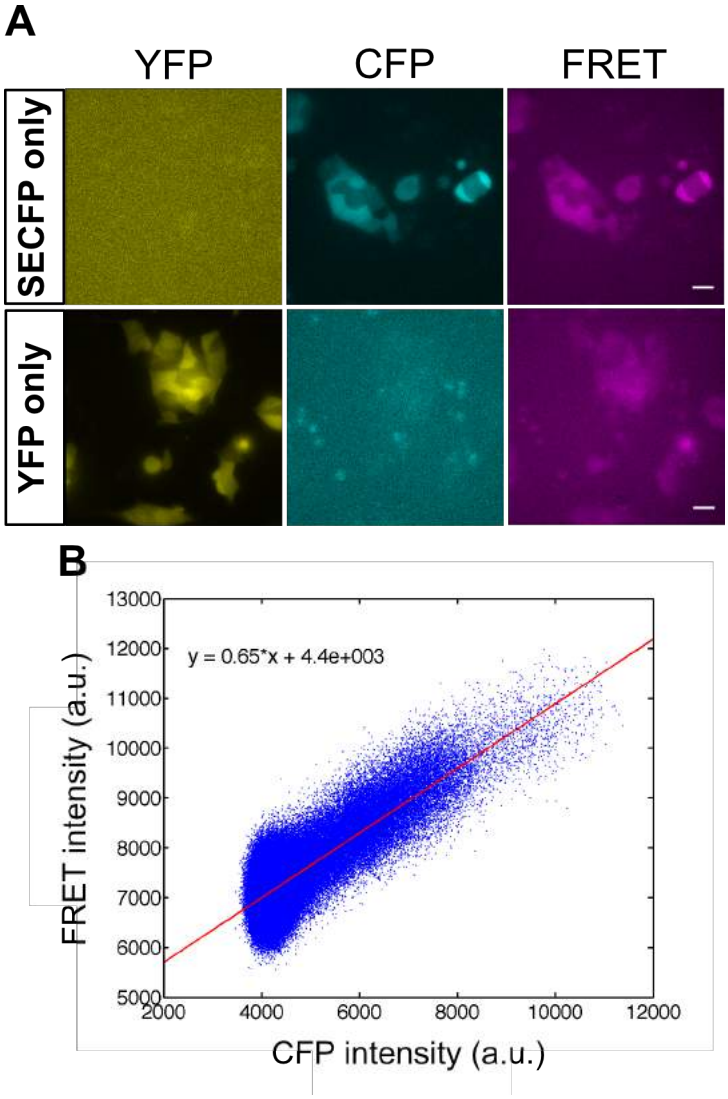


**Figure 3.7: Calculating proportion of FRET signal caused by bleed-through.** (A) Image of ES cells expressing YFP-only or CFP-only captured with the Zeiss Axiovert 200 wide-field system. Scale bars = 20$\mu$m (B) Pixel values in the CFP channel plotted against pixel values in the FRET channel of SECFP-only expressing ES cells. Line of best fit is drawn through the data points and its gradient was measured (m=0.65). Data shown represents values from 1 FOV

through the points and its gradient was calculated. The gradient of the line signifies the proportion of FRET signal that is the consequence of bleed-through. All the gradients calculated from each FOV were averaged together to generate a value that could then be subtracted from the ratiometric image of the biosensor ensuring all remaining signal is a representation of FRET and not bleed-through.

To test the effect bleed-through was having on ratiometric FRET values, I calculated the mean FRET ratio values of cells over 5 FOV before and after bleed-through was subtracted (Figure3.8A). Correction for bleed-through caused a negative shift in FRET ratio values (Figure 3.8B). However, as the bleed-through contribution calculated was a constant value, removal of this value resulted in a uniform decrease in FRET ratio levels across the ratiometric image. Consequently, there was no significant impact on the qualitative difference in FRET signal between

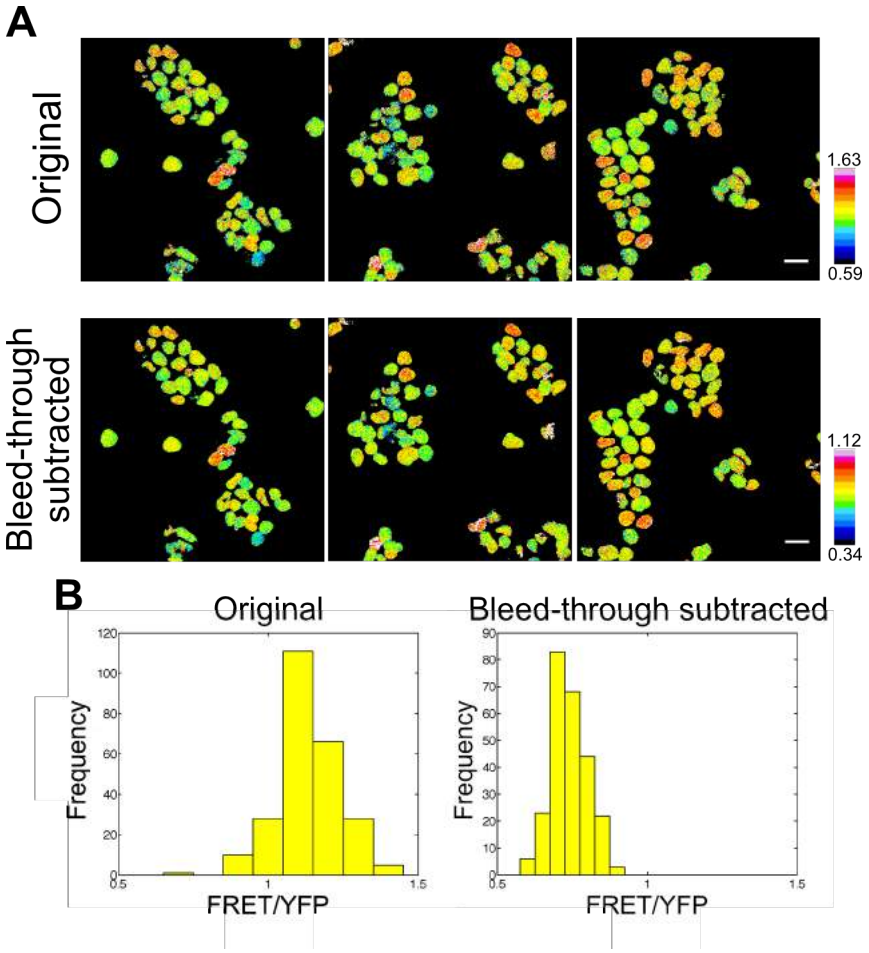


**Figure 3.8: Subtraction of FRET signal caused by bleed-through.** (A) Ratiometric images of ES cells expressing EKAREV in serum/LIF. YFP and FRET channel images were ratioed as before (Original). For bleed-through subtraction the FRET channel images were multiplied by the calculated bleed-through contribution value (0.65 for example shown) prior to the YFP and FRET channel image being ratioed together. LUT was applied to both ratio images showing the distribution of FRET levels to be the same. 3 FOV from one experiment are shown. Scale bars = 20$\mu$m (B) Quantification of mean FRET ratio of individual cells before and after bleed-through subtraction

different cells of a population and the relationship between cells remained relatively unchanged (Figure 3.8A). These data would suggest that bleed-through contribution is having a negligible affect on the observed relative differences in FRET ratio values between cells, and as a result bleed-through was not corrected for in subsequent FRET experiments.

### 3.4.4 The EKAREV biosensor reliably reports on ERK activity in ES cells

Previous studies have shown ERK activity can be highly heterogeneous between cells of a population (Albeck et al., 2013; Aoki et al., 2013) and pERK immunostaining of ES cells has shown pERK levels to be varied between cells (Figure 3.1A). Figure 3.9 shows that under serum/LIF culture conditions a range of FRET ratio levels can be seen, with a small sub-population of cells displaying high levels of FRET. FRET ratio values should correlate with the level of ERK activity suggesting that ERK activity is heterogeneous within an ES cell population.

In order to test that the FRET signal being measured was representative of ERK activity levels, cells were treated with a MEK inhibitor PD0325901 (PD) for 3h and 24h prior to imaging. FRET images were captured over 5 FOV for each condition and ratiometric analysis was carried out in imageJ. ES cells once again displayed a range of FRET ratios, signifying ERK activity to be heterogeneous under standard serum/LIF culture conditions (Figure 3.10A). FRET ratio values appeared to be slightly lower in 3h PD treated cells compared to untreated cells, and high levels of FRET could no longer be detected (Figure 3.10A). However, not as substantial a decrease could be observed following 24h treatment and high levels of FRET could be detected in a small portion of cells (Figure 3.10A). An ES cell line expressing EKAREV with a T/A phosphosite mutation in the substrate domain (EKAREV-TA), was also employed to act as an additional negative control. The EKAREV-TA expressing ES cells displayed very low levels of FRET under serum/LIF culture conditions due to the biosensor being unable to respond to changes in ERK activity (Figure 3.10A).

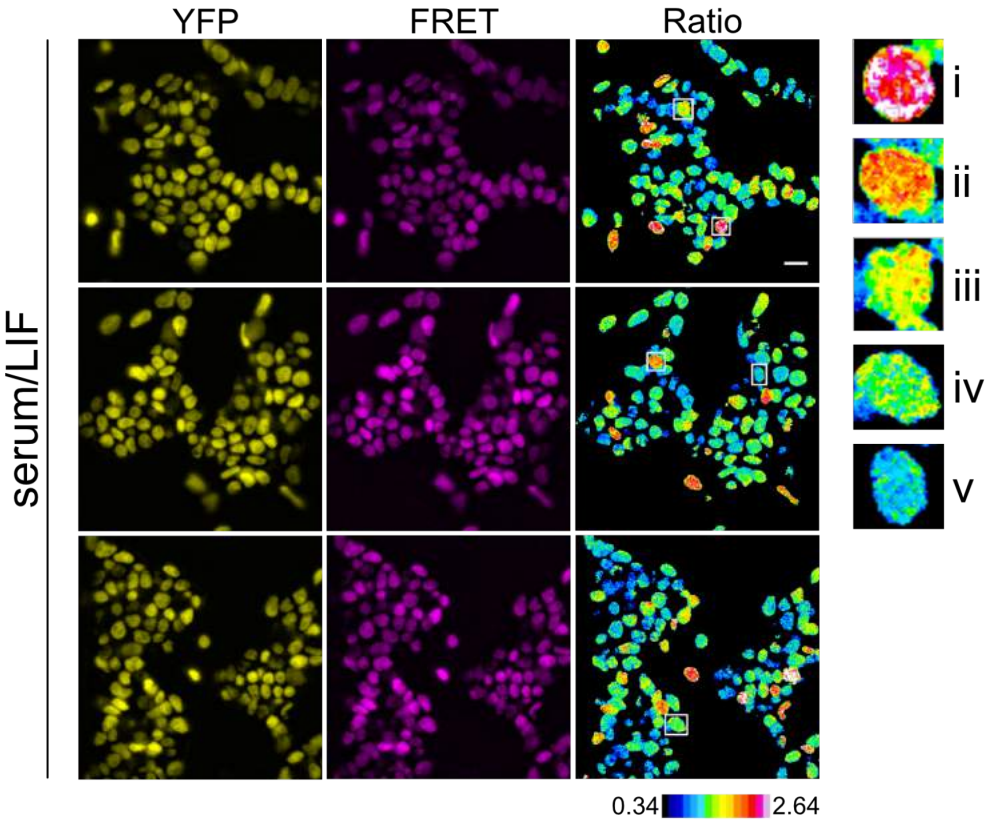


**Figure 3.9: Utilising the FRET based biosensor identified heterogeneous ERK activity.** Ratiometric FRET imaging of ES cells expressing the EKAREV biosensor under serum/LIF culture conditions identified heterogeneous ERK activity. A YFP channel, FRET channel, and ratiometric image are shown for 3 FOV from one experiment. LUT applied demonstrates the range of FRET values detected and an example of cells with distinct FRET ratios is shown on the right. Cells shown on the right hand side are outlined and numbered I-V in order of descending levels of FRET. Scale bar = 20$\mu$m

Quantification of FRET ratio values revealed a statistically significant ($P \leq 0.001$) decrease in FRET signal, following 3h treatment with a MEK inhibitor (Figure 3.10C). Furthermore, 3h MEK inhibition resulted in a smaller range of FRET ratio values, signifying that heterogeneity in relation to ERK activity had been lost (Figure 3.10B). 24h PD treatment also resulted in a statistically significant decrease in FRET ratio values ($P \leq 0.001$). 24h PD treatment did not cause as strong a decrease in FRET ratio values as 3h treatment and FRET ratio values measured appeared more similar to the FRET signal of untreated cells (Figure 3.10A and B). Quantification also identified a strong negative shift in FRET ratio

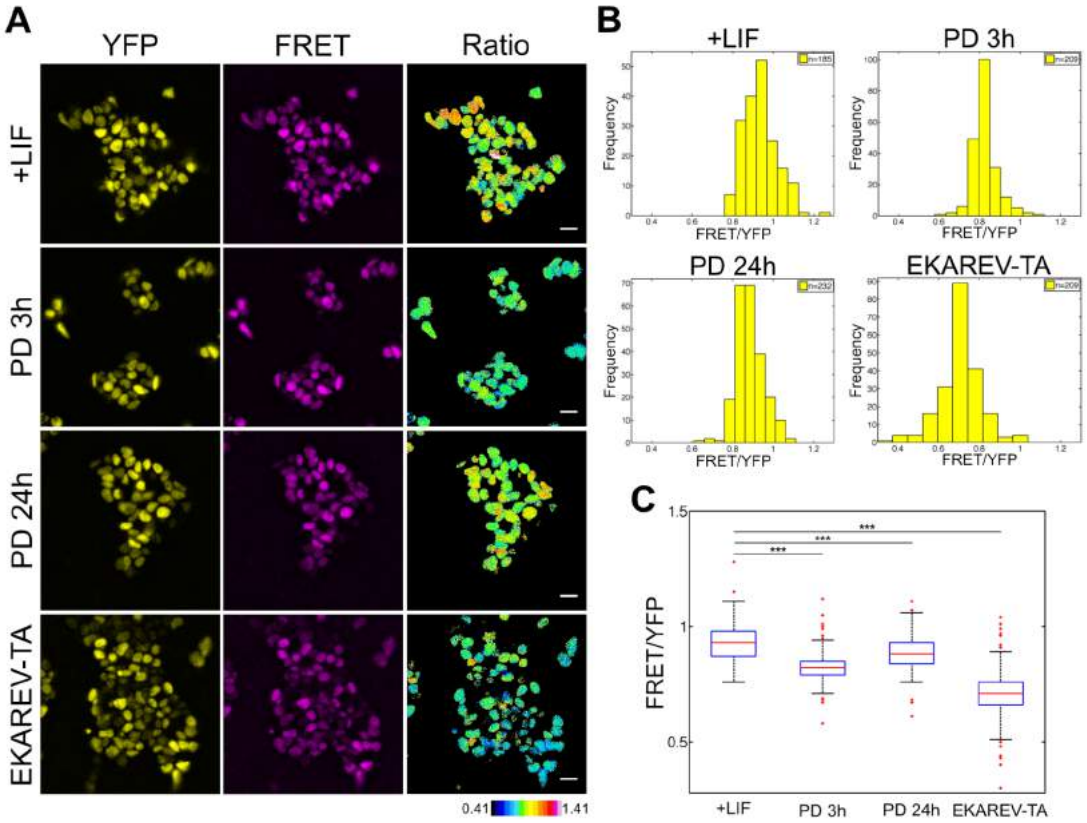


**Figure 3.10: Inhibition of the MAPK pathway causes a loss in FRET signal.** (A) YFP channel, FRET channel and ratiomteric images of ES cells expressing the EKAREV biosensor following treatment with a MEK inhibitor (PD) (10$\mu$M) 3h or 24h prior to imaging, or untreated in serum/LIF as a control (+LIF). YFP channel, FRET channel and ratiometric image were also acquired for ES cells expressing the phospho-site mutated biosenser EKAREV-TA under serum/LIF culture conditions. 5 FOV were captured for each condition (B) mean FRET ratio value of control cells (+LIF) (n=185), PD 3h (n=209) and PD 24h (n=232) treated cells, and EKAREV-TA expressing cells (n=209). Scale bars = 30$\mu$m (C) Boxplot of FRET ratio values for each condition. FRET ratio values were compared against control (+LIF) using an unpaired Student's t-test and found to be significantly different.*** signifies p$\leq$0.001

values of EKAREV-TA expressing cells compared to EKAREV-NLS expressing ES cells (P$\leq$0.001) (Figure 3.10C). These results suggest that the FRET ratio values detected are caused by phosphorylation of the EKAREV biosensor, as loss of this phosphorylation site resulted in a decreased FRET efficiency.

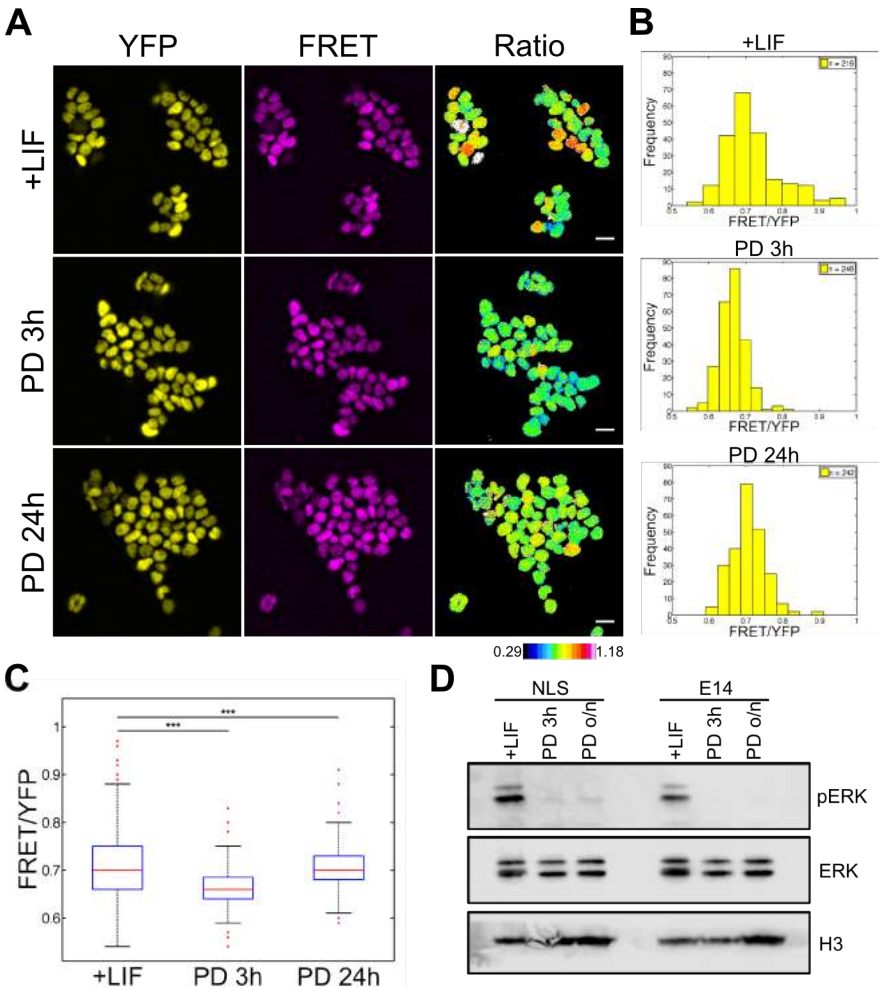


**Figure 3.11: Western blot corroborates that treatment with a MEK inhibitor causes a loss in FRET signal.** (A) YFP channel, FRET channel and ratiometric images of ES cells in serum/LIF (+LIF), treated with 10$\mu$M of PD for 3h (PD 3h) or 24h (PD 24h) prior to imaging. (B) Quantification of FRET ratio values of individual cells over 5 FOV for all 3 conditions. scale bars = 20$\mu$m (C) Boxplot of FRET ratio values measured in +LIF, PD 3h, and PD 24h and FRET ratio values were found to be significantly different compared to control (+LIF) using an unpaired Student's t-test. *** signifies p$\leq$0.001. (D) ES cells expressing EKAREV-NLS (NLS) and wild-type ES cells (E14) were simultaneously treated with PD (10$\mu$M) for 3h or 24h, or left untreated as a control (+LIF). Western blots were performed with anti-phospho-ERK, anti-ERK and anti-H3 antibodies. pERK levels decreased following 3h and 24h treatment with a MEK inhibitor in E14 and EKAREV-NLS expressing cells

To investigate the potency of our MEK inhibitor and the specificity of the biosensor, I decided to repeat the experiment carrying out a western blot in parallel. A western blot was also carried out on wild-type ES cells (E14) to ensure expression of the biosensor was not impeding ERK activity responses. Cells were cultured in serum/LIF, as before, and treated with a MEK inhibitor for 3h or 24h prior to imaging. 5 FOV were captured for each condition and ratiometric images were generated using the imageJ plugin RatioPLUS. A drop in FRET signal could be observed following 3h PD treatment, exhibited by the negative shift in the mean FRET ratio values measured (Figure3.11B). A negative shift in FRET ratio values was also identified following 24h PD treatment (Figure 3.11B). In agreement with previous data, the overall decrease in FRET signal was not as strong compared to cells treated for 3h, and high FRET ratio values appeared more similar to untreated cells (Figure 3.11A and B). A significant decrease in ERK activity following 3h MEK inhibition could also be detected by western blot, demonstrating that loss in FRET signal is the result of decreasing ERK activity (Figure 3.11D). A significant decrease in pERK levels could also be observed following 24h PD treatment, implying that ERK activity is much lower than the ratiometric FRET data would suggest (Figure 3.11D). From Figure 3.11A we can see that only a small portion of 24h PD treated cells displayed high levels of ERK activity which could be masked by population averages, and ERK activity may appear lower as a result. Nevertheless, we can not rule out the possibility that increases in FRET ratio could be caused by the EKAREV cross reacting with other signalling components, and this possibility should be considered when carrying out further FRET analysis.

To determine the dynamic range in which changes in FRET can be measured it is important to generate positive and negative controls (Komatsu et al., 2011). Using the EKAREV-TA expressing ES cell line and a MAPK pathway inhibitor as negative controls, I have been able to establish a lower FRET limit of the EKAREV biosensor. To establish the upper FRET limit of EKAREV expressing ES cells I employed a phosphatase inhibitor known as okadaic acid (OD) that has been used previously to establish the range of the EKAR FRET biosensor in fibroblasts

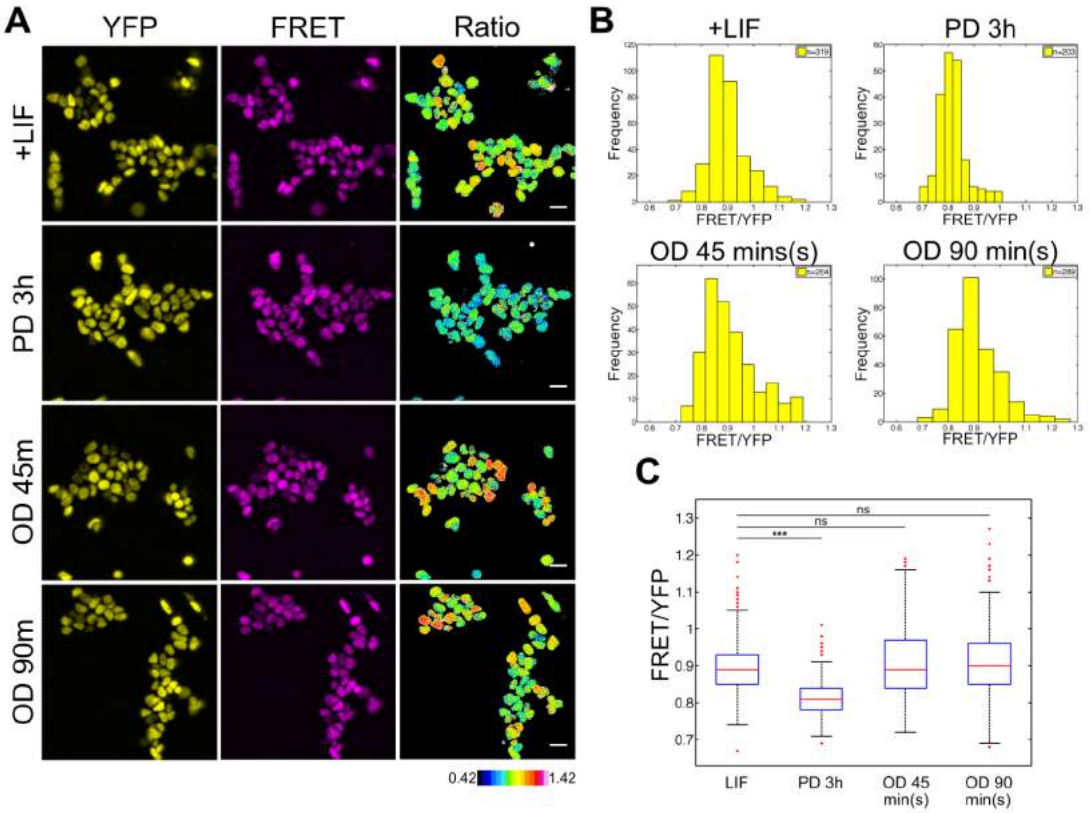


**Figure 3.12: Phosphatase inhibition has a negligible affect on FRET ratio levels.** (A) ES cells expressing EKAREV were treated with a MEK inhibitor (10$\mu$M) for 3h (PD 3h), or treated with a phosphatase inhibitor (20nM) (Okadaic Acid) for 45m (OD 45 min(s)) and 90m (OD 90 min(s)) prior to imaging or left untreated in serum/LIF as a control (+LIF). A YFP channel, FRET channel and ratiometric image were acquired for each condition over 5 FOV. scale bars = 20$\mu$m (B) mean FRET ratio values of individual cells were measured for each condition. +LIF (n=319), PD 3h (n=203), OD 45 min(s) (n=264), OD 90 min(s) (n=289) (D) Boxplot of FRET ratio values for control (+LIF), 3h PD treated (PD 3h), and 45 min(s) and 90 min(s) OD treated cells. FRET ratio values were compared against control(+LIF) using an unpaired Student's t-test. *** = $p \leq 0.001$, **ns** = $p > 0.05$

(Ahmed et al., 2014). Cells were treated with 20nM of OD for 45 min(s) and 90 min(s) prior to imaging, or with a MEK inhibitor for 3h to act as negative control. A YFP channel and FRET channel image were acquired over 5 FOV for each inhibitor treatment, and ratiometric FRET analysis was carried out in imageJ. A statistically significant decrease in FRET ratio values was observed following inhibition with 3h PD treatment, as had been shown previously (Figure 3.12B and C). Cells treated with OD for 45 min(s) and 90 min(s) displayed a range of FRET ratio values,

and FRET ratio levels appeared higher in a small portion of cells compared to non-treated (Fig 3.12A). Quantification analysis, however, revealed no significant difference in the FRET ratio values of OD treated cells compared to non-treated (+LIF) cells (Figure 3.12C). A western blot carried out in parallel identified a small increase in pERK levels following 90 min(s) OD treatment in both EKAREV expressing ES cells (NLS) and wild-type ES cells (E14) (Figure 3.13). However, an increase in pERK levels could not be detected in the EKAREV expressing cells following 45m OD treatment (Figure 3.13). It is important to note that okadaic acid blocks the function of multiple phosphatases and is not specific to phospatases of the MAPK pathway. Consequently, negative feedback from phosphatases is still likely to be occurring and changes in ERK activity levels caused by OD treatment may be too small to be detected by ratiometric FRET. A more specific phosphatase inhibitor should be used in future, to produce a stronger change in ERK activity.

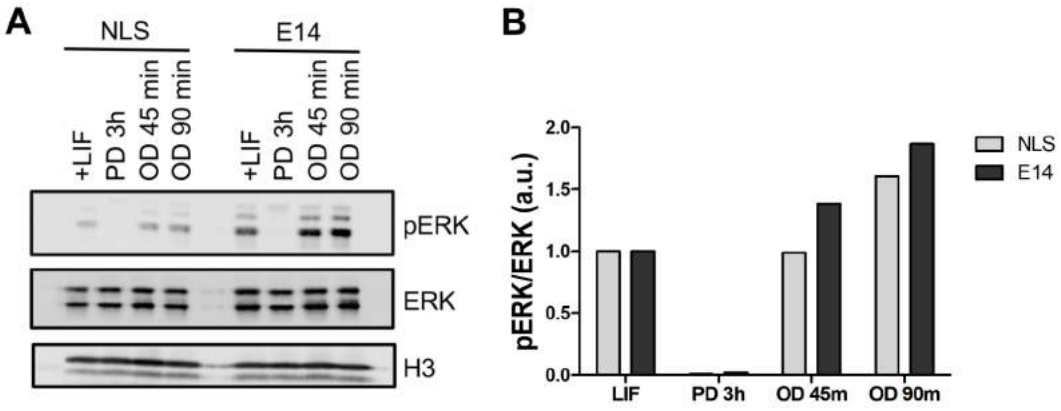


**Figure 3.13: Western blot reveals phosphatase inhibition to have a weak affect on pERK levels.** (A) Western blots were performed with anti-phospho-ERK, anti-ERK and anti-H3 antibodies on ES cells expressing EKAREV-NLS (NLS) and wild-type ES cells (E14). Cells were treated with a MEK inhibitor (10$\mu$M) for 3h (PD 3h), or with 20nM of a phosphatase inhibitor (Okadaic Acid) (OD) for 45 min(s) and 90 min(s) (n=1) (B) Quantification of bands from (a). Active ERK levels were determined by the ratio of pERK/ERK and data are presented relative to +LIF control levels

A reduction in FRET ratio values following the blockage of the MAPK pathway with a MEK inhibitor has been highly reproducible, especially following 3h treatment. In addition, by using a mutated biosensor I have shown that the

FRET signal being detected is dependant on the phosphorylation of the EKAREV biosensor. Collectively, these results support the suitability of the EKAREV biosensor as a method for measuring ERK activity in ES cells.

### 3.4.5 EKAREV reliably reports on changes in ERK activity with changing culture conditions

Hitherto I have shown, using the EKAREV biosensor, ERK activity of ES cells to be highly heterogeneous under serum/LIF culture conditions (Figure 3.9). As previously mentioned ES cells can also be cultured in the presence of 2i, which is comprised of a MEK and GSK3 inhibitor that suppresses MEK and promotes the Wnt pathway respectively, and inhibition of these two pathways maintains the ES cells in a state of naïve pluripotency (Ying et al., 2008). I therefore wanted to determine how changing between 2i/LIF and serum/LIF ES cell culture conditions affected ERK activity.

ES cells expressing the EKAREV bisosensor were cultured in 2i/LIF for a minimum of 2 passages and 2i was removed from the media 3h, 6h and 24h prior to imaging. FRET ratiometric images were acquired as before over 5 FOV and FRET ratio values were quantified in imageJ. At 0h FRET ratio levels appear low, due to the presence of 2i which contains an inhibitor of the MAPK pathway (Figure 3.14A). Quantification identified a statistically significant ($P \leq 0.001$) increase in ERK activity 3h after the removal of 2i, which could still be detected at 6h (Figure 3.14A and B). By 24h FRET ratio values had decreased to similar levels as seen under serum/LIF culture conditions and ERK activity appeared heterogeneous within a population (Figure 3.14A and B).

As well as the MEK inhibitor PD, 2i also contains a highly selective inhibitor of GSK3, which is a signalling component of the Wnt pathway (Ying et al., 2008). To test that the changes in FRET signal that had been observed were a consequence of loss of MAPK pathway inhibition, the experiment was repeated removing either PD only or the GSK3 inhibitor (GSK3i) from the culture composition. PD only removal caused an increase in FRET ratio values at 3h, which decreased at 6h and

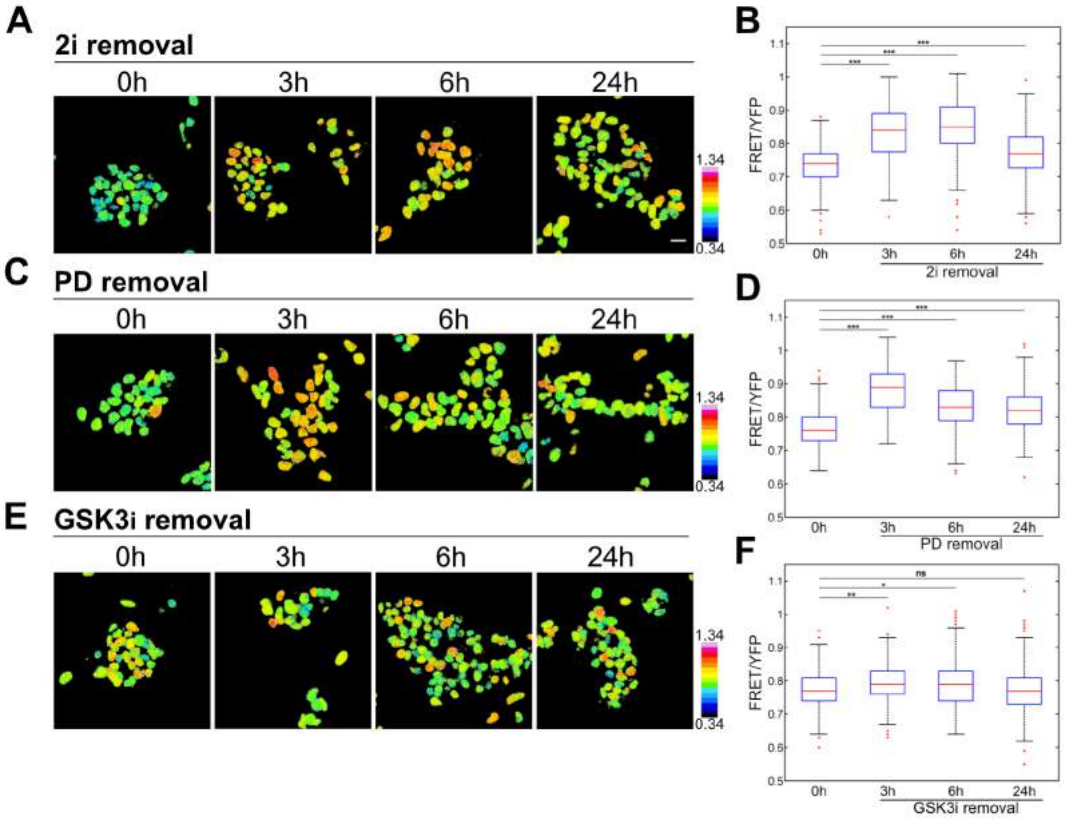


**Figure 3.14: EKAREV reliably reports on changes in ERK activity with changing culture conditions.** ES cells expressing the EKAREV biosensor were cultured in 2i/LIF and media composition was changed by either removing 2i (A and B), removing PD only (C and D), or removal of GSK3i (E and F). FRET images were taken at 0h, 3h, 6h and 24h after the removal of the inhibitor(s) and the 3 experiments were carried out in parallel. 5 FOV were taken at every time-point for each experiment and FRET ratio values of individual cells were quantified and represented in boxplots (B, D and F). FRET ratio values were compared against 0h for each experiment using an unpaired Student's t-test. *** = $p \leq 0.001$, ** = $p \leq 0.01$, * = $p \leq 0.05$, **ns** = $p > 0.05$

returned to similar levels as seen in serum/LIF culture conditions by 24h (Figure 3.14C and D). Conversely, cells cultured in the presence of the GSK3i in the absence of PD, exhibited FRET ratio levels similar to serum/LIF culture conditions, due to the MAPK pathway no longer being repressed (Figure 3.14E). Figure 3.14E suggests that removal of GSK3 inhibition had no affect on FRET ratio values with FRET ratios appearing relatively similar at 3h, 6h and 24h after the removal of GSK3i. However, quantification of FRET ratios identified a statistically significant

increase in ERK activity 3h and 6h after the removal of GSK3 inhibition (Figure 3.14F). The natural heterogeneous nature of ERK activity in ES cells is likely to cause variation in ERK behaviour between sample populations and a statistically significant difference is likely to be observed even in the absence of perturbations to the ERK signalling pathway. Additionally, this slight increase in ERK activity could be the result of changing media and the addition of fresh serum increasing activation of the MAPK pathway. Although a statistically significant increase in ERK activity has been identified, this change was not as significant as the increase observed following the removal of 2i and PD only (Figure 3.14B and D).

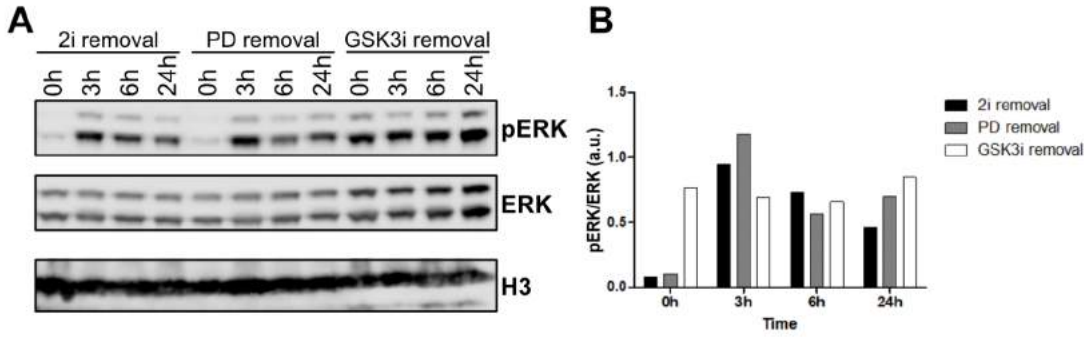


**Figure 3.15: Western blot corroborates changes in ERK activity identified by FRET.** (A) Western blots were performed using a anti p-ERK, anti-ERK and anti-H3 antibody on ES cells expressing EKAREV-NLS. Cells were harvested at 0h, 3h, 6h and 24h following the removal of 2i, PD only, and GSK3i (n=1) (B) Quantification of bands from (a)

A western blot was carried out in parallel to determine whether changes in pERK levels reflected the change in ERK activity that had been seen by FRET ratio analysis (Figure 3.15). An increase in pERK can be seen following the removal of 2i, and PD only, at 3h and 6h (Figure 3.15). However, an increase in pERK levels was not detected following the removal of GSK3 inhibition, and pERK levels remained relatively constant (Figure 3.15). From these data it would appear that changes in FRET ratio levels observed by the removal of 2i were caused by the loss of MEK inhibition rather than any other possible changes in media composition. These results further corroborate the specificity of the EKAREV biosensor as a reporter of ERK activity in ES cells.

### 3.4.6 Using the EKAREV reporter to identify distinct ERK activity dynamics

Thus far I have used the EKAREV FRET biosensor to look at ERK activity of ES cells at single snap shots in time and have found ERK activity levels to be heterogeneous under serum/LIF culture conditions. As well as offering a single cell resolution read outs of ERK activity, the EKAREV biosensor can also be used to follow changes in ERK activity over time. To determine whether distinct ERK activity patterns as well as levels, could be identified, FRET time lapse imaging of ES cells expressing the EKAREV-NLS biosensor was carried out over a 16h period in serum/LIF. A YFP channel and FRET channel image was taken every 20 minutes and ratoimetric images were acquired in imageJ as before. In order to monitor changes in ERK activity, cells were tracked and the FRET ratio value of each cell was quantified at every time-point. FRET tracks were subsequently smoothed to remove experimental noise and facilitate the identification of dynamics behaviours.

Figure 3.16 shows an example of three different ERK activity dynamics that were observed following FRET time-lapse imaging of the EKAREV biosensor. Cell 1 represents FRET levels that are oscillatory throughout the time series, suggesting ERK activation levels can be varied within a cell over time. In contrast, the FRET levels of Cell 2 appear relatively steady suggesting differences in ERK activity behaviour between cells of a population. Ratiometric FRET intensity of Cell 3 is initially high and then decreased, followed by a small increase in FRET later in the time series, thus representing another distinct ERK activity dynamic. From this preliminary FRET time-lapse imaging it appears that not only ERK activity levels but also ERK activity dynamics can be heterogeneous in a ES cell population under serum/LIF culture conditions.

### 3.4.7 Time-lapse imaging identifies a pulse in ERK activity following the removal of 2i

Hitherto I have shown that removal of MEK inhibition causes an increase in ERK activity at 3h returning to levels similar to those observed under serum/LIF culture conditions by 24h (Figure 3.14). These observations however were obtained from

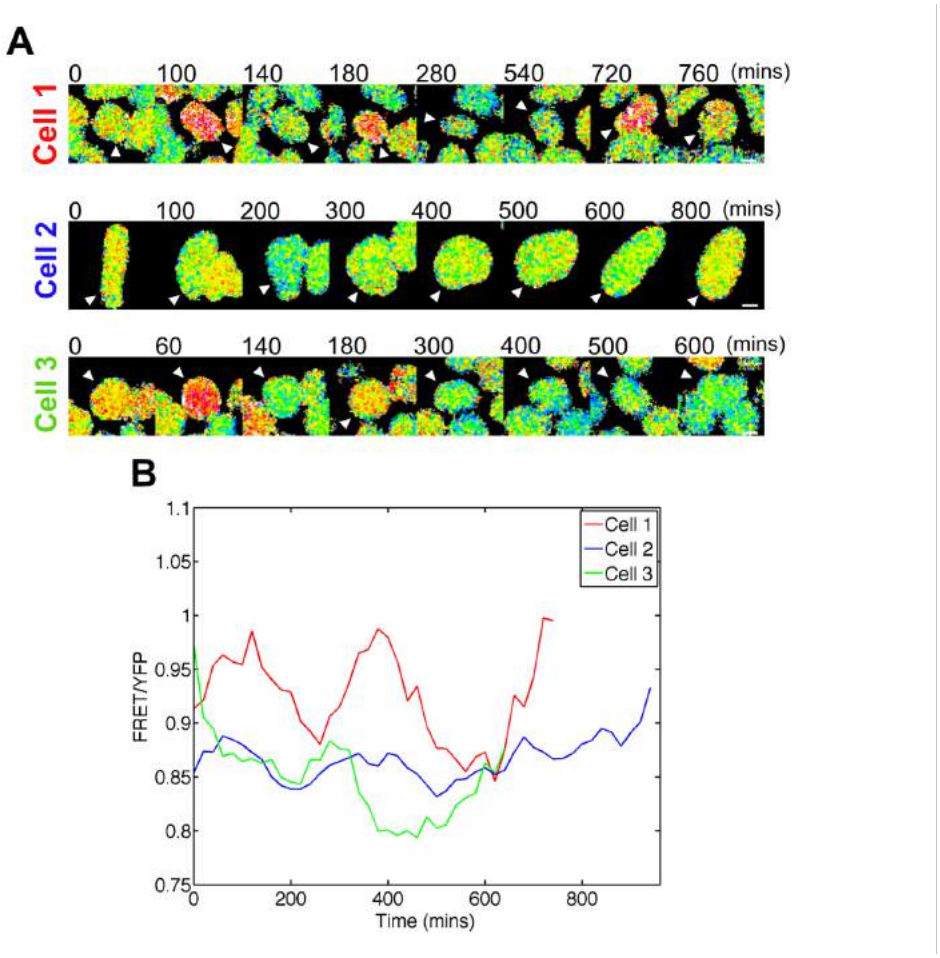


**Figure 3.16: Using the EKAREV reporter to identify distinct ERK activity dynamics.** FRET time-lapse imaging of ES cells expressing EKAREV-NLS in serum/LIF. A YFP and FRET channel image were captured every 20 minutes for 16h and a ratiometric image was acquired in imageJ for each time-point (A) Ratiometric images of individual cells at the indicated time points. White arrows indicate cell of interest. Scale bar = 10$\mu$m (B) FRET ratio levels of cells shown in (a) were quantified and plotted over time. Cell tracks were smoothed using an inbuilt MATLAB function prior to plotting

the study of ERK activity at static points in time and additional dynamic behaviours within this response may have been precluded. I therefore wanted to investigate the dynamics of this response at a much greater time resolution using FRET time-lapse imaging to monitor the ERK activity dynamics of cells following the removal of 2i.

Cells were cultured in the presence of 2i/LIF for a minimum of 2 passages and 2i was removed from the medium. FRET imaging was carried out as stated in Material and Methods with a z-stack image taken every 5 minutes over a 4 hour

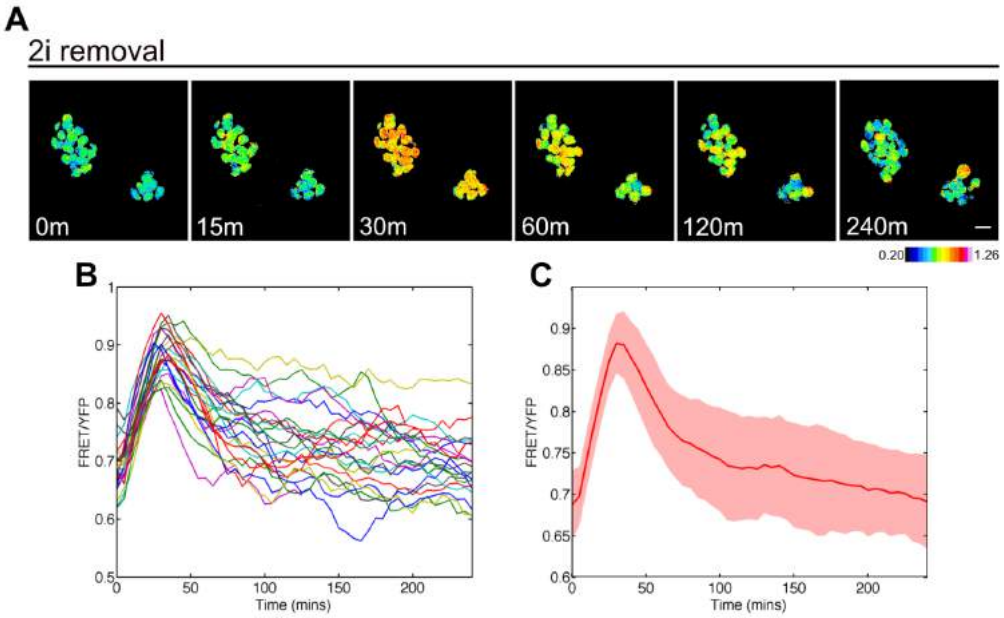


**Figure 3.17: Time-lapse imaging identifies a pulse in ERK activity following the removal of 2i.** (A) ERK activity of ES cells expressing EKAREV-NLS following 2i removal represented by ratiometeric FRET. Scale bar = 30$\mu$m (B) FRET ratio values of each cell in (a) were quantified over time as described in Materials and Methods. Tracks were smoothed prior to plotting using an inbuilt MATLAB function (n=23) (C) Red line represents the mean FRET ratio of all cells shown in (a). Shaded area specifies the region between the standard deviation of the mean

period. From time-lapse imaging I was able to identify an immediate increase in FRET signal following the removal of 2i, occurring within the first 5-10 minutes, which then decreased slowly over time (Figure 3.17A). To investigate changes in the FRET signal further, each cell was tracked and its FRET ratio value was quantified at every frame. Quantification showed a rapid increase in FRET signal following the removal of 2i, that appeared relatively homogeneous within the population (Figure 3.17B and C). FRET ratio levels peaked around 40 minutes and as FRET signal decreased FRET ratio values became more heterogeneous, represented by an increase in the standard error of FRET signal detected (Figure 3.17C).

To test whether this peak in FRET signal following 2i removal was caused by a loss in MAPK pathway inhibition, the experiment was repeated with the addition of a control. For the control 2i/LIF media was changed as before, however the

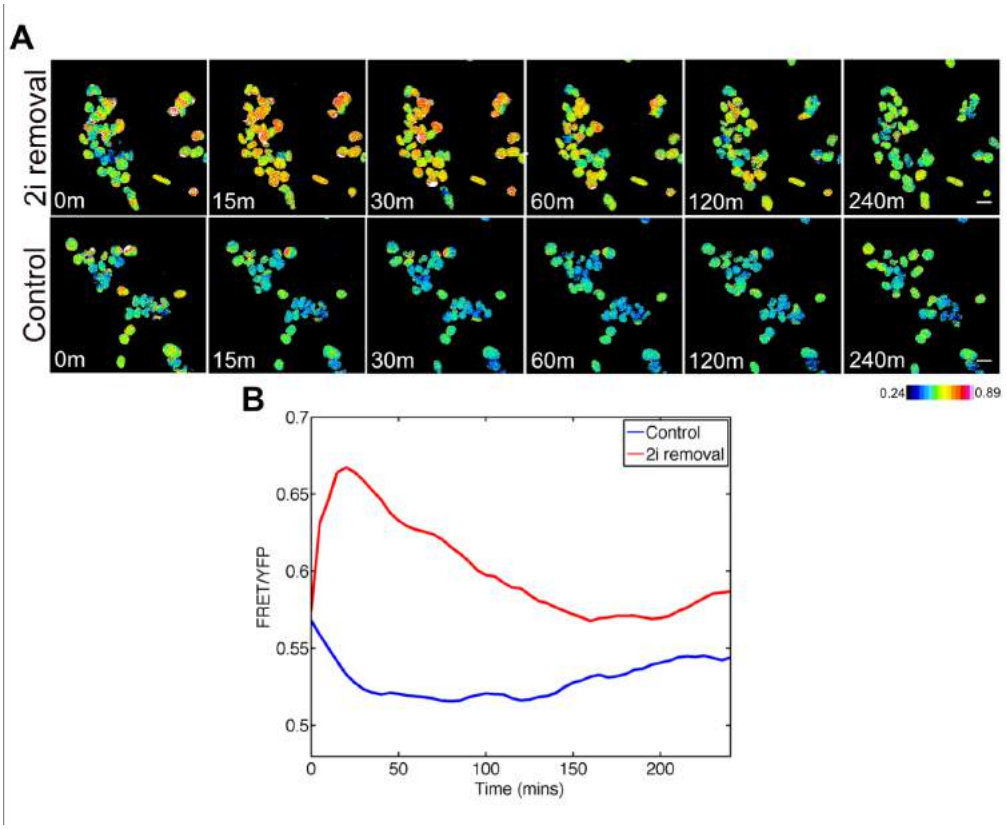


**Figure 3.18: Release from 2i causes pulse in ERK activity.** (A) Ratiometric FRET images of ES cells expressing EKAREV-NLS at indicated time-points after media was changed to either serum/LIF (2i removal) or serum+LIF supplemented with 2i (control). Scale bars = 30$\mu$m (B) Mean FRET ratio of all cells shown in (a) for 2i removal (red) and continued 2i supplementation control (blue)

media was replaced with the same 2i/LIF media to maintain the suppression of ERK activity. A rapid increase in FRET signal was once again observed following the removal of 2i, and a peak in FRET signal could be detected at around 40 minutes (Figure 3.18A and B). FRET time-lapse imaging was unable to identify a peak in FRET signal following the maintained suppression of ERK signalling under control conditions (Figure 3.18A and B). This would suggest that this peak in FRET signal was caused by the removal of 2i and is thus representative of changing ERK activity. Moreover, this further substantiates that the EKAREV biosensor is able to reliably report on the ERK activity dynamics of ES cells.

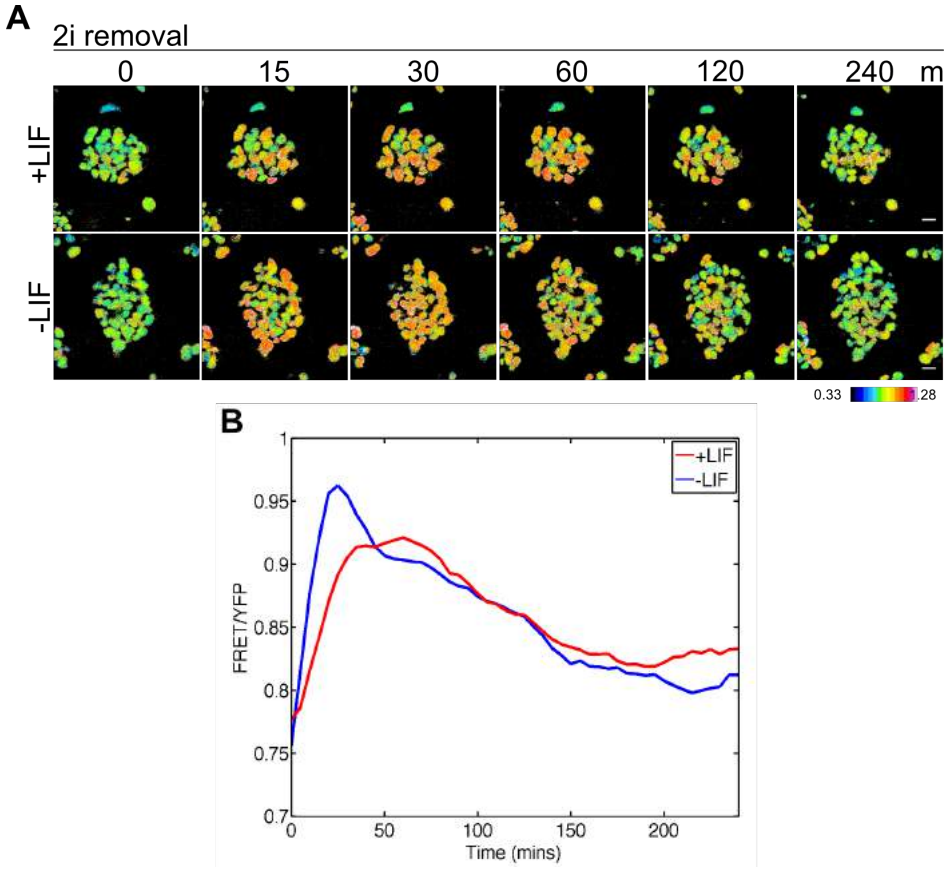


**Figure 3.19: Release from 2i in the presence and absence of LIF** (A) Ratiometric FRET images of ES cells after media was changed from 2i/LIF to media supplemented with LIF (+LIF) or to media free from 2i and LIF (-LIF). scale bars = 30$\mu$m (B) mean FRET ratio of cells shown in (a) over time. +LIF = red and -LIF = blue (n=1)

Differentiation of ES cells is induced by the removal of 2i, however the presence of LIF is predicted to delay the onset of differentiation (Dunn et al., 2014). To assess whether removal of LIF simultaneously with 2i affects this pulse in ERK activity, cells were cultured in 2i/LIF and media was changed to either media free from 2i and LIF (-LIF) or media free from 2i but still supplemented with LIF (+LIF). A pulse in ERK activity was observed following the release from 2i in the presence and absence of LIF (Figure 3.19A and B). Figure 3.19B shows removal of LIF simultaneously with 2i resulted in a slightly increased peak of ERK activity compared to removal of 2i only. However, the rate of decline of ERK activity appeared similar for both 2i only removal and removal of 2i and LIF (Figure 3.19B). A western blot was carried out in parallel and an increase in pERK

levels could be observed following the removal of 2i in the absence and presence of LIF (Figure 3.20A). Quantification of pERK levels identified a pulse in ERK activity that is representative of the changes in ERK activity shown by ratiometric FRET (Figure 3.20A). However, a substantial difference in the peak levels of ERK activity following the removal of 2i with (-LIF) or without LIF (+LIF) could not be identified. A pulse in ERK activity was also detected by immunofluorescence (Figure 3.20B), as well as western blot, further validating this ERK behavioural response (Figure 3.20C). Collectively, these findings are consistent with previous work that has shown ERK activity to increase rapidly following release from 2i, with cells exhibiting a similar temporal pattern of activation to the data I have shown here (Yang et al., 2012; Nett et al., 2018).

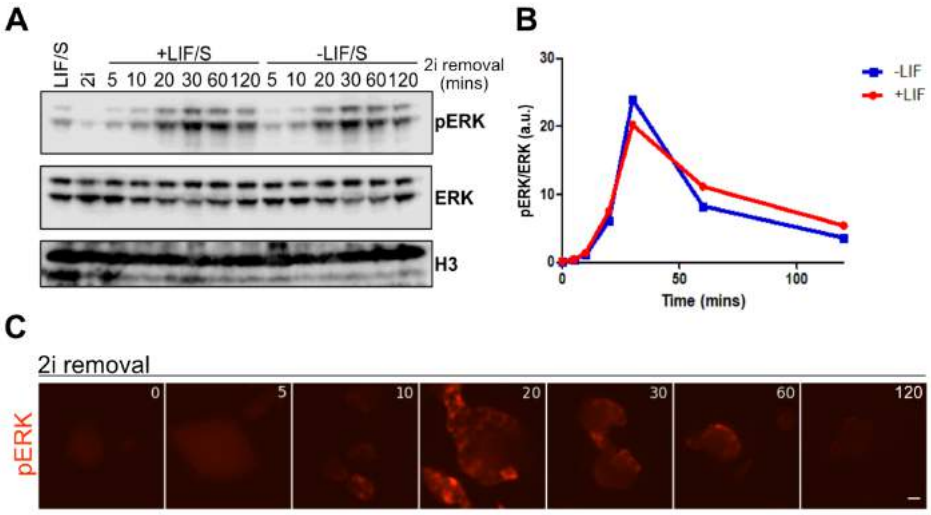


**Figure 3.20: A pulse in ERK activity following release from 2i is supported by western blot and immunofluorescence.** (A) Immunoblot for pERK and ERK from ES cells expressing EKAREV after media was changed from 2i/LIF to media supplemented with LIF (+LIF) or media free from LIF and 2i (-LIF). Cells were harvested at the indicated time points after media was changed and anti-H3 was used as a loading control (n=1) (B) Quantification of bands in (a). Removal of LIF with 2i (-LIF) = blue and continued LIF supplementation after 2i removal (+LIF) = red (C) Immunofluorescence of wild-type ES cells (E14 cells). Cells were cultured in 2i/LIF and were immunostained for pERK (red) following removal of 2i at the indicated time-points (n=1). Scale bar = 30$\mu$m

## 3.5 Summary

In this chapter I have used the reporter lines TNGA (Chambers et al., 2007) and OCRG9 (Toyooka et al., 2008) to examine the relationship between ERK activity and expression of pluripotency factors Nanog and Rex1. A strong relationship between the levels of pERK and expression of either reporter could not be identified using single cell quantification tools (Figure 3.1 and 3.2). pERK immunostaining also identified a significant decrease in pERK levels following the removal of LIF (Figure 3.3) and a similar response could also be seen by western blot (Figure 3.4).

In order to investigate ERK activity at a greater time resolution a FRET based biosensor was employed that has been used to reliably report on spatial and temporal regulation of ERK in other systems. Visualisation of FRET signals using the methodology I had established showed FRET levels between ES cells expressing the EKAREV biosensor to be highly variable implying that ERK activity is heterogeneous under serum/LIF culture conditions (Figure 3.9). This was further substantiated by a series of control experiments using inhibitors of the MAPK pathway and a FRET-null reporter, that showed FRET ratio levels to reliably report on changes in ERK activity of ES cells (Figures 3.11, 3.10, and 3.12). Furthermore, time-lapse imaging identified distinct ERK activity patterns in individual ES cells under serum/LIF culture conditions, indicating ERK activation kinetics, as well as levels, to be heterogeneous across a population (Figure 3.16).

An examination into the affects of changing culture conditions identified a rapid increase in ERK activity following the release from 2i, followed by a steady decline in activity (Figure 3.17). This pulse in ERK activity appeared highly robust among multiple experiments, and could be detected by other experimental techniques (Figure 3.20). Removal of 2i and LIF allows ES cell to exit self-renewal and enter lineage commitment. This pulse in ERK activity following release from 2i/LIF could therefore play an important role in the rate of exit from pluripotency and the future fate choice of a cell. Previous work has shown that manipulation of this pulse in ERK activity to alter the expression of lineage and pluripotency markers (Yang

et al., 2012). Release from 2i induces an overall uniform response in ERK activity, however dynamics of this response such as amplitude and falling rate were variable between cells (Figure 3.17B).

# Chapter 4

# Investigating the dynamics of ERK activity in relation to pluripotency

## 4.1 Introduction

Exit from pluripotency is an asynchronous process and the temporal kinetics of down and up regulation of factors involved in this transition varies between cells (Kalkan et al., 2017). ERK signalling is required for progression out of naïve pluripotent state, however I was unable to identify a correlation between levels of pERK1/2 and the expression of pluripotency markers, Nanog and Rex1, at the single cell level. Previous studies of ERK signalling in other systems, have shown that differences in the level and timing of ERK activation can result in different cellular responses (Marshall, 1995; Santos et al., 2007; Albeck et al., 2013; Aoki et al., 2013; Schröter et al., 2015). Therefore, differences in ERK activity profiles of ES cells following exit from pluripotency could be driving this asynchronous ES cell transition.

In the previous chapter I have shown that using a FRET based biosensor, EKAREV, it is possible to follow the ERK dynamics of ES cells at the single cell level, and I have established a methodology for imaging, tracking and quantifying the FRET ratio values of individual cells over time. Utilising this method I have shown

induction of ES cell differentiation, by release from 2i/LIF, causes a pulse in ERK activity across the entire population (Figure 3.17). This ERK activation response during the onset of differentiation has been shown in ES cells previously by other experimental methods (Yang et al., 2012; Nett et al., 2018). However, these methods have relied on population averages, which mask variation between cells. Our methodology offers a tool in which to measure the ERK dynamics of individual ES cells as they transition from naïve pluripotency towards lineage commitment, and determining the functional consequences of these dynamics on the asynchronous exit from pluripotency could provide novel insights into the molecular mechanisms of pluripotency and differentiation.

In this chapter I will describe the development of our method for studying ERK activity in ES cells and the different analysis tools that can be applied to examine the dynamics of ERK activity following 2i/LIF withdrawal. I will also demonstrate how the ERK dynamics identified by FRET time-lapse imaging can be compared to the pluripotent state of a cell, and will discuss different dynamics that I have observed. Finally, I will examine the cell-cell variability of different dynamic features of the activation kinetics of ERK following exit from pluripotency, and will compare these features to the expression of Nanog.

## 4.2 Identification of a marker of pluripotency for comparison against ERK activity

In order to identify an appropriate factor to compare ERK activity dynamics against, I wanted to assess the expression dynamics of different pluripotency markers in our EKAREV-NLS expressing ES cell line. To monitor changes during the early stages of ES cell differentiation cells were cultured in 2i/LIF, supplemented with serum, for a minimum of 2 passages and plated on to gelatin coated dishes 24h prior to the withdrawal of 2i/LIF. Cells were immunostained for Nanog, Sox2 or Esrrb, at 0h, 9h, 24h and 48h following release from 2i/LIF and fluorescent intensities of individual cells were quantified using a custom built MATLAB software created by

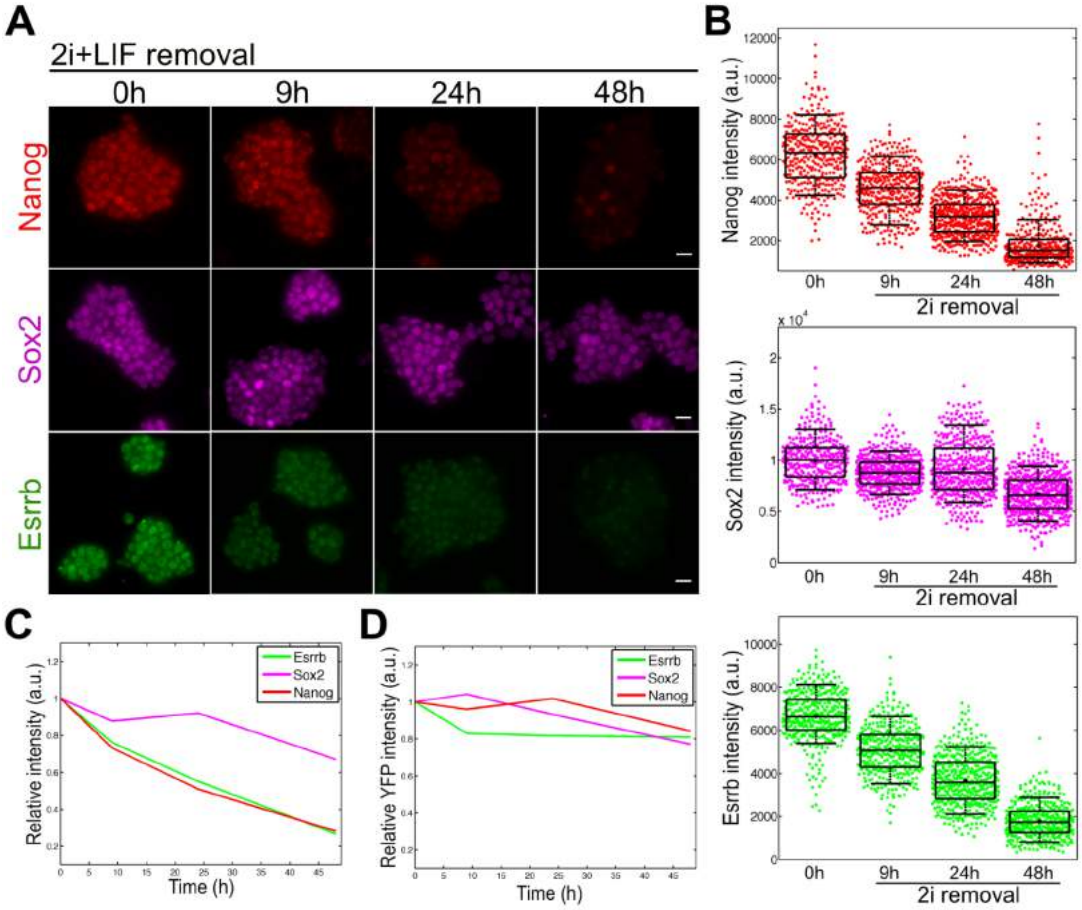


**Figure 4.1: Identifying a marker of pluripotency for comparison against ERK activity.** (A) EKAREV-NLS expressing ES cells were immunostained for Nanog (red), Sox2 (magenta), and Esrrb (green) following the removal of 2i/LIF at indicated time-points. Scale bar = 20$\mu$m (B) Measured fluorescent intensities of Nanog (red), Sox2 (magenta), and Esrrb (green) at each time point from individual cells over 5 FOV with box-plots overlaid (C) Average relative intensity of Nanog (red), Sox2 (magenta), Esrrb (green) following withdrawal from 2i/LIF in relation to the expression of each marker at 0h. (D) Relative intensity of YFP expression after immunostaining following 2i/LIF withdrawal in relation to YFP expression at 0h.

a post-doc in the lab (Adam Corrigan). In brief, cell positions were recorded using a mouse click to generate a coordinate for each cell. Intensities were then extracted by calculating the median pixel intensity in cylinders of 5x5x3 voxels centred around each of these manually selected coordinates, which should be representative of the levels for immunostained protein within each cell.

All three pluripotency factors were highly expressed at 0h and expression levels appeared relatively uniform across the population (Figure 4.1A). A clear decrease in expression of both Nanog and Esrrb was evident 9h after the release from 2i/LIF, with expression continuing to decline 24h and 48h post 2i/LIF removal (Figure 4.1A and B). In contrast, expression of the core pluripotency factor Sox2 remained largely unchanged following 2i/LIF withdrawal, and a small decrease in expression could only be detected at 48h (Figure 4.1A and B). The delayed down-regulation of Sox2 is in accordance with previous finding that have shown Sox2, alongside Oct4, to be indispensable to the maintenance of pluripotency resulting in their maintained expression during the dismantling of the naïve pluripotency network (Ivanova et al., 2006; Dunn et al., 2014). A YFP intensity could also be extracted from each selected coordinate due to the presence of the EKAREV-NLS biosensor. Figure 4.1D shows YFP intensities remained relatively unchanged following the withdrawal of 2i/LIF demonstrating that differences in the expression of markers detected is representative of changing protein levels and is independent of the expression of the ERKAREV biosensor. Moreover, a signal could not be detected following secondary only staining of the EKAREV-NLS cell lines verifying the specificity of our immunostaining.

The early detectable decrease in Esrrb and Nanog following withdrawal of 2i/LIF, makes both markers useful candidates for comparison against ERK activity dynamics as cells exit from pluripotency. Relative intensity measurements of all three markers, at each time point in relation to 0h, would suggest that Essrb and Nanog expression are down-regulated at similar rates (Figure 4.1C). In accordance with previous findings I have also observed variability in Nanog and Esrrb expression levels following release from 2i/LIF (Chambers et al., 2007; van den Berg et al., 2008). Quantification of cell-cell variability using the coefficient of variation (CV), defined by the ratio of the standard deviation to the mean ($CV = \frac{\sigma}{\mu}$), showed Nanog expression to be more variable at 24h (CV = 0.32) and 48h (CV = 0.55) than Esrrb expression (CV = 0.29 and CV = 0.43 for 24h and 48h respectively). The increased cell-cell variability of Nanog expression provides

a greater range of expression levels in which to compare different ERK activity dynamics against. Consequently, expression levels of Nanog were chosen to act as a functional determinant of different ERK activity dynamics for future assays.

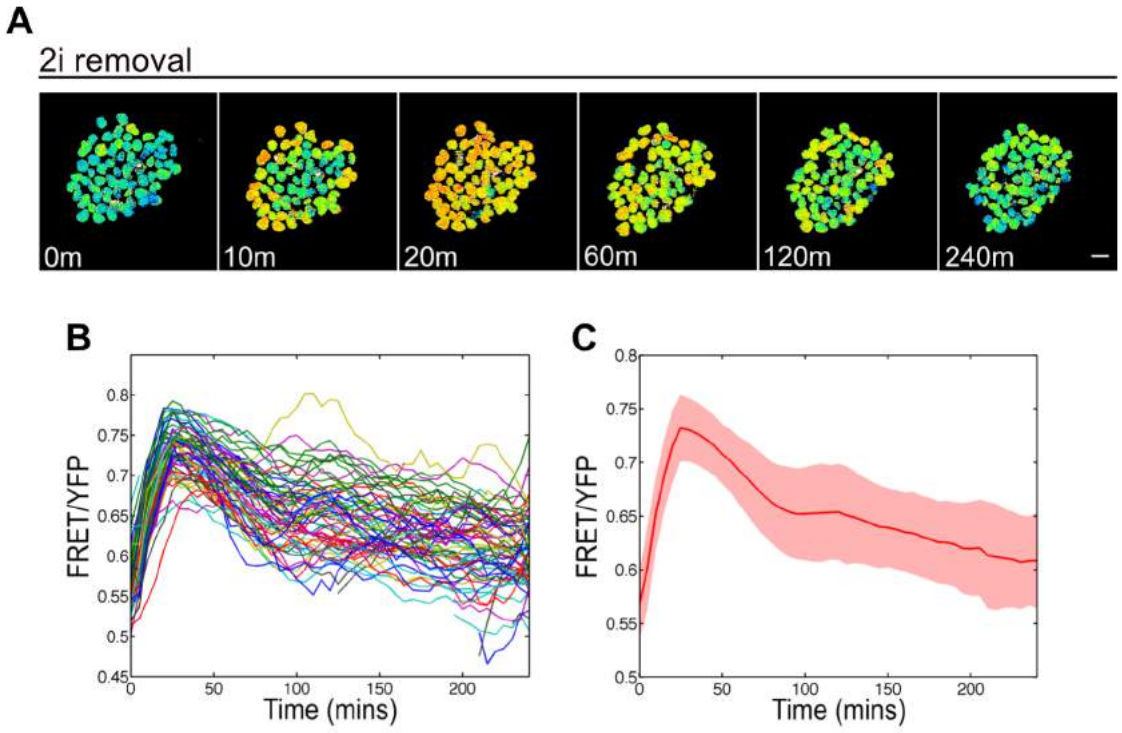


**Figure 4.2: Testing ERK dynamics of 2i release following plating on Laminin.** (A) Ratiometric FRET images of ES cells expressing EKAREV-NLS plated on laminin coated imaging dishes at indicated time-points following the removal of 2i. Scale bar = 20$\mu$m (B) FRET ratio values of each cell in (a) were quantified over time as described in Materials and Methods. Tracks were smoothed prior to plotting using an inbuilt MATLAB function (C) Red line represents the mean FRET ratio of all cells shown in (a). Shaded area specifies the region between the standard deviation of the mean

Hitherto, all experiments, both in this Chapter and Chapter 3, have been carried out using gelatin-coated dishes. ES cells cultured on gelatin will have a tendency to grow over each other in an overlapping manner, which can make it difficult to distinguish between cells. This will reduce the number of cells that can be comprehensibly tracked and analyzed from each experiment. Cells plated on laminin form more of a monolayer structure, making it easier to identify and track individual cells. Differentiation of ES cells has been carried out on laminin as well

as gelatin previously (Abranches et al., 2014; Kalkan et al., 2017), and laminin coated dishes could therefore be used to study the dynamics of ERK as cells exit pluripotency. In order to test whether laminin could be used in replace of gelatin it was important to ensure that both the ERK activity dynamics I had already observed and the down-regulation kinetics of Nanog expression were not compromised by the use of laminin.

I have already shown that ES cells plated on gelatin-coated dishes display an immediate peak in ERK activity following the removal of 2i (Figure 3.17). To asses whether laminin was having a significant impact on this ERK activity response, ES cells expressing the EKAREV-NLS biosensor were plated on to laminin coated dishes, 2i was withdrawn from the media, and FRET time-lapse imaging was carried out as before. A peak in FRET was detected following release from 2i in all cells, indicating that using Laminin instead of gelatin was not impeding this pulse in ERK activity that had been detected (Figure 4.2). Plating on laminin resulted in a higher number of cells (n=77) that could be tracked compared to plating on gelatin, which resulted in the attainment of roughly 25-30 tracks per FOV. From Figure 4.2A it would appear that cells at the edge of a cell colony experience an increase in ERK activity initially, which then spreads into the more densely populated portions of the colony. However, it is of note that experimental repeats of 2i removal on laminin coated dishes could not always reproduce this positional response (data not shown). How cell density and a cells position within a colony affects ERK activity following 2i/LIF removal will be discussed further in Chapter 5.

To test the expression profile of Nanog, ES cell expressing the EKAREV-NLS biosensor were plated on either laminin or gelatin coated dishes in 2i/LIF, supplemented with serum, 24h prior to 2i/LIF removal. Cells were immunostained for Nanog 0h, 4h, 9h and 12h post release from 2i/LIF, and the fluorescent intensity of each cell was measured as before. Cells plated on gelatin displayed higher levels of Nanog overall which is likely to be the result of combinatorial fluorescent intensities of cells that sit on top of one another (Figure 4.3A and B). Although,

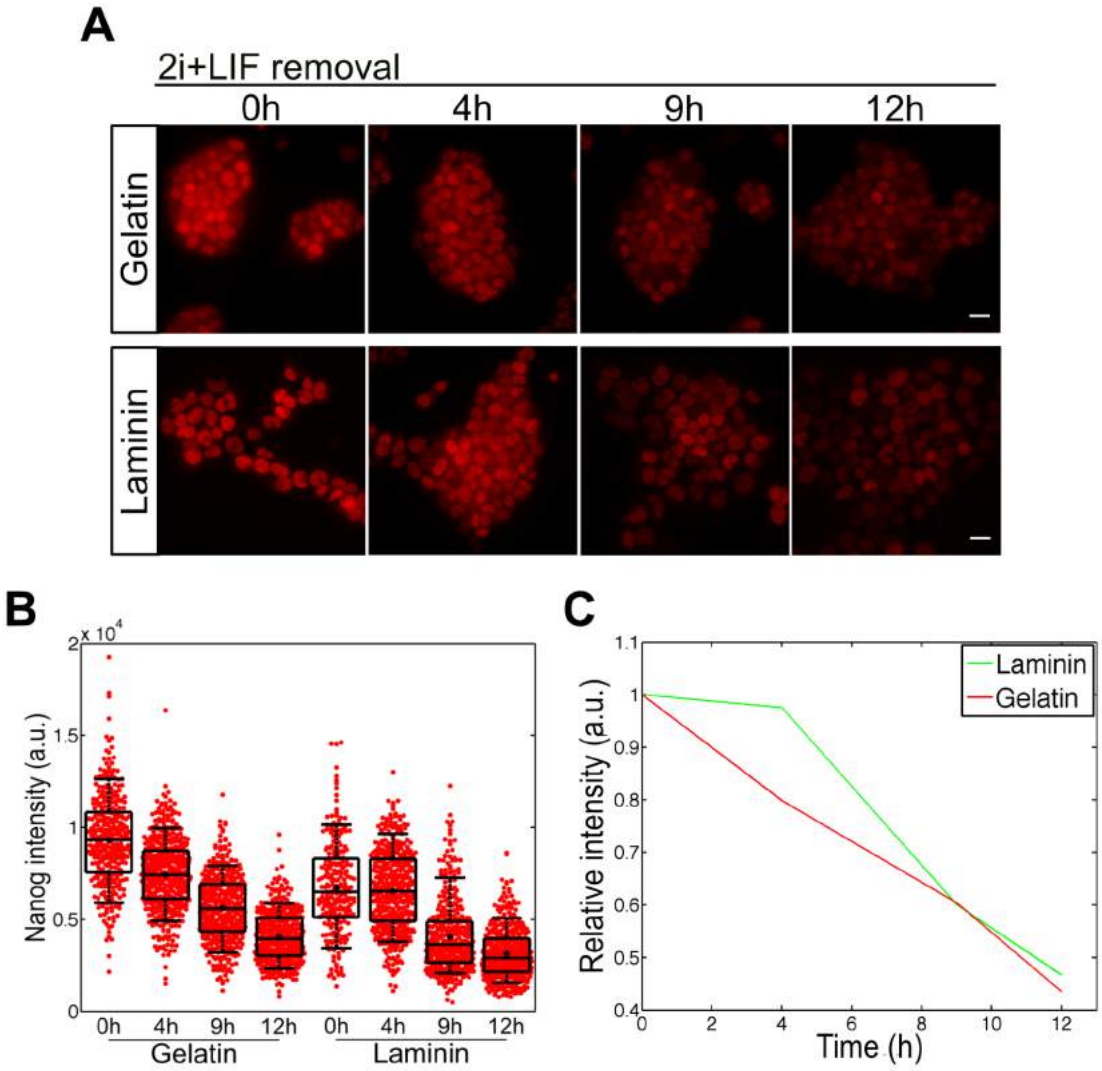


**Figure 4.3: Down-regulation kinetics of Nanog expression are comparable following plating on Laminin or gletain.** (A)ES cells expressing EKAREV-NLS were plated on gelatin or laminin coated imaging dishes and cells were immunostained for Nanog at the time points indicated following the removal of 2i/LIF. Experiments were carried out in parrallel. Scale bar = 20$\mu$m (B) Measured fluorescent intensities of individual cells at each time-point over 5 FOV with box-plots overlaid (C) Mean expression of Nanog following release from 2i/LIF from cells plated on laminin (green) and gelatin (red). Expression levels are shown as relative to the mean Nanog expression at 0h

there is a slight disparity in Nanog expression between the two coating conditions at the early stages of differentiation, the level of decline in Nanog expression appeared relatively equal by 9h (Figure 4.3C). These results suggest that laminin coated dishes provide a viable alternative in which to measure changes in Nanog expression, as well as an optimized imaging condition for measuring changes in ratiometric FRET.

## 4.3 Application of our methodology to monitor ERK signalling dynamics in relation to the expression of Nanog

By combining all experimental methods that discussed so far I have been able to establish a method for linking ERK activity dynamics of individual ES cells to the expression of different pluripotency associated factors, and have applied this method to the study of ERK activity dynamics during the onset of differentiation in relation to the expression of Nanog. Specifically, FRET time-lapse imaging was carried out to monitor the ERK activity of individual cells in the early phase of transition following release from 2i/LIF. Cells were monitored over a 16h period and were immediately fixed and immunostained for Nanog following completion of time-lapse imaging (Figure 4.4A). A 16h period for monitoring changes in ERK activity was chosen as a compromise between the viability of cells following this length of FRET time-lapse imaging and being able to detect noticeable enough differences in the expression levels of Nanog.

Immunofluorescence images were acquired for the same group of cells that had previously been captured during the FRET time-lapse in order to compare the ERK activity dynamics of each cell to its corresponding Nanog intensity post 2i/LIF removal. An example of the ratiometric FRET time-lapse images acquired from a single FOV and the corresponding Nanog immunofluoresence image of the same cell population is shown in Figure 4.4B and Figure 4.4C respectively. This experiment was repeated 3 times and cell tracks were pooled from 4-5 FOV for

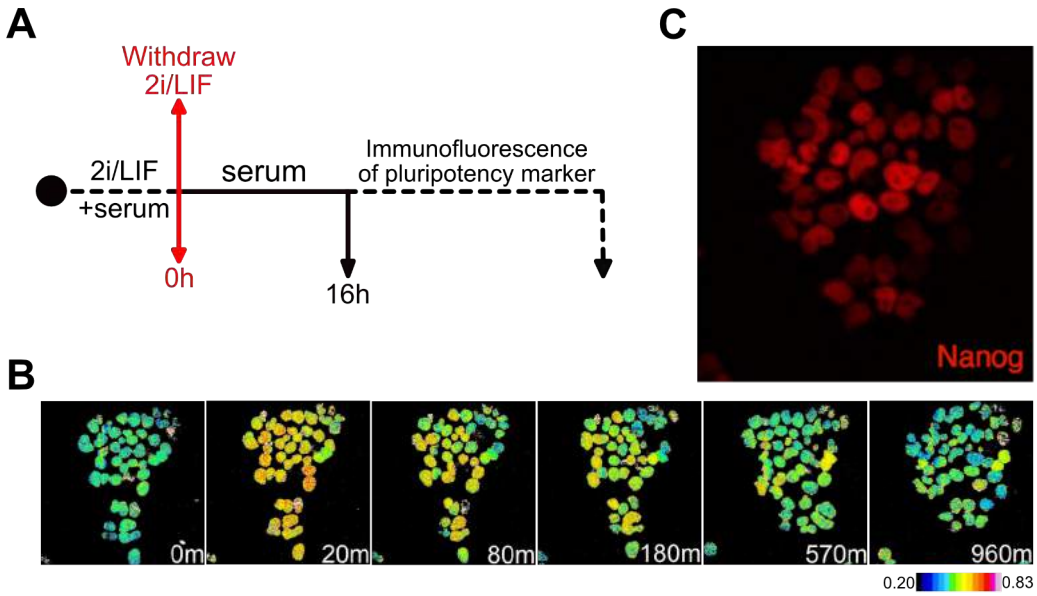


**Figure 4.4: Experimental set-up for tracking ERK dynamics in relation to Nanog expression.** (A) Protocol for following ERK activity dynamics during the early stages of naïve ES cell differentiation by 2i/LIF withdrawal and comparing observed dynamics to expression of pluripotency factors. Figure adapted from (Kalkan et al., 2017) (B) Ratiometric FRET images of ES cells following release from 2i/LIF at time-points indicated. Example of 1 FOV of data from protocol described in (a) (C) Cells from (b) immunostained for Nanog 16h following release from 2i/LIF and subsequent FRET time-lapse imaging

each experiment. Cell tracks from each replicate are shown in Figure 4.5 and the average FRET signal measured from each experiment is shown below.

A pulse in ERK activity was observed in all 3 replicates following the induction of differentiation, with a peak in ERK activity occurring 25 $\pm$ 5m after the removal of 2i/LIF (Figure 4.5). A slight disparity in the rate of decline in ERK activity was observed between experimental replicates following this peak in ERK activation, particularly for replicate 1, which showed a more enhanced gradient of declining activity (Figure 4.5A). In addition, the range of FRET ratio values also differed between experimental replicates, and the FRET ratio values of replicate 1 appear reduced in relation to replicates 2 and 3 (Figure 4.5). Although imaging acquisition settings were kept constant between replicates these experiments were not carried out in parallel thus there is likely to be some biological, as well as experimental

variation between them. The rest of my results will focus on the data I have acquired from these three experiments. I will demonstrate the different analysis tools that can be applied to this data set and will discuss some current findings from the use of these tools.

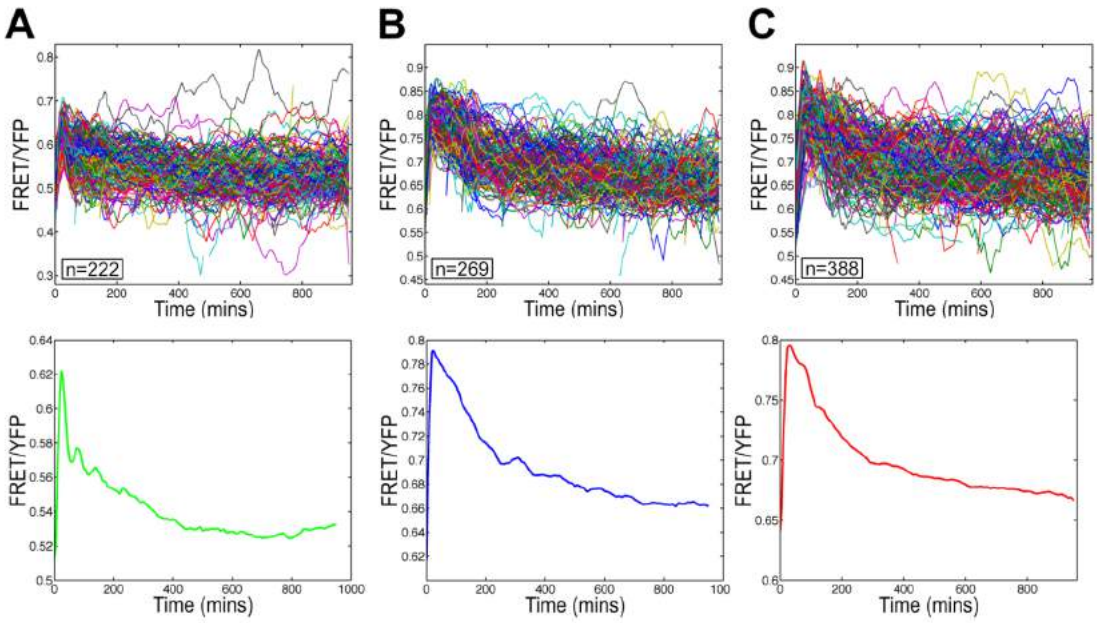


**Figure 4.5: 2i/LIF withdrawal causes a pulse in ERK activity in all experimental replicates.** FRET Ratio values of cells following release from 2i/LIF pooled from 4-5 FOV using protocol described in 4.4A with average mean FRET ratio value of all cells shown below (A) Cell tracks from experiment 1 (green) (n=222) (B) Cell tracks from experiment 2 (blue) (n=269) (C) Cell tracks from experiment 3 (red) (n=388). Colours used here to represent each experimental replicate will be used for all remaining results

## 4.4 Comparing Nanog expression to differences in the activation profile of ERK activity

To determine whether overall ERK activity levels influence Nanog expression at the single cell level, the mean ERK activity of each cell over the 16h time-lapse was plotted against its corresponding Nanog intensity (Figure 4.6). A correlation between mean ERK activity and Nanog intensity levels could not be identified by Pearsons correlation in either experimental replicate (Figure4.6). This result is in broad agreement with previous immunofluorescence data that showed pERK levels

of individual cells to be poorly correlated to the expression of a reporter for Nanog (Figure 3.1). Collectively, these data support the idea that absolute ERK activity levels alone do not influence the expression of Nanog and more information may be in encoded in the dynamics of the ERK activity response of individual cells following induction of differentiation.

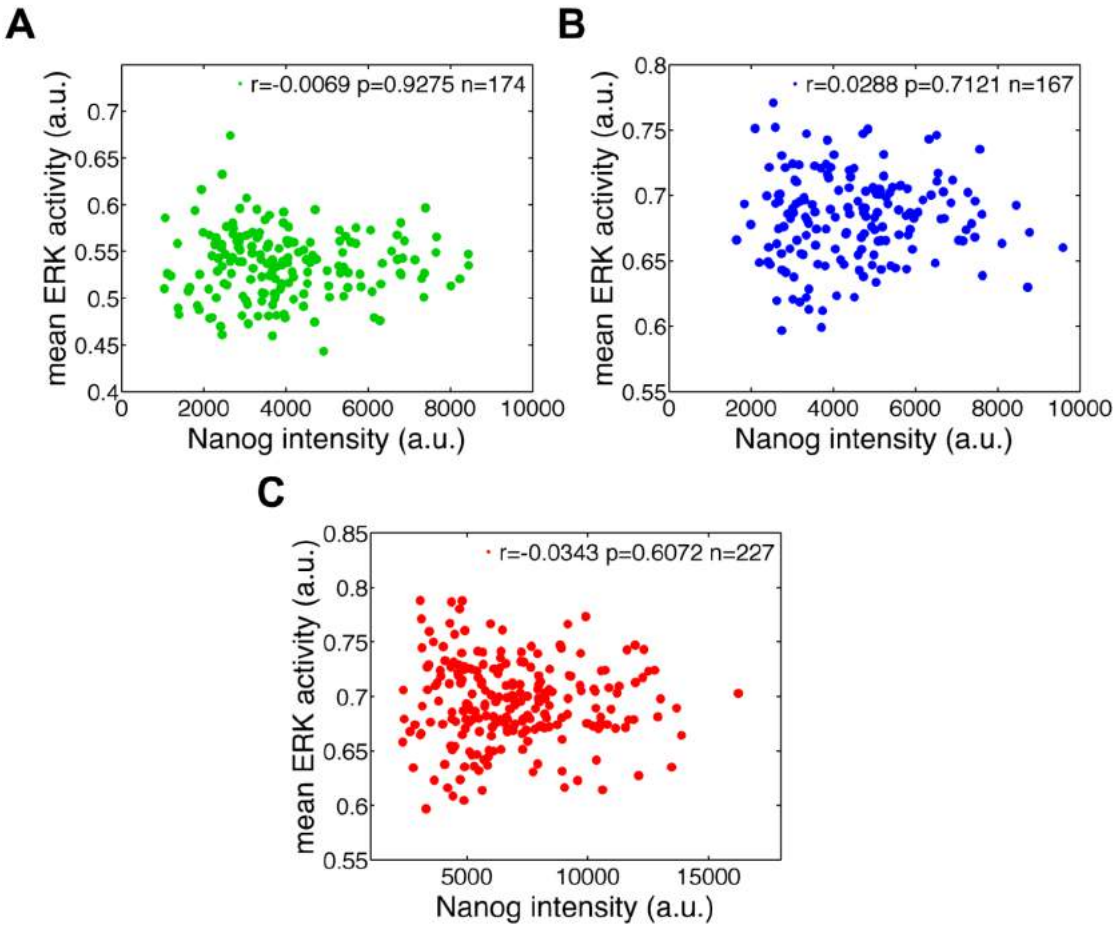


**Figure 4.6: Correlation of mean ERK activity against Nanog expression of individual cells.** Mean ERK activity plotted against its corresponding Nanog intensity of each cell from (A) Experiment 1 (r=-0.0069, p=0.9275, n=174) (B) Experiment 2 (r=0.0288,p=0.7121, n=167) and (C) Experiment 3 (r=-0.0343, p=0.6072, n=277)

The ERK activity dynamics of this initial pulse response, following removal of 2i/LIF, was found to be variable across a population and distinct dynamic properties within this pulse could be influencing the expression of Nanog in individual cells. To quantify variability in the dynamics of this pulse in ERK activity that

had been observed, I parametrised the ERK activity of each cell into a set of descriptors that have been used to define response profiles of cells in previous studies (Cohen-Saidon et al., 2009; Lee et al., 2014). A measurement for the initial levels of FRET prior to the 2i/LIF removal ($F_i$), peak level of FRET ($F_{max}$), levels of FRET at 180m ($F_{t=180}$), and the final FRET levels for each cell track ($F_{t=end}$) was obtained for each cell and these values were correlated with same-cell Nanog intensities (Figure 4.7).

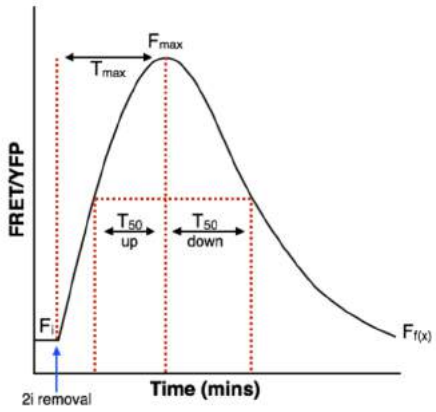


| Descriptor | Definition |
|---|---|
| $F_i$ | initial FRET signal |
| $F_{max}$ | Maximal FRET signal |
| $F_{t=180}$ | FRET levels at t = 180 minutes |
| $F_{t=end}$ | FRET levels at end of track |
| $F_{max}/F_i$ | Maximum fold change in FRET |
| $F_{max}$ - $F_i$ | Amplitude of change in FRET |
| $T_{50up}$ | Time to reach 50% of maximal FRET during increase |
| $T_{50down}$ | Time to reach 50% of maximal FRET during decrease |

**Figure 4.7: Definition of parameters in the activation kinetics of ERK in response to 2i/LIF withdrawal.** All measurements were quantified from FRET ratio values of individual cells and were obtained following smoothing and interpolation of each cell track

To evaluate which descriptors could be predictors of Nanog expression levels each descriptor was plotted against its corresponding Nanog intensity and the coefficient of determination was calculated ($R^2$) (Figure 4.8). Coeffiecient of determination is used to predict how much of the variance of the dependent variable, Nanog protein level, can be predicted by each descriptor. Figure 4.8D (top panel) shows that the final level of ERK activity ($F_{t=end}$) for each cell track accounted for 6% observed Nanog protein variability in replicate 1, and a weak negative correlation between the two variables was identified by Pearsons correlation (r=-0.2522 p=0.01). However, this negative correlation was lost in replicates 2 and 3 (Table 4.1) and final ERK activity levels were no longer a predictor of variation in Nanog protein levels ($R^2$=0.008 and $R^2$=0.0019 for replicates 2 and 3 respectively) (Figure 4.8D; middle

and bottom panel). ERK activity levels at 180 minutes ($F_{t=180}$) were negatively correlated with Nanog intensities in replicate 2 (r=-0.3445 p=0.01) and accounted for 12% of the variance in Nanog protein levels (Figure 4.8C; middle panel). However, once again this correlation was not reproducible between experimental replicates (Table 4.1). Other descriptors of ERK activity response were extremely weak predictors of Nanog protein level, in all 3 replicates, and a consistent significant correlation between the two variables could not be identified (Figure 4.8). A summary of correlation values calculated is presented in Table 4.1.

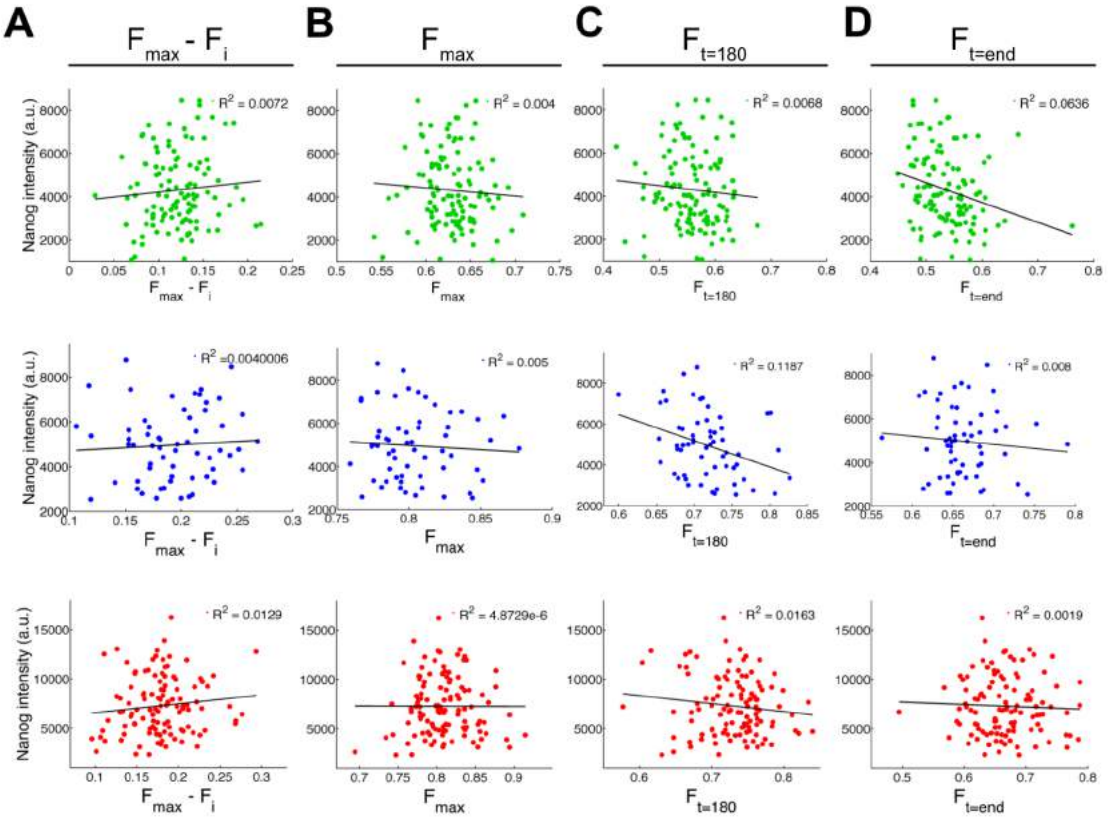


**Figure 4.8: Relationship between parameters of ERK activity response and Nanog expression.** The following ERK activity parameters were plotted against same-cell Nanog intensity for each cell (A) $F_{max}$-$F_i$ (B) $F_{max}$ (C) $F_{t=180}$ (D) $F_{t=end}$. Coefficient of determination ($R^2$) was calculated to indicate which variable is a predictor of variance in Nanog expression and black lines represent the linear regression of each scatter. Experimental replicates are colour coded green for experiment 1, blue for experiment 2, and red for experiment 3

I next wanted to test whether descriptors that quantify changes in ERK activity over time could be stronger predictors of Nanog protein levels. The following descriptors for each cell were plotted against same-cell Nanog protein levels and coefficient of determination and Pearsons correlation were calculated. Fold change response, defined by $F_{max}/F_i$, was unable to predict variation in Nanog expression, in all three replicates (Figure 4.9A) and a significant correlation between these two variables could not be identified (Table 4.1) . Time taken to reach half the maximal FRET signal during increase ($T50_{up}$) and decrease ($T50_{down}$) were also poor predictors of Nanog protein levels and no significant correlation could be identified (Figure 4.9B) (Table 4.1) .

| | **Replicate 1** | | **Replicate 2** | | **Replicate 3** | |
|---|---|---|---|---|---|---|
| **Descriptor** | R | P | R | P | R | P |
| $F_{max}$-$F_i$ | 0.0898 | 0.37 | 0.0632 | 0.63 | 0.1136 | 0.23 |
| $F_{max}$ | 0.0633 | 0.51 | -0.0674 | 0.61 | 0.0022 | 0.98 |
| $F_{t=180}$ | -0.0826 | 0.38 | -0.3445* | 0.01 | -0.1277 | 0.18 |
| $F_{t=end}$ | -0.2522* | 0.01 | -0.0874 | 0.51 | -0.0434 | 0.65 |
| $F_{max}/F_i$ | 0.0921 | 0.33 | 0.0841 | 0.52 | 0.1229 | 0.19 |
| $T50_{down}$ | -0.0544 | 0.57 | -0.2341 | 0.07 | -0.1325 | 0.17 |
| $T50_{up}$ | 0.0539 | 0.57 | -0.0883 | 0.5 | 0.1226 | 0.19 |
| $F_{max}$-$F_i$ vs $F_i$ | -0.5651* | $2.76 \times 10^{-14}$ | -0.7017* | $8.29 \times 10^{-23}$ | -0.6268* | $6.81 \times 10^{-30}$ |

**Table 4.1: Summary of correlations between parameters of the activation profile of ERK and Nanog expression.** Pearson's correlation coefficient values (R) were calculated in MATLAB for all experimental replicates to measure the linear correlation between Nanog expression and dynamics of ERK activity. Basal levels of ERK activity ($F_i$) were also correlated against amplitude of increase in ERK ($F_{max}$-$F_i$) for all experimental replicates and the values calculated are shown in the bottom row. Correlations assigned a p-value $\leq 0.05$ are considered significant and are marked with *.

From these data it appears that ERK activity dynamics during this initial pulse in ERK activity are poorly correlated with Nanog protein levels, suggesting that ERK activity dynamics after this pulse could play a more important role in regulating Nanog expression. However, it is of note that the Nanog intensities recorded are reporting on Nanog protein levels 16h after the induction of differentiation, occurring hours after this initial pulse. It is therefore possible that dynamic features of this initial response could be more correlated with Nanog expression at earlier

stages in development and measuring changes in Nanog expression levels during this time could reveal a more consistent relationship. In addition, these results are limited to the descriptors of ERK dynamics that have been chosen and other features of the ERK activity response, that have not been described here, may be better predictors of Nanog protein levels.

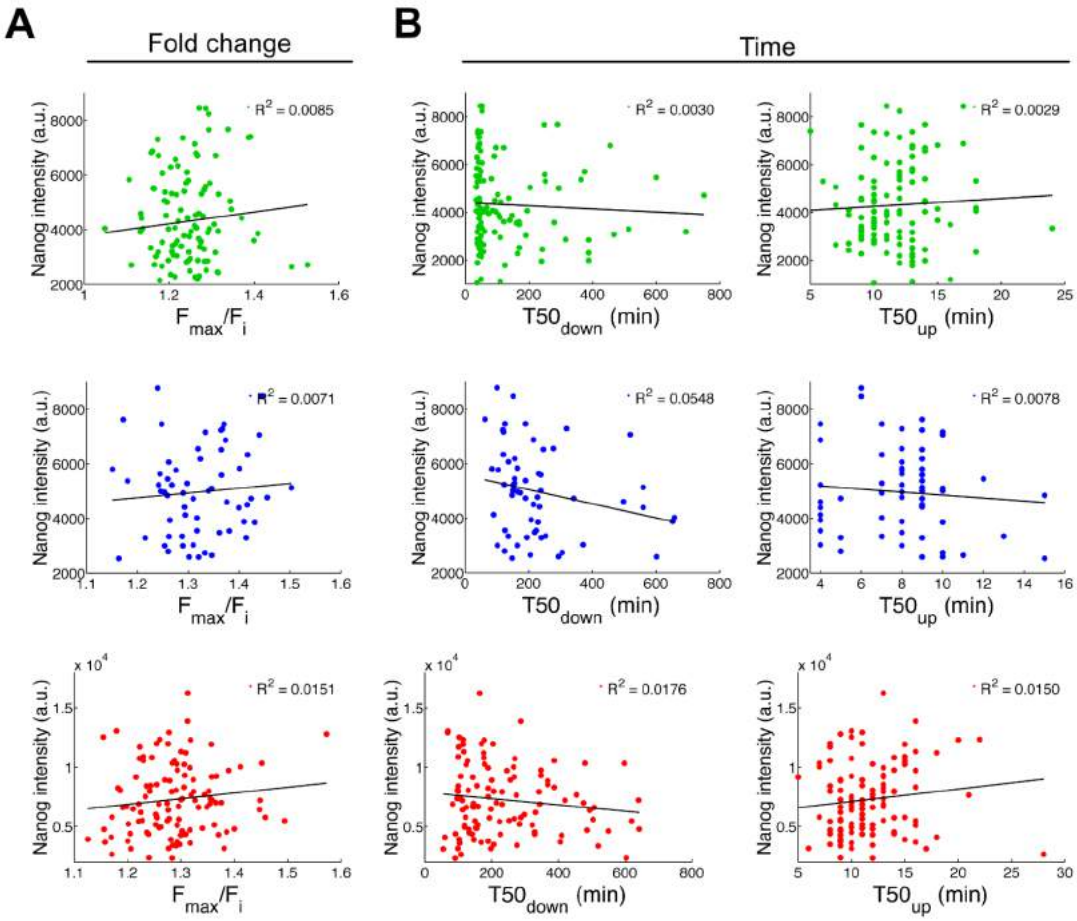


**Figure 4.9: Relationship between time related parameters of ERK activity response and Nanog expression.** Nanog intensity of each cell was plotted against (A) Fold change in ERK activity ($F_{max}/F_i$) (B) Time related parameters of ERK activity $T50_{down}$ and $T50_{up}$. Coefficient of determination ($R^2$) was calculated to indicate which variable is a predictor of variance in Nanog expression and black lines represent the linear regression of each scatter. Experimental replicates are colour coded green for experiment 1, blue for experiment 2, and red for experiment 3

To determine the cell-cell variation in ERK activity dynamics the coefficient of variation (CV) was calculated for each descriptor and values were averaged across all 3 experimental replicates (Figure 4.10A). CV values under 30% were observed for all ERK activity level descriptors, $F_i$, $F_{max}$, $F_{t=180}$, and $F_{t=end}$, as shown in Figure 4.10A. Descriptors associated with temporal dynamics such as, $T50_{up}$ and $T50_{down}$, showed a greater cell-cell variability; particularly in response fall time ($T50_{down}$) which was highly variable between cells (CV=0.77). Additionally, I found the amplitude of increase in FRET ratio values of cell tracks, defined by $F_{max}$-$F_i$, to be anti-correlated to initial basal levels of FRET, in all three replicates ($r=-0.5651$ $P\leq0.001$, $r=-0.7017$ $P\leq0.001$, $r=0.6268$ $P\leq0.001$ for replicates 1, 2 and 3 respectively) (Figure 4.10B). This would suggest that cells are showing an *absolute response* where the peak ERK activity level reached within each cells is approximately the same following 2i/LIF withdrawal, regardless of initial basal levels in activity. This is in contrast to the findings of Cohen-Saidon et al. (2009) who identified a *fold-change response* in ERK activity following EGF stimulation, meaning high initial ERK activity results in a larger absolute increase in ERK activity. It is of note that ERK activity levels were monitored by measuring nuclear levels of YFP tagged ERK2 of individual and use of this alternative method for measuring ERK activity could be causing the discrepancy between our findings. Moreover, the ERK response was measured in a non-small cell carcinoma line (H1299) implying that ERK activity kinetics are likely to vary between cell lines.

Our data suggest that ERK activity increases to a similar level of activity in each cell following removal of 2i/LIF, which could imply that a threshold of ERK activity is reached following the induction of differentiation. This is highlighted further by the low variability in $F_{max}$ levels between cells (CV=0.04). However, it is possible that this threshold in ERK activity is the consequence of pixel saturation during imaging, or the result of all available biosensors within a cell being phosphorylated despite ERK activity continuing to increase. It would therefore be interesting to see if this *absolute response* could be replicated using YFP tagged ERK2, or another alternative method for monitoring ERK activity in single cells.

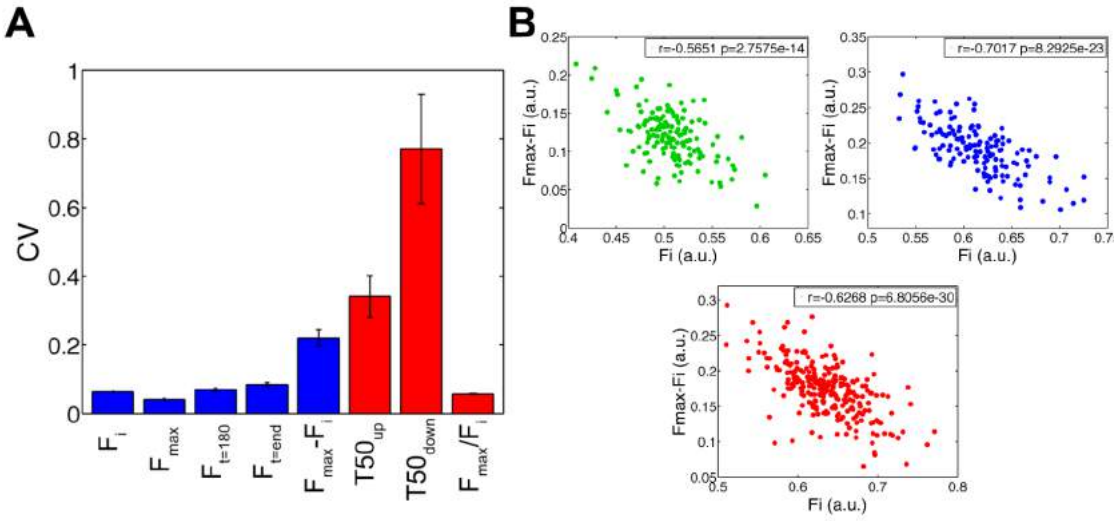


**Figure 4.10: Temporal dynamics of ERK activity are more variable than ERK activity level parameters.** (A) Cell-cell variability measured as the CV ($\frac{\sigma}{\mu}$) of different dynamic features of the activation kinetics of ERK following exit from pluripotency. Blue bars represent measurements of ERK activity levels, and red bars represent time-related parameters. CV values were averaged across all 3 experimental replicates and error bars represent the standard error between experimental replicates. (B) Scatter of $F_{max}$-$F_i$ against $F_i$ from three independent replicates

## 4.5 Clustering suggests two distinct ERK signalling responses

Thus far I have defined ERK activity behaviours based on single parameters, such as absolute ERK activity levels or temporal dynamics of ERK. The majority of analysis I have shown has focused on this initial peak in ERK activity, following withdrawal from 2i/LIF, and ERK dynamics beyond this point have not been taken into consideration. Data positioning algorithms, such as k-means clustering, are commonly used to help find groups within data by clustering data points based on features of similarity. I therefore wanted to investigate if k-means clustering could identify distinct ERK activity patterns, following the onset of differentiation.

In order to determine the optimum number of groups that the data can be clustered into a silhouette evaluation criteria was applied using the *evalcluster* MATLAB function. Silhouette criterion value is calculated for each data point based on

how similar that data point is to its cluster compared to points in other clusters (Rousseeuw, 1987). Higher scores indicate that a data point is well matched to its cluster and the clustering solution that produces the highest average silhouette score represents the optimum number of groups the data should be split into. The potential number of clusters ranged from 1 to 6, and this process was repeated 50 times. The most occurring optimum cluster number (k=2) will become the designated k value. Application of other evaluation criteria, such as Gap and DaviesBouldin, identified the same optimum of number of clusters as Silhouette implying that the optimal number of clusters is independent of the criteria choice for our data set.

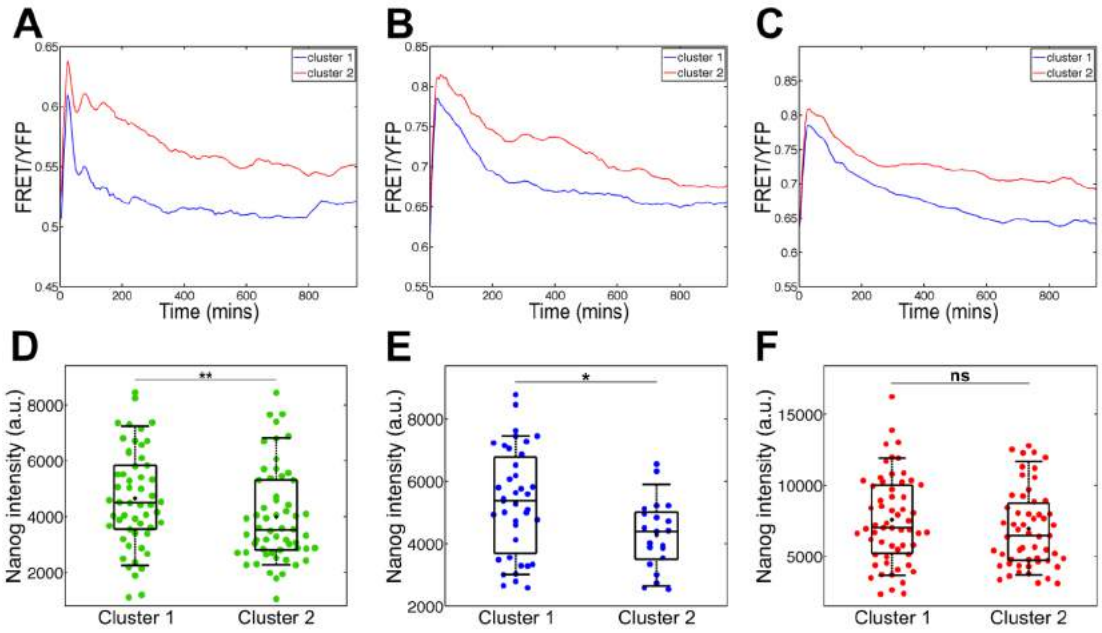


**Figure 4.11: Distinct ERK activity dynamics identified by clustering are weakly related to Nanog expression levels.** Average FRET intensities of cell tracks grouped by k-means clustering for (A) cluster 1 (n=55) and cluster 2 (n=59) of experiment 1 (B) cluster 1 (n=40) and cluster 2 (n=21) of experiment 2, and (C) cluster 1 (n=59) and cluster 2 (n=55) of experiment 3. Measured Nanog intensities of each cell from (D) clusters shown in (a) (E) clusters shown in (b) and (F) clusters shown in (c). Nanog levels were found to be significantly different for experiments 1 and 2 using a KS-test and no statistical difference was found for experiment 3. ** signifies $p \leq 0.01$, * signifies $p \leq 0.05$, and **ns** signifies $p \geq 0.05$

The k-means algorithm works by randomly selecting data points to become centroids and clusters data by assigning each data point to its closest centroid. New centroid values are then obtained by averaging the data points within each cluster and the process starts again. The algorithm will undergo a number of iterations until the centroid position stops changing or a defined maximum number of iterations is reached. K-means clustering, using a cluster number of two as defined by silhouette evaluation, was applied to all cell tracks for each experimental repeat using the *kmeans* MATLAB function. Clustering was repeated 100 times using new random initial cluster centroid positions each time and a score was applied to each replicate. The clustering result from the replicate with the lowest score is then kept.

Figure 4.11A-C shows the average FRET intensities of the two groups of cell tracks as defined by k-means clustering for each experimental replicate. From k-means clustering I was able to identify two distinct ERK signalling behaviours and these two responses appeared robust between experimental repeats. These data suggest that following withdrawal from 2i/LIF cells can be separated into sub-populations based on the rate of decrease in ERK activity following this initial peak. Cells that fall into cluster 1 demonstrated a more transient ERK activity response following the induction of differentiation, whereas ERK dynamics of cells that fell into cluster 2 was more sustained as development progressed (Figure 4.11A-C). It is interesting to note that cells in cluster 2 showed a greater peak in ERK activity compared to cells of cluster 1, in all 3 experimental replicates, implying that differences in the rate of loss in ERK activity may be related to the level of peak ERK activity.

Having identified these two distinct ERK signalling dynamics I next wanted to assess how these ERK activation profiles related to Nanog expression. Nanog intensity of individual cells in each cluster was plotted for all three experimental replicates, as shown in Figure 4.11D-F. A statistically significant decrease in the expression of Nanog between the two clusters was identified using a Kolmogorov-Smirnov test (KS-test), for replicates 1 ($P \leq 0.001$) and 2 ($P \leq 0.05$). Although a statistically significant difference could not be detected in replicate 3

(P=0.2657). These data suggest that Nanog expression is related to the rate at which ERK activity falls. However, it is important to note this effect is relatively weak and only a small difference in the expression of Nanog was observed between these k-means clustering defined groups of cells (Figure 4.11D and E).

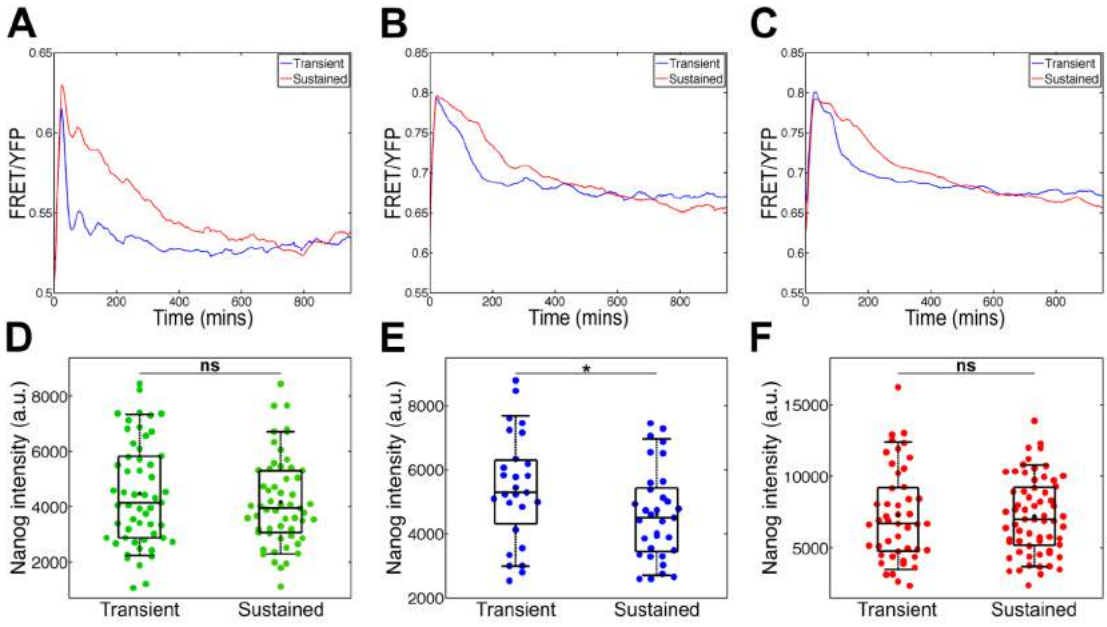


**Figure 4.12: Partition of cells into groups of sustained or transient ERK activity responses suggests Nanog expression levels are not related to declining rates in ERK activity.** Cell tracks were separated into groups of transient (blue) or sustained (red) ERK activity based on their $T50_{down}$ value. The average FRET intensities of (A) Transient (n=61) and Sustained (n=51) cell tracks of experiment 1 (B) Transient (n=28) and Sustained (n=33) cell tracks of experiment 2, and (C) Transient (n=53) and Sustained (n=58) cell tracks of experiment 3 (D-F) Measured Nanog intensities of transient and sustained cell tracks are shown in the plots below each graph of its corresponding experimental replicate. Nanog levels were found to be significantly different for experiment 2 using a KS-test and no statistical difference was found for experiments 1 and 3. ** signifies $p \leq 0.01$, * signifies $p \leq 0.05$, and **ns** signifies $p \geq 0.05$

Another parameter of ERK activity that could be used to separate cell tracks into sub-population of transient and sustained ERK activity responses is the descriptor $T50_{down}$ (Figure 4.7). $T50_{down}$ value represents the time it takes for each cell to reach half its maximal ERK activity level as activity levels decrease following the initial peak. Consequently, cells demonstrating sustained ERK activity will

have high $T50_{down}$ values and cells demonstrating transient ERK activity will be represented by low $T50_{down}$ values. A $T50_{down}$ value was calculated for each cell and the median of these values was determined for each replicate. Cells were subsequently separated into two equally sized groups of sustained and transient ERK activity based on whether their $T50_{down}$ value was above or below the median, and the average FRET signal of these two group was subsequently plotted. Figure 4.12A-C demonstrates that $T50_{down}$ values can reliably separate cells into sustained and transient ERK activity responses that are comparable to the ERK activity dynamics identified by clustering.

A statistically significant difference in the expression of Nanog between the two groups of cells exhibiting either a transient or sustained response, could only be identified for experimental replicate 2 ($P \leq 0.05$) (Figure 4.12D-F), suggesting that Nanog expression levels are not strongly related to the rate of decline in ERK activity. This indicates that differences in the expression of Nanog between clustered groups of cells in replicates 1 and 2, is unlikely to be the result of ERK activity being sustained or transient, and instead may be related to other dynamic features of ERK activity within these two clusters. Indeed, if we compare the average ERK activity dynamics of cells grouped by clustering to those grouped using the $T50_{down}$ value, it would appear that similarities in the average ERK activity dynamics of cells grouped by these two methods become increasing disparate towards later portions of the time series (Figures 4.11A-C and 4.12A-C).

To investigate whether ERK dynamics after the initial pulse in activity could influence the expression of Nanog, the same k-means algorithm was applied to the clustering of tracks from 5h to the end of the time series. Cells of cluster 1 demonstrated overall lower levels of ERK activity compared to cells of cluster 2, and a slight dip in ERK activity in the cells of cluster 1 could be observed, which was particularly apparent in replicate 3 (Figure 4.13A-C). In agreement with the results obtained from clustering of the whole time series, a statistically significant lowering in the expression of Nanog was observed between clustered groups of cells

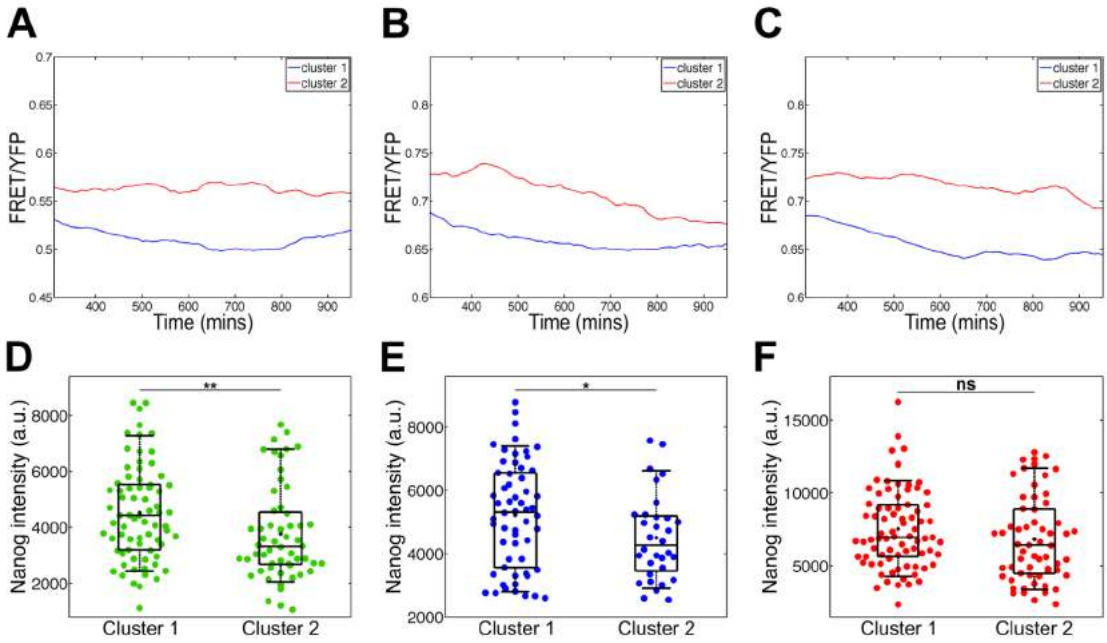


**Figure 4.13: Differences in expression of Nanog are the result of ERK activity after the initial pulse response.** Average FRET intensities of cell tracks clustered from 5h to the end of the time series for (A) Cluster 1 (n=73) and cluster 2 (n=56) of experiment 1 (B) Cluster 1 (n=58) and cluster 2 (n=32) of experiment 2, and (C) Cluster 1 (n=79) and cluster 2 (n=61) of experiment 3. Measured Nanog intensities of each cell from (D) clusters shown in (a) (E) clusters shown in (b) and (F) clusters shown in (c). Nanog levels were found to be significantly different for experiments 1 and 2 using a KS-test and no statistical difference was found for experiment 3. ** signifies $p \leq 0.01$, * signifies $p \leq 0.05$, and **ns** signifies $p \geq 0.05$

for both replicate 1 ($P \leq 0.01$) and replicate 2 ($P \leq 0.05$) (Figure 4.13D-E), suggesting Nanog expression is partially regulated by ERK signalling dynamics that occur after this initial pulse in activity. However, once again a statistically significant difference in Nanog expression between clusters could not be identified in all 3 replicates and the magnitude of difference in expression between clustered groups was small indicative of an overall weak affect.

## 4.6 Summary

In this chapter I have discussed the development of a method for using the FRET based biosensor, EKAREV, to examine ERK signalling dynamics following the

onset of differentiation. As well as monitoring ERK activity, the Nanog intensity of individual cells was quantified at the end of the developmental time course to act as a determinant for the functional consequence of different ERK activity dynamics. Nanog intensities were chosen as a read-out of pluripotency as result of the heterogeneous nature of its expression and a significant decrease in its expression being observed at early stages during the transition from naïve pluripotency (Figure 4.1)

A peak in ERK activity was evident immediately after the removal of 2i/LIF in all three experimental replicates, followed by a decline in ERK activity reaching a basal plateau at around 4h (Figure 4.5). Parametrization of this ERK activity response to a set of descriptors was unable to identify a distinct feature of ERK activity dynamics that correlated with Nanog expression across all three replicates (Figures 4.8 and 4.9). Clustering of cells identified two distinct ERK signalling responses, of sustained or transient ERK activity following the initial peak, and quantification of Nanog intensities revealed a significant difference in the expression of Nanog between cells of these two clusters (Figure 4.11). However, this affect was only observed in two out of three replicates and differences in Nanog expression were small, indicating a weak relationship between these dynamics and the expression of Nanog.

Differences in Nanog expression were lost when cells were separated into groups of transient or sustained ERK activity response using the $T50_{down}$ parameter (Figure 4.12). Furthermore, clustering of cell tracks after the initial pulse in ERK activity resulted in distinction in Nanog expression between clusters for experiments 1 and 2, thus replicating the findings of whole track clustering (Figure 4.13). Together these data suggest that the rate at which ERK activity declines does not influence Nanog expression and ERK activity dynamics after this initial pulse could be playing a greater regulatory role.

# Chapter 5

# Investigating spatial regulation of ERK activity in ES cell colonies

## 5.1 Introduction

The lineage determination of stem cell is highly dependent on its surrounding environment (Fuchs et al., 2004). Environmental factors such as cell density, cytoskeletal tensions, and cell-cell interactions have all been shown to influence the self-renewal capacity of ES cells (Fernandes et al., 2010; Murray et al., 2013; Taleahmad et al., 2017; Redmer et al., 2011). Micro patterning approaches have shown governing the size and density of stem cell colonies can spatially control signalling cues to alter gene expression (Peerani et al., 2009; Warmflash et al., 2014; Morgani et al., 2018a). Monitoring of ERK signalling in other model systems has shown spatial regulation, as well as temporal dynamics, to play an important role during development and location of activation is able to guide cell fate choices (Johnson et al., 2017; de la Cova et al., 2017). However, the spatial regulation of ERK activity in ES cells and how this relates to the expression patterns of pluripotency is poorly understood.

In the previous chapter I showed how the EKAREV biosensor can be used to monitor the temporal dynamics of ERK activity following exit from pluripotency.

From these data I was able to quantify levels of ERK activity over time and relate differences in the activation profiles of ERK to the expression of Nanog. As well as being able to extract information on the quantification levels of ERK activity, from these data it is also possible to obtain information on the position of each cell over time. Previous studies of ERK activity in ES cell colonies have been limited by the use of population averages, which results in a loss of structural information. Our data therefore offers a novel opportunity to monitor differences in ERK activity dynamics in relation to the spatial arrangement of cells within an ES cell colony, which could further our understanding of the role ERK signalling plays in the maintenance of pluripotency.

In this chapter I will describe the approaches I am using to quantify spatially related features from the three data sets that were collected in chapter 4. I will discuss how these quantified values can be used to demonstrate how environmental factors, such as cell density and neighbouring interactions, influence ERK activity, using multiple analysis methods. Finally, I will discuss how our data can be used to examine the ERK activity of daughter cells to investigate whether similar ERK activity behaviours are the result of proximity or inheritance.

## 5.2 Differences in cell density influences ERK activity levels

To investigate the possibility of environmental effects on ERK signalling I first wanted to assess how ERK activity of individual cells relates to its localized density. ERK activity has been shown to be highly stochastic in other cell lines and the frequency of different ERK activity pulses has been found to be cell density related (Aoki et al., 2013; Albeck et al., 2013). Cell density is a metric for differences in local environment and has been shown to play an influential role in the expansion of ES cells (Fernandes et al., 2010).

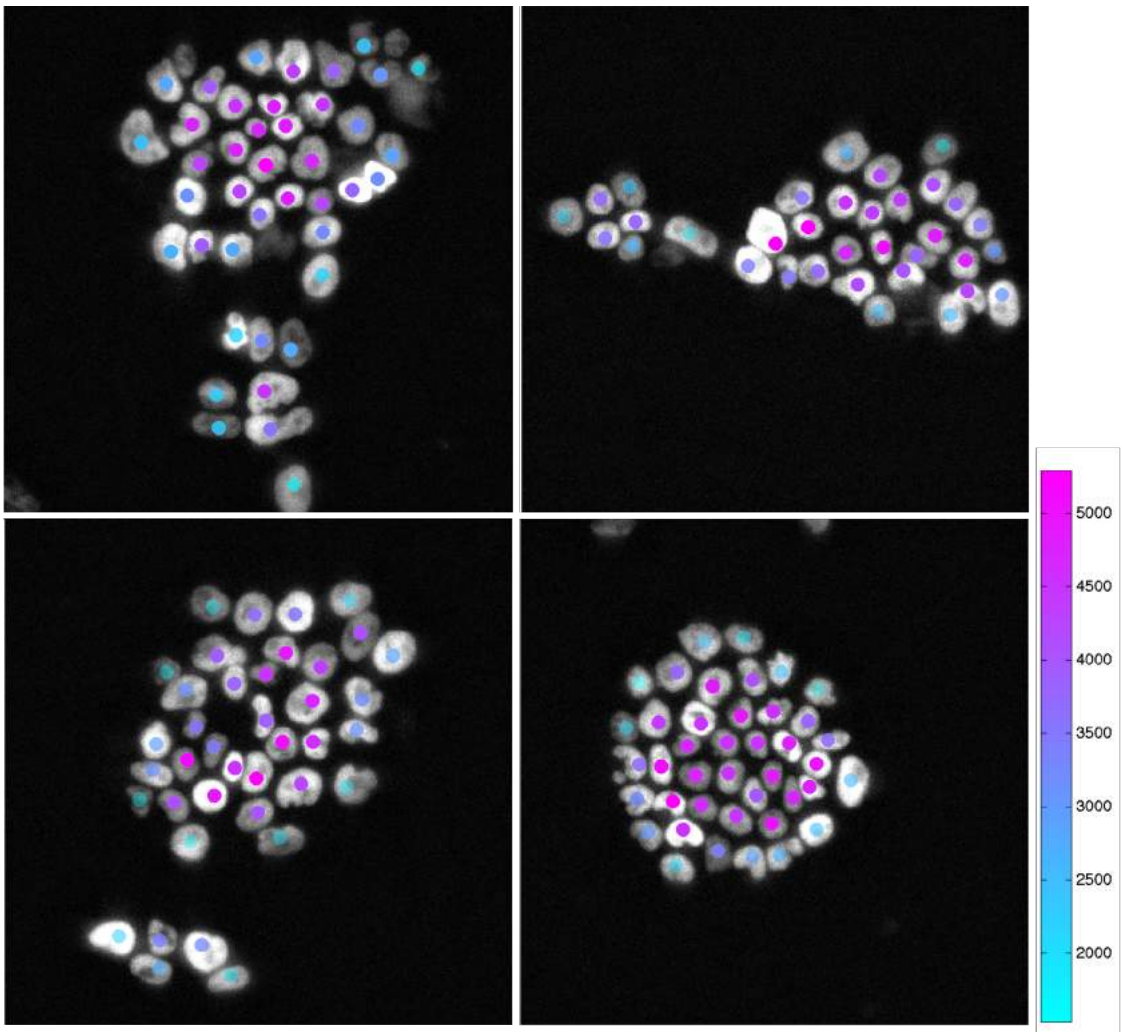


**Figure 5.1: An example of the density values applied to cells in the initial imaging frame.** Density of the environment surrounding each cell was calculated using a custom-built MATLAB script (Vlatka Antolovic). High density values represent cells in a densely populated area (i.e. at the colony centre) whilst low density values represent cells in more sparsely populated regions (i.e. at the colony edge). A LUT was applied to the cell density values of each cell and a scale bar of these values is shown on the right hand side.

Cell density was determined by measuring the density of the environment surrounding each cell using a custom-built MATLAB script (Vlatka Antolovic). In brief, a 50 pixel diameter circle was centred on the coordinates of each cell, that were generated during tracking, at every time-point in a single field of view (FOV). In parallel, images were binarized and a density value was assigned by summing up pixel values within each circle; the larger the proportion of cells that fall within a circle the higher this value will be. Consequently, cells at the centre of colonies, where the environment of a cell will be densely populated, will be represented by high values and low values will be assigned to cells at the edge of colonies, where the proportion of cells is smaller (Figure 5.1). A cell density value was calculated for each cell at every time-point to generate a single cell read-out of density over time, which could be corroborated with changing ERK activity dynamics. This analysis was applied to all three experimental replicates of the data collected for Chapter 4 and the results from each replicate are shown below.

To test how cell density influences ERK activity, the mean cell density of each cell was plotted against its corresponding mean ERK activity level, and values were compared using Pearsons correlation coefficient (r). A weak negative correlation was identified for replicates 2 (r=-0.2863 p=$1.80\times10^{-06}$) and 3 (r=-0.1396 p=0.0059) (Figure 5.2B and C), implying that increased cell density causes a decrease in the levels of ERK activity. Although, a negative correlation between mean cell density and mean ERK activity was also detected for replicate 1 (r=-0.1142), the correlation was found to be marginally non-significant (p=0.0894) (Figures 5.2A). These findings are in broad agreement with Aoki et al. (2013) who observed a decrease in basal ERK activity with increasing cell densities. Correlation values observed suggest that the relationship between density and ERK activity is relatively weak. Investigating how the local density of a cell's environment changes over time in relation to its ERK activity could provide a more detailed insight into the correlation between these two variables.

## 5.3 High density and low density culture environments exhibit distinct ERK dynamics during the initial peak response

Removal of 2i/LIF allows cells to exit pluripotency and transition towards lineage commitment. An increase in ERK activity is immediately evident at the onset of this transition, which peaks at around 25-30 minutes, followed by a decrease in activity with rates in decline varying between cells (Figure 4.5). In the previous chapter I briefly discussed possible positional affects of this response following plating on laminin, which increases the spreading of cells (Figure 4.2). From ratiometric images of this experiment it appears that cells at the edge of a colony display increasing levels of ERK activity prior to cells in the centre more densely populated

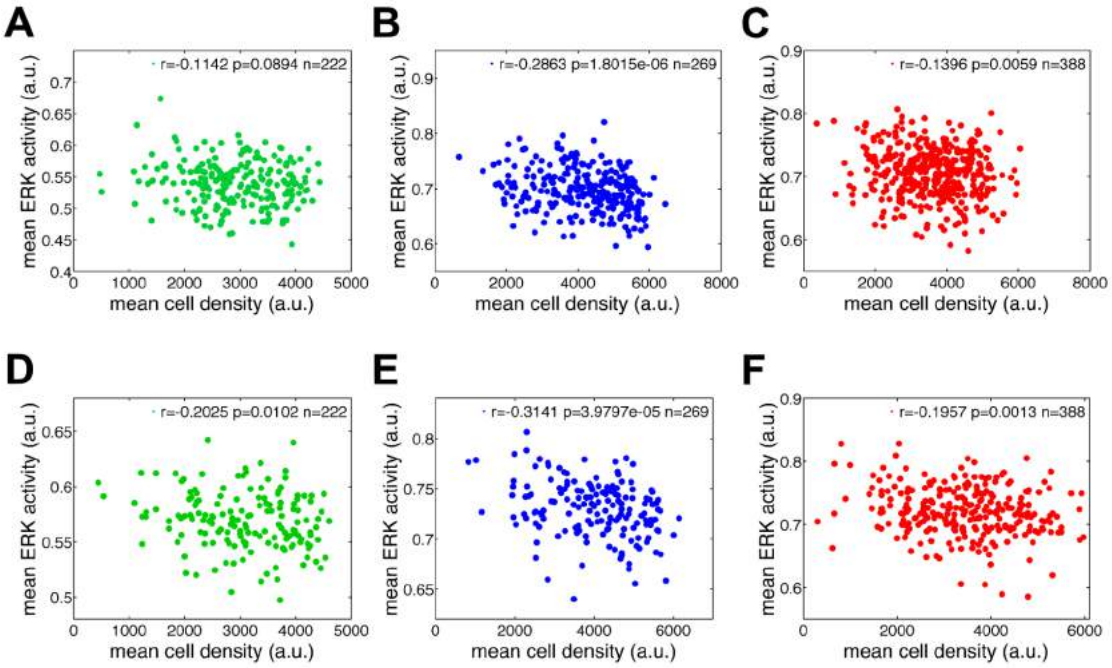


**Figure 5.2: Correlation of mean cell density and ERK activity.** (A-C) Mean cell density of each cell over time was calculated and plotted against its corresponding mean ERK activity level. (D-F) Scatter plot of mean cell density and mean ERK activity of each cell in the first 6 frames of the time-series (25m). Scatters for each experimental replicate are shown; experiment 1 (green), experiment 2 (red), and experiment 3 (red). Pearsons correlation coefficient between variables are shown on the corresponding scatter plot

region (Figure 4.2A). I therefore wanted to investigate if a stronger correlation between ERK activity levels and cell density could be observed during the earlier stages of our time series.

First, I calculated the mean cell density around each cell during the first 6 frames (25 min) of the time series, when this initial increase in ERK activity is occurring. I subsequently plotted the mean cell density around each cell against its corresponding mean ERK activity during this period, and correlated values using Pearsons correlation coefficient. A negative correlation was identified in all 3 experimental replicates, suggesting that cell density has a greater affect during this initial increase in ERK activity (r=-0.2025 p=0.012, r=-0.3141 p=$3.98\times10^{-05}$, and r=-0.1957 p=0.0013, for replicates 1, 2 and 3 respectively) (Figure 5.2D-F). This would imply that cells of a lower density, which are likely to be at the edge of a colony, have a greater increase in ERK activity during this initial peak, thus agreeing with previous observations (Figure 4.2A). Once again these correlations are relatively weak, I therefore wanted to carry out some additional analysis to examine these findings further.

To investigate differences in the activation kinetics of ERK during this initial increase, k-means clustering was carried out on the first 6 time-points of each cell track using the method described in chapter 4. Clustering identified two distinct ERK activity responses during this initial peak in all three experiments, with basal activity, and final amplitude levels differing between the two clusters (Figure 5.3 A-C). To determine whether these distinct ERK activity dynamics, identified by clustering, could be the result of cell density, the mean cell density from frames 1 to 6 were calculated for each group of clustered cells. Figure 5.3 shows the mean FRET intensities of clustered cells and the average cell density of each cluster is represented in the bar charts below.

Clustering demonstrated differences in initial levels of ERK activity between cells (Figure 5.3). Moreover, groups of cells with high initial ERK activity levels also displayed higher levels of ERK activity at 25 minutes, and this affect was

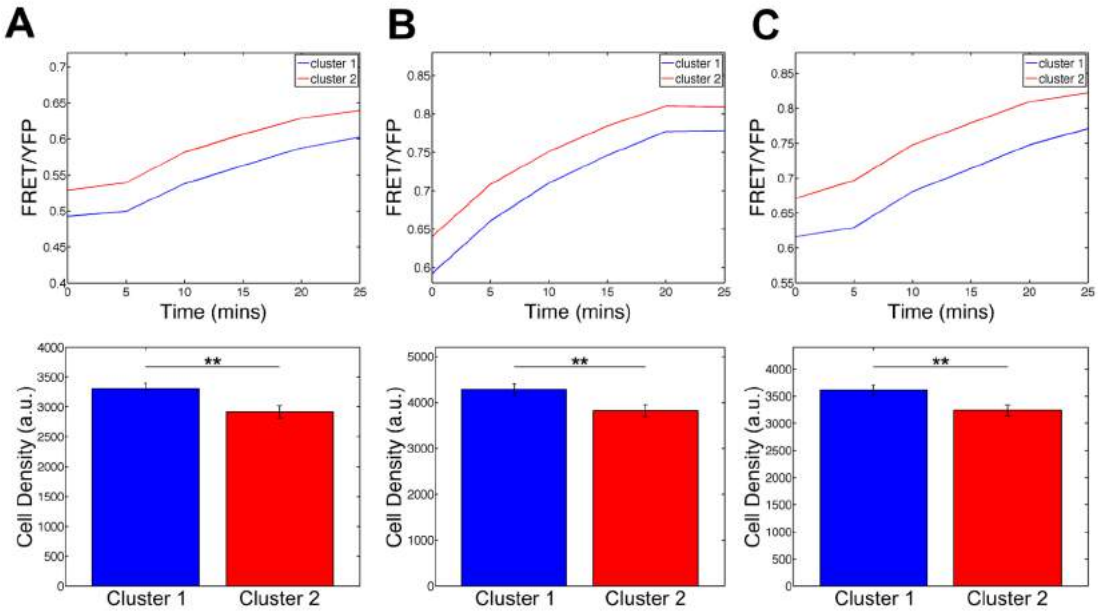


**Figure 5.3: Clustering identified two cell density related ERK activity responses during the initial peak.** Mean FRET ratio levels of cells grouped by clustering during the first 25 minutes the time-series are shown in the first row and the corresponding cell density of each cluster is shown below, for experiment 1 (A), experiment 2 (B), and experiment 3 (C). Differences in cell density between clusters were found to be significantly different using Wilcoxon signed ranks test. ** signifies $p \leq 0.01$

reproducible across all three replicates. To investigate the rate of increase in average ERK activity between these clustered groups of cells the gradient of the curve was calculated for each cluster using the MATLAB function polyfit. Cells of cluster 1 were found to have a greater rate of incline compared to cells of cluster 2, in replicates 2 and 3. However, this difference in gradient was very small and could not be reproduced across all three experiments. Thus the main distinction in ERK activation kinetics between these two clusters is likely to be the initial basal level rather than rate of increase in activity. A statistically significant decrease in cell density values of cell of cluster 2 was detected by Wilcoxon signed ranks test suggesting a disparity in the features of ERK activity between these two clusters is partially related to the density of the environment (Figure 5.3).

To test this finding further, I next wanted to ask if this cell density dependent affect could be reproduced using an alternative method of analysis. The average

cell density values of each cell, from frames 1 to 6, were sorted into ascending order and were divided to three equally sized groups of Low density, Mid density and High density cells. An example of the density values for each cell, from replicate 1, and the division of these three groups is represented in Figure 5.4A, with each group's mean cell density shown in Figure 5.4B. The mean ERK activity of each group was subsequently plotted and a significant difference between the ERK activity response of cells with high density values and cells of the low density group was identified by Wilcoxon signed ranks test in all three replicates (Figure 5.4C). Conversely, cells demonstrating mid range cell density values demonstrated a varied ERK activity response between replicates, with ERK activity dynamics appearing similar to either the low density or high density group of cells (Figure 5.4C). Cells with low density values demonstrated an increased level of basal ERK activity and a reduced rate of incline, which is representative of the average ERK activity response of cells belonging to cluster 2. In contrast, cells of the high density group displayed reduced basal levels of ERK activity and an enhanced rate of incline, making them representative of the more densely populated cells of cluster 1 (Figure 5.4C). However, once again it is of note that differences in the rate of increase were small and could only be observed in experimental replicates 2 and 3.

Distinctions in the ERK activity dynamics of cells in areas of high density, and in areas of low density, were comparable between these two methods. Both analysis methods showed the greatest difference in the activation kinetics of ERK between cells in high density and low density populated areas is the initial level of ERK activity. Accordingly, I have found initial basal levels of ERK activity to be negatively correlated to the average cell density of each cell in the first 25 minutes of the time-lapse series in all 3 experimental replicates ($r=-0.164$ $p=0.0421$, $r=-0.2839$ $p=0.0005$, and $r=-0.1276$ $p=0.0394$, for replicate 1, 2 and 3 respectively). Collectively, these data suggest that cells in areas of low density demonstrate increased basal levels of ERK activity prior to 2i/LIF removal, which could in turn be influencing the rate at which ERK activity increases during this initial peak. However, it is of note that the affect of cell density on rates of increase in ERK

activity was relatively weak. Examining this peak in ERK activity at a much greater time resolution could establish stronger variations in the kinetics of this response that may be more highly correlated with cell density. In addition, it may also be interesting to examine the ERK activity dynamics of cells isolated from colonies and study how these dynamics compare to cells with high density values.

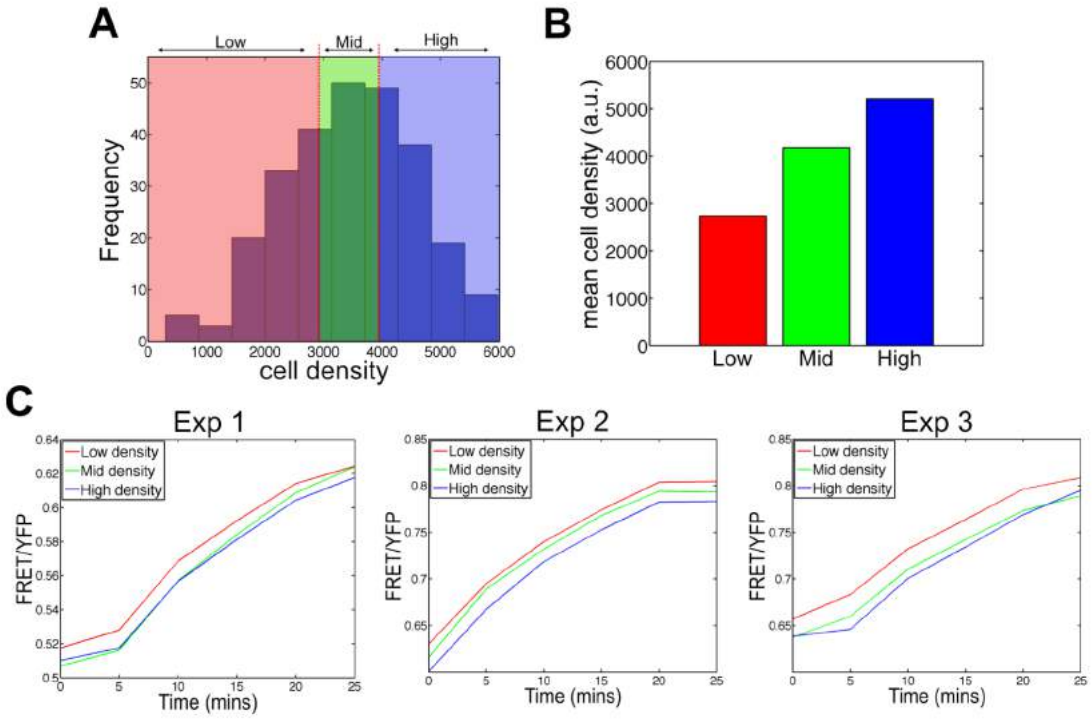


**Figure 5.4: High density and low density cells exhibit distinct ERK dynamics during the initial peak response.** (A) Histogram of average cell density values from the first 6 frames of all cells in experiment 1. Colours represent separation of cells into three groups of Low density (red), Mid density (green), and High density (blue). (B) Mean cell density value of each group shown in (a). (C) Mean FRET ratio values of cells grouped based on density values for all 3 experimental replicates. Differences in FRET ratio values between the high and low cell density group were found to be statistically significant ($p \leq 0.001$) using Wilcoxon signed ranks test in all three experiments.

## 5.4 Cell density influences the expression of Nanog

The data I have shown thus far suggests that ERK activity levels can be modulated by changes in cell density within an ES cell colony. The environmental dynamics of cell density have also bee associated with the self-renewal capacity of ES cells,

which is largely inferred by the idea that cells at the edges colonies have a reduced pluripotency potential represented by their flattened more polarized morphology (Murray et al., 2013). Moreover, recent studies, using both experimental and computational approaches, have shown density to be correlated with the expression of both Nanog and Rex1 (Cannon et al., 2015; Herberg et al., 2015). I therefore wanted to investigate if this trend of cell density regulated expression of pluripotency associated factors could also be deduced from our data sets.

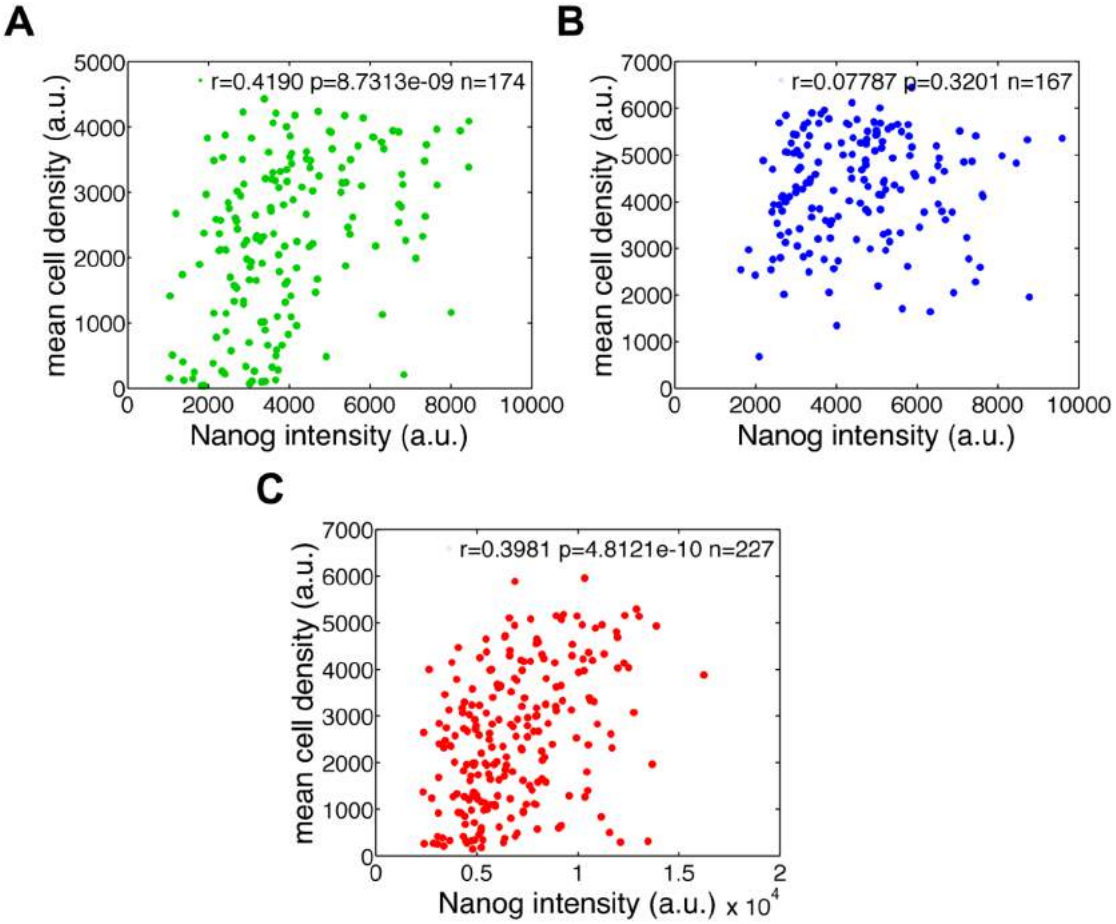


**Figure 5.5: Correlation between Nanog expression and cell density.** Mean cell density value of each was correlated against its corresponding Nanog intensity for (A) experiment 1 (green), (B) experiment 2 (blue) and (C) experiment 3 (red). Pearsons correlation coefficient value for each experiment are shown on the corresponding scatter plot

To assess whether cell density influences pluripotency, I utilized the quantified Nanog intensity values I had gathered in chapter 4 from all three experimental replicates, and correlated these values to the mean cell density of each cell (Figure 5.5). Pearson correlation coefficient identified a significant positive correlation between Nanog intensity and mean cell density for experimental replicate 1 (r=0.4190 p=$8.73\times10^{-09}$) and 3 (r=0.3941 p=$4.81\times10^{-10}$), implying that Nanog expression increases proportionally with cell density, which is in agreement with previous reports (Cannon et al., 2015). A significant correlation could however not be identified for replicate 2 (r=0.0779 p=0.3201), which may result from perturbation of cell density averages by enhanced cell motility thereby precluding a correlation between Nanog and density. However, there is currently no quantification data on the motility of cells within each experiment, so this theory is highly speculative at this stage. Nevertheless, overall these data support the idea that cells at the centre of a colony, where density is higher, have a greater pluripotent potential, represented by an increase in the expression of Nanog.

## 5.5 Neighbouring cells demonstrate similar ERK activity dynamics

Hitherto I have shown that cells in highly dense portions of an ES cell colony demonstrate lower levels of ERK activity compared to cells at the edge where density is lower. This cell density dependent affect on ERK activity would suggest that some form of environmental affect is occurring. Previous studies have shown that ERK activity is able to propagate between neighbouring cells both *in vitro* and *in vivo* (Aoki et al., 2013; Hiratsuka et al., 2014). Local cell density affects on ERK activity could therefore be arising from intercellular interactions. To address this I decided to compare the ERK activity of neighbouring cells using a different methods of analysis that will be discussed in detail below.

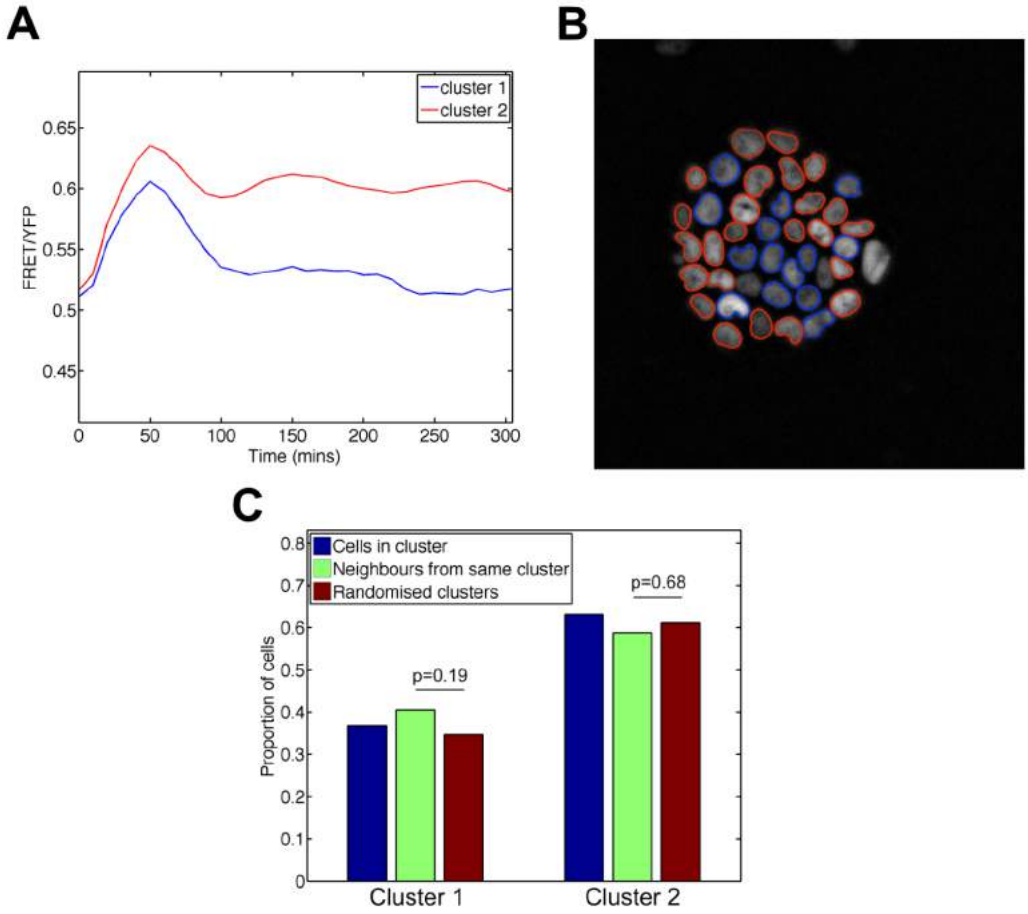


**Figure 5.6: Spatial distribution of ERK activity dynamics identified by clustering.** (A) Mean FRET ratio values of cells grouped by k-means clustering taken from a single FOV. Cluster 1 = blue (n=13) and Cluster 2 = red (n=24). (B) Location of cells from clusters shown in (a). (C) Proportion of cells in each cluster (blue), proportion of cell in a cluster that neighbour one another (green), average proportion of cells from each cluster that are neighbours taken from randomised data sets (red). Data are typical of all experiments

In the previous chapter I described how k-means clustering identified two distinct ERK activity dynamics of transient or sustained ERK activity following release from 2i/LIF (Figure 4.11). These dynamics can occur between cells of the same population, I therefore wanted to explore whether the localization of cells within a colony had any influence on these two observed dynamics. K-means clustering requires track lengths to be of equal size. Consequently, clustering of 16h data would result in the exclusion of cells that have been lost by cell death or division during imaging. To allow for a larger number of cells to be analysed the subsequent

analysis was carried on data k-means clustered from the first 5h of the time series, where these distinct ERK activity dynamics can still be observed. An example of the average ERK activity of k-means data from a single FOV that was used for this analysis is shown in Figure 5.6A.

The location of cells from each k-means cluster was determined using a custom built MATLAB script that uses the mouse clicked coordinates recorded during manual tracking to couple cell positions with the corresponding cell track (Vlatka Antolovic). The location of cells of k-means cluster 1 (blue) and k-means cluster 2 (red), is represented in Figure 5.6B. At a first glance, it appears that cells in k-means cluster 1 group together primarily in the centre of the colony, whilst cells of k-means cluster 2 congregate more towards the edge. To quantify the spatial distribution of these ERK activity dynamics, we decided to evaluate what proportion of neighbouring cells are from the same k-means cluster. To test this the nearest neighbours of each cell was determined using a custom built MATLAB script (Vlatka Antolovic). In brief, a 30 pixel diameter circles was centred around each cell using the coordinates manually selected in the first frame of a time-lapse, and the cells whose corresponding circle areas overlap are considered to be neighbours.

First, the proportion of cells in each k-means cluster was calculated by dividing the number of cells in a cluster by the total number of analysed cells. Following the identification of neighbouring cells we next determined how many neighbours of each cell are in the same or opposing k-means cluster. We then calculated the ratio of neighbours of the same k-means cluster to total number of neighbours for each cluster separately. To test whether this proportion of cells within a k-means cluster could neighbour each other by chance the data was bootstrapped by randomly assigning cells into clusters. This process was repeated 1000 times and the proportion of neighbours from the same cluster was calculated for each randomised data set. If the previously calculated proportion of neighbours that are from the same k-mean cluster occurs at a probability greater than 0.05 by random sampling, the spatial pattern of distribution of cells from each k-means cluster is

considered to be the result of chance.

Figure 5.6C represents the proportion of cells in cluster 1 and cluster 2 that neighbour cells of the same k-means cluster from the FOV shown (green bars) and the average proportion of cells from each cluster that are neighbours taken from randomised data sets (red bars). Randomisation of the data by bootstrapping, identified a 0.19 and 0.68 probability that cells of k-means cluster 1 and cells of k-means cluster 2 would neighbour themselves to the extent observed by chance (Figure 5.6), implying that the proportion of k-means cluster 1 and k-means cluster 2 cells that neighbour one another does not constitute an effect. Here I have only shown an example of data generated from a single FOV using this analysis method. However, application of this analysis method to different FOV has found this trend to be consistent across multiple ES cell colonies.

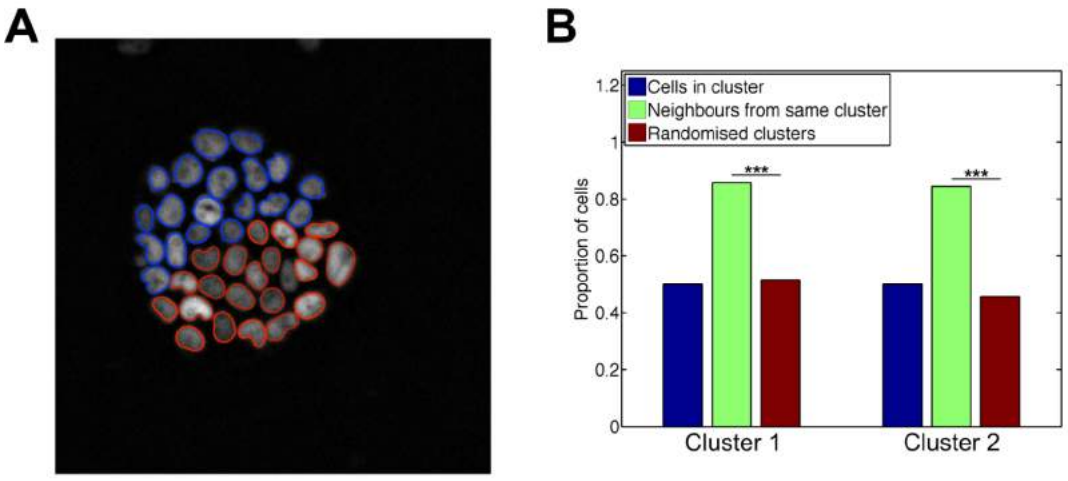


**Figure 5.7: Testing method for determining spatial distribution of ERK activity dynamics defined by clustering.** (A) Cells were manually assigned into two groups of cells based on their location within the colony. Cluster 1 = blue and cluster 2 = red. (B) Proportion of cells in each cluster (blue), proportion of cell in a cluster that neighbour one another (green), average proportion of cells from each cluster that are neighbours taken from randomised data sets (red).*** signifies probability of $\leq$0.001

In order to test the sensitivity of our methodology the analysis was repeated on cells that had been manually allocated into clusters based on their localization. The colony was divided into two roughly equal sized areas and the cells congregating within each area were assigned to either cluster 1 (blue) or cluster 2 (red), and the proportion of neighbouring cells from within a cluster was calculated as before. Figure 5.7 shows the proportion of cluster 1 cells that neighbour each other is extremely high, and this high proportion is also apparent for the cells of cluster 2. Moreover, bootstrapping identified a probability of less than 0.001 of getting this distribution of neighbouring cells from the same cluster by chance. These data demonstrate the reliability of our method for detecting whether cells of a cluster localize together, which further supports the above finding.

Overall these data suggest that these distinct dynamics of ERK activity, identified by k-means clustering, do not occur in defined areas of a colony and are therefore unlikely to be mediated by localised cell organisation. This would imply that activation kinetics of ERK is a cell autonomous event, as the dynamics within a cell appear poorly related to its neighbours. However, this analysis has only incorporated the ERK activity profiles of two groups of cells and has been restricted to defined portion of the time series. Analysis of the whole time series, incorporating multiple features of ERK activity dynamics, might provide additional insight into the relationship in ERK activity between neighbouring cells.

To assess how the ERK activity of a cell relates to the dynamics of its nearest neighbours, the cell tracks of all neighbouring cells were correlated using Pearsons correlation coefficient. This was carried out across all FOV and the probability distribution of all the correlation values collected were plotted for each experimental replicate, represented by the blue line in the graphs of Figure 5.8. Each cell was sequentially correlated to all other cells in the population, excluding those it neighboured, and an average of these correlation values was recorded. The average correlation value assigned to each cell, that represents comparisons between all cells in the population, were pooled from all FOV and the probability distribution of these

correlation values was plotted (red line) for all experimental replicates, as shown in Figure 5.8. Tracks lengths will vary in length as a result of cell divisions or cells being lost during tracking. Correlations between cells tracks that overlapped by less than 10 frames were discounted from the data set.

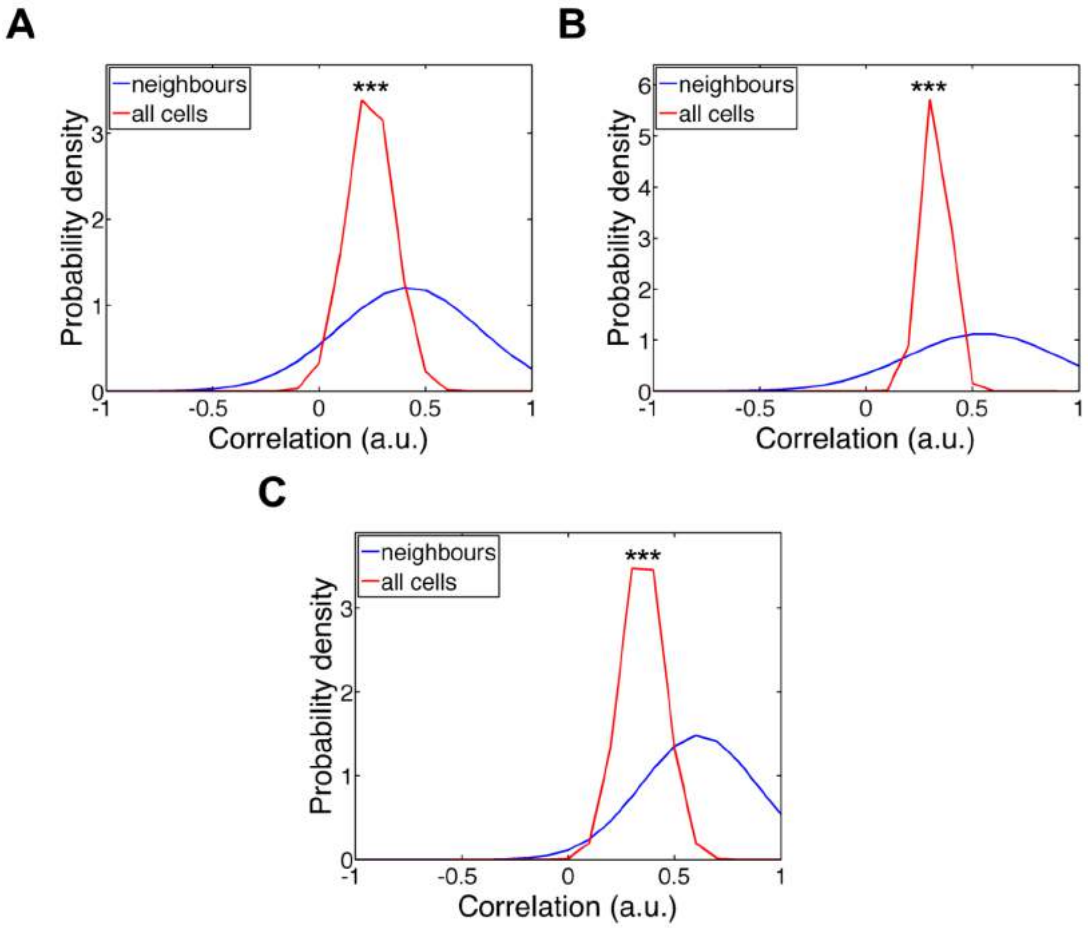


**Figure 5.8: Comparing the ERK activity of neighbouring cells in relation to correlations between all cells in a population.** Each cell was correlated to its nearest neighbours (blue) and all other cells (red) in the first frame of each FOV using Pearsons correlation coefficient. Correlation values were pooled from all FOV in an experiment and the probability distribution of values collected is shown for (A) experiment 1, (B) experiment 2, and (C) experiment 3. Data was fitted using the 'normpdf' function in MATLAB. Wilcoxon signed ranks test identified a statistically significant difference between the correlation values of neighbouring cells and correlations of all cells in a population in all three experimental replicates.*** signifies probability of $\leq$0.001

Correlation values calculated between neighbouring cells were found to be of an overall higher distribution compared to correlations between all cells of a population (Figure 5.8). The distribution of correlation values between neighbours and all cells was found to be statistically significantly in all three replicates by Wilcoxon signed ranks test, implying that cells are more similar to their neighbours, in terms of ERK activity, than they are to other cells within the colony. It important to consider that correlation values were calculated using neighbours assigned to each cell at the start of the time-lapse, which could result in the inclusion of correlation values between cells that are no longer neighbours. As motility of ES cells is relatively negligible during exit from pluripotency, the cells immediately surrounding one another are unlikely to change and the correlation of neighbouring cells at the start of each time-lapse should provide a good indication of how ERK activity dynamics of neighbouring cells relate to one another.

To test this finding further I decided to measure the mean difference in FRET ratio levels between neighbouring cells. FRET levels were averaged for each cell and differences in average FRET values between cells that neighboured one another was recorded. Differences in ERK activity of neighbouring cells were pooled from all FOV and the average of these values, for each experimental replicate, is represented by the observed (Obs) bar shown in Figure 5.9. Neighbours were then randomly assigned to each cell, using a bootstrapping approach, and the mean difference in ERK activity between randomly assigned neighbours was calculated. This procedure was repeated 1000 times for each FOV of an experimental replicate and the average difference in ERK activity from these randomized data sets (Rnd) was calculated (Figure 5.9). A statistically significant difference in the mean difference in ERK activity of observed neighbours (Obs) compared to those that were randomly assigned (Rnd) was identified for all three experimental replicates. These data therefore further substantiates the idea that ES cells in close proximity to one another display more similar levels of ERK activity. It is important to note that neighbours have been assigned based on nuclei coordinates, and there may be cell contact sites that fall outside of this 30 pixel assigned radius. The presence of

a membrane dye, would facilitate the identification of neighbouring cells and could provide a more accurate representation of the spatial arrangement of cells within an ES cell colony from which to analysis the positional affects of ERK signalling.

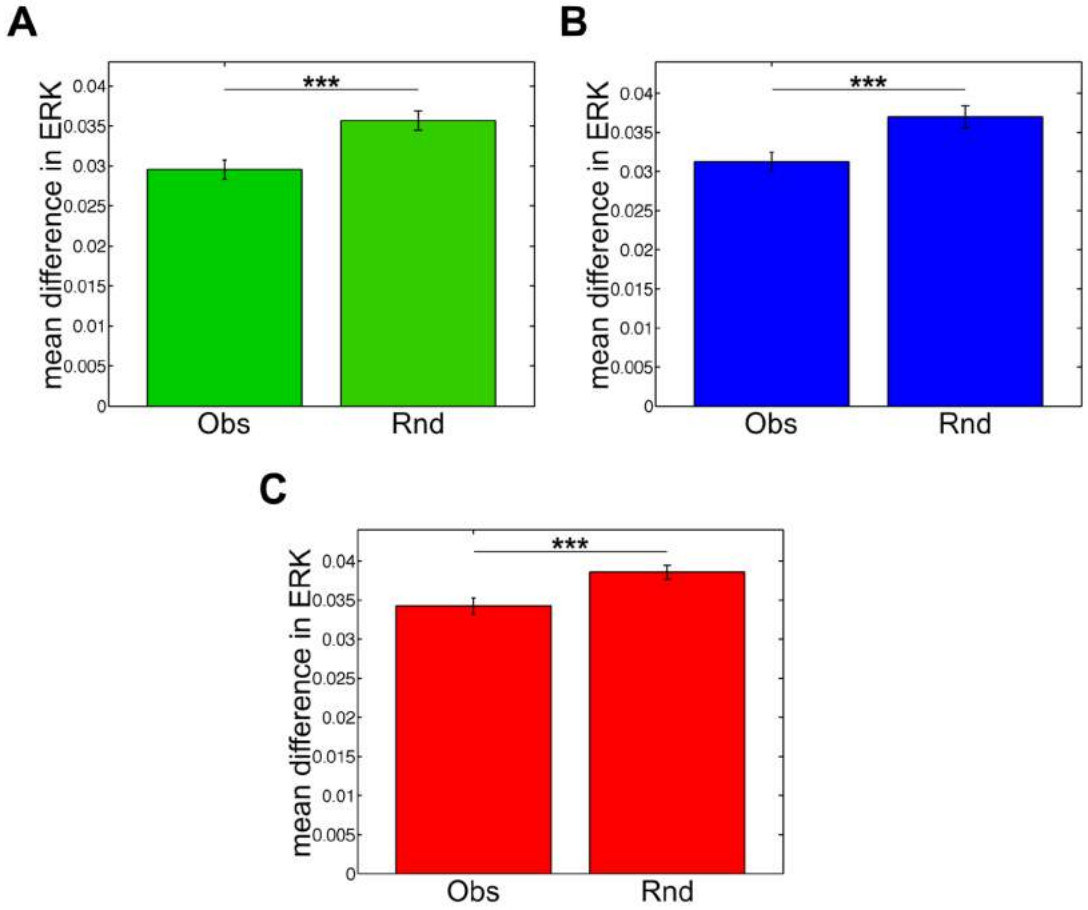


**Figure 5.9: Differences in ERK activity between neighbours and neighbours randomly assigned by bootstrapping.** Mean difference in ERK activity between neighbours (Obs) and randomly assigned neighbours (Rnd) are shown for (A) experiment 1 (green), (B) experiment 2 (blue), and (C) experiment 3. Error bars represent the standard deviation (Obs) and standard error (Rnd) from the mean. A statisitically significant difference between Obs and Rnd values was identified by Wilcoxon ranks sum test. *** signifies $p \leq 0.001$

## 5.6 Investigating the ERK dynamics of daughter cells

I have shown how the positional coordinates generated during tracking can be used to study the effects local environmental factors have on ERK activity, and have shown cells in close proximity to display similar ERK activity dynamics.

Similarities in the behaviour of ES cell have also been associated with inheritance and closely related cells have been shown to have more similar cycle times and expression patterns of pluripotency markers (Cannon et al., 2015; Kumar et al., 2014). Could the similarities in ERK activity between cells observed here be the result of inheritance rather than proximity?

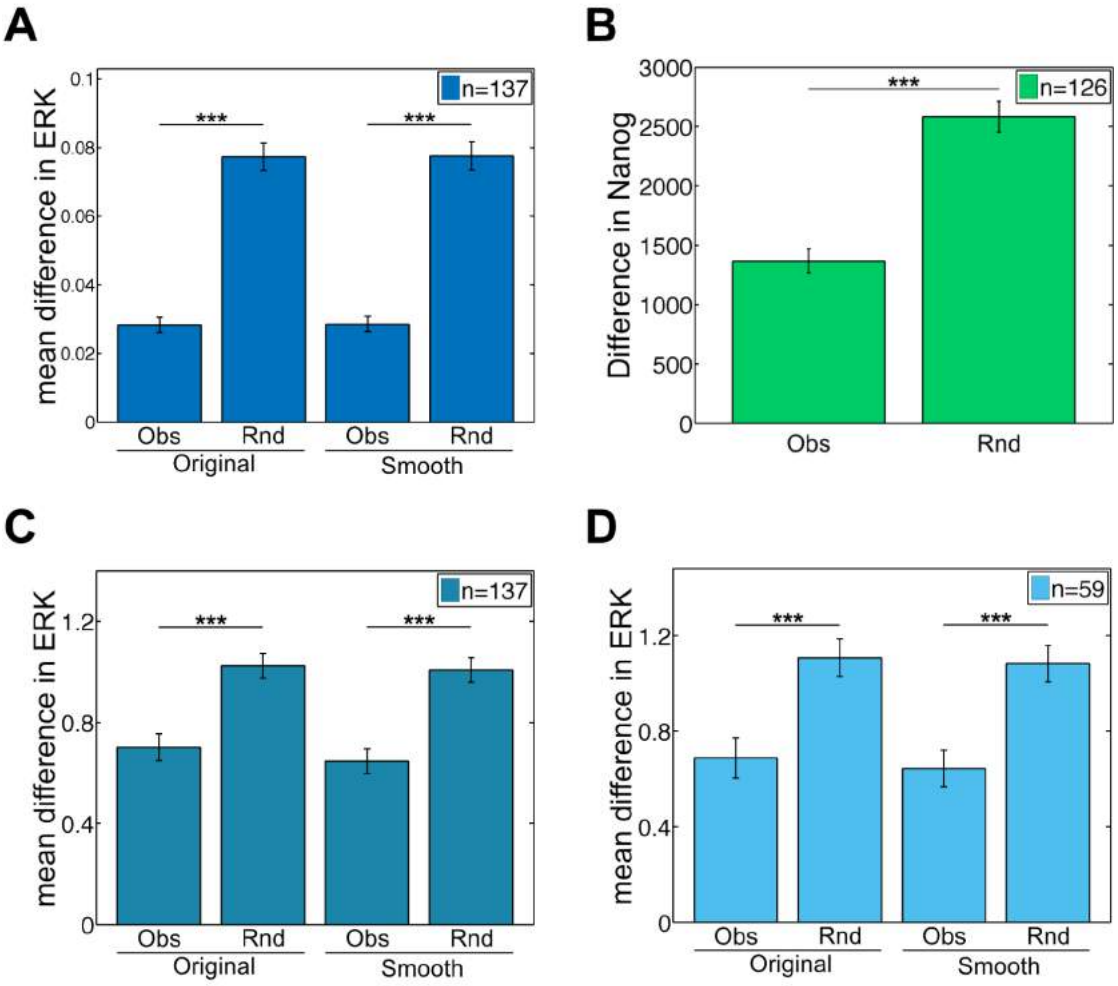


**Figure 5.10: Differences in mean ERK activity of daughter cells.** (A) Differences in mean ERK activity of daughters (Obs) and differences following re-sampling of the data by bootstrapping (Rnd). Analysis was carried on both raw (original) and filtered (smooth) FRET tracks of daughter cells. (B) Differences in quantified Nanog intensity of daughters (Obs) and randomised daughter Nanog intensities (Rnd). (C) Differences in mean ERK activity of Obs and Rnd daughters following normalisation. (D) Differences in normalised mean ERK activity of daughters pairs from experimental replicate 3. Statistical significant differences shown were calculated using Wilcoxon ranks sum test.*** signifies $p \leq 0.001$

To address this question, cell tracks (n=137) for daughter pairs were extracted from each experimental replicate and pooled. The first five frames of each daughter track was removed from the FRET data prior to analysis due to the convolution effects generated by the mitotic shape of cells immediately after division, which can introduce artefacts into the FRET levels being tracked (Cannon et al., 2015). Differences in the mean ERK activity of each daughter pair was calculated, and is referred to as the observed (Obs) difference between daughters, as shown in Figure 5.10A. The mean ERK activity of daughters was subsequently randomized using a bootstrapping approach. Mean ERK activity values of randomised daughters were re-sampled 1000 times and differences in mean activity between daughters was calculated for each of the randomized data sets. The average difference in mean ERK activity of randomized data (Rnd) is presented in Figure 5.10A.

A non-parametric Wilcoxon ranks sum test identified a statistically significant increase in the measured differences between daughters following randomisation of the data (Figure 5.10A), implying that closely related cells display more similar levels of ERK activity. This trend was consistent following analysis on original and smoothed data, signifying that similarity had not been introduced by smoothing (Figure 5.10A). The difference in Nanog expression between daughter pairs was also calculated and randomization of these values, using the same approach, resulted in a significant increase in the average difference in Nanog between pairs (Figure 5.10B). These findings are in agreement with a previous work (Cannon et al., 2015) that showed expression of a reporter for Nanog to be more strongly correlated in closely related cells of a lineage and stable along cell lineages (Singer et al., 2014; Filipczyk et al., 2013).

In order to generate a large data set for this analysis daughter pairs were pooled from all three experimental replicates. Consequently, this increased difference in ERK activity following the randomization of daughters could result from the random sampling of pairs from different experimental days. In addition, random sampling currently does not take into account the portion of the time series in

which a daughter appears. For example, daughters of earlier dividing cells that appear during the initial peak in activation will have a tendency to be different from randomly selected daughters that appear later in the time series when cells exhibit overall lower levels of ERK activity. To address these issues the mean ERK activity of each daughter was normalised to the average ERK activity of cells, from the same replicate, for the same segment of time. Differences in the ERK activity between daughters were calculated, following normalisation and normalised mean ERK activity values of daughters were subsequently randomised, using the same bootstrapping. Differences between randomised pairs was then calculated for each re-sampled data set (Figure 5.10C).

Randomisation of normalised mean ERK activity values resulted in a statistically significant increase in the difference in ERK activity of daughter pairs (Figure 5.10C). These findings are in agreement with the bootstrapping analysis carried out on the non-normalised mean ERK activity levels (Figure 5.10A), indicating that the shared time range of daughter pairs is not the underlying cause of this observed similarity. However, normalisation did lead to a reduction in the degree of separation between the mean differences in ERK activity of the observed (Obs) and randomised (Rnd) pairs, suggesting the similarity between daughters to be partially influenced by when they appear within the time series (Figure 5.10C). In order to investigate if increased differences in ERK activity were caused by random sampling of pairs between replicates, the analysis was repeated to only include the daughter pairs from one experimental day. Analysis was carried out on experimental replicate 3, which has the highest proportion of daughter pairs (n=57), using normalised values of mean ERK activity (Figure 5.10D). A significant increase in the mean differences in ERK activity of randomized pairs could still be identified following analysis of replicate 3, with observed and randomized pairs exhibiting similar differences in ERK activity to daughters pooled from all three replicates (Figures 5.10C and D).

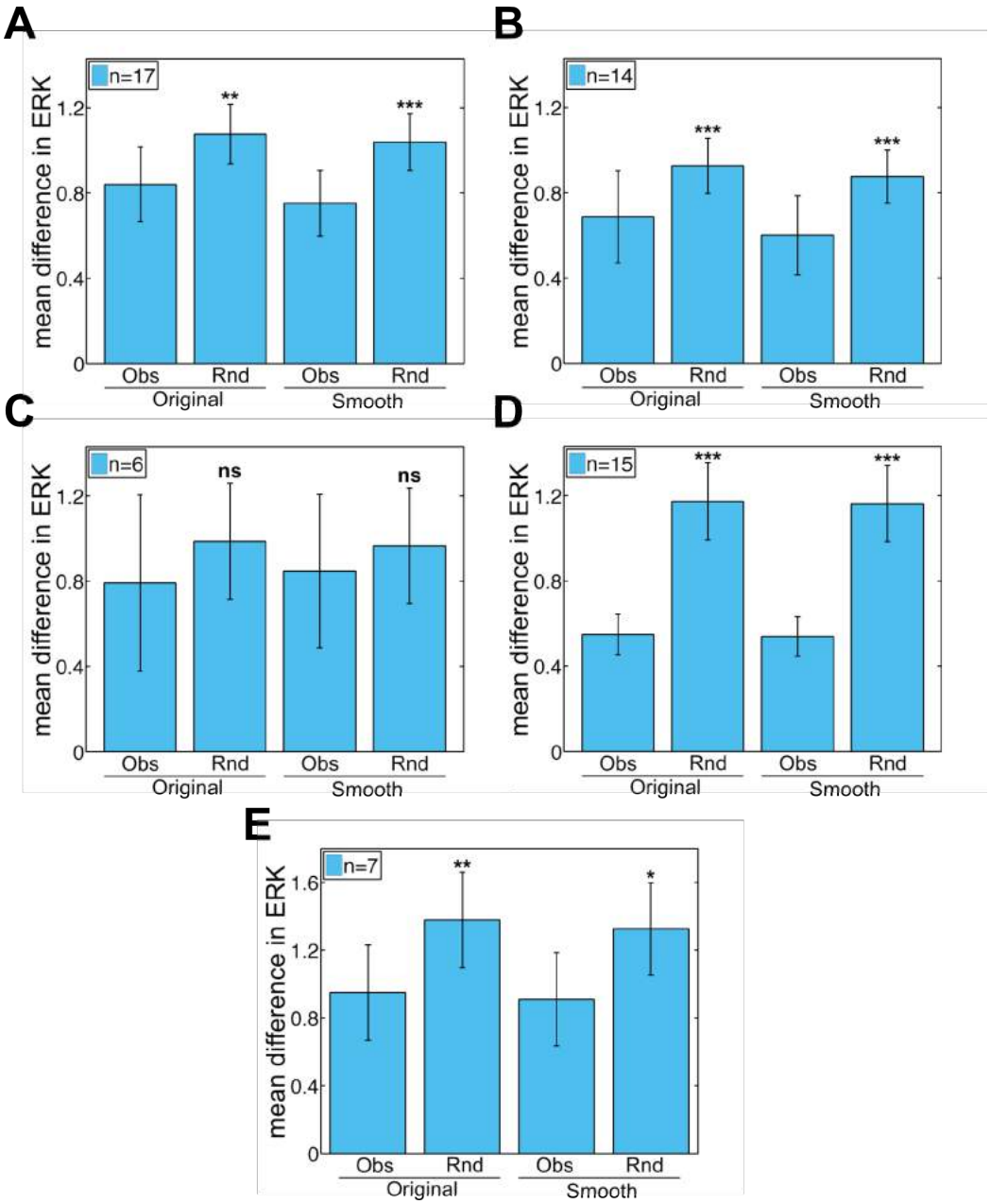


**Figure 5.11: Differences in mean ERK activity of daughter cells within a single FOV** Differences in mean ERK activity of daughters (Obs) and differences following re-sampling of the data by bootstrapping (Rnd). Analysis was carried on both raw (original) and filtered (smooth) FRET tracks of daughter cells. (A) corresponds to FOV 1, (B) FOV 2, (C) FOV 3, (D) FOV 4, and (E) FOV 5. Differences in ERK activity or randomised pairs were compared against observed values using Wilcoxon ranks sum test.*** signifies $p \leq 0.001$

Although correlations in the ERK activity behaviour of daughter cells does not appear to be effected by experimental replicate, it is possible that increased differences in ERK activity following randomisation may arise from the comparison of cells in different FOV. In order to account for this possibility the same bootstrapping analysis was carried out on daughter pairs from each separate FOV of experiment replicate 3. A statistically significant increase in the measured differences between daughters was once again identified following randomisation of the data for 4 out of 5 FOV (Figure 5.11). A statistically significant difference could not be identified between the observed and randomised pairs in FOV 3, which is likely to result from the small number of daughter pairs being analysed and the enhanced variation in mean difference in ERK activity values, exhibited by the increased error bar size (Figure 5.11C). Consistent with this, the small number of pairs being analysed in the FOV 5 also resulted in a reduced level of significance in the mean difference in ERK activity between observed and randomised pairs (Figure 5.11C). Although not significant randomisation of daughters within these FOV did result in an increased difference in ERK activity, in agreement with the trends observed in all other FOV. These data collectively demonstrate that similarities in the ERK activity behaviour of daughters are unlikely to be due to differences between FOV.

I next wanted to investigate how similarities in the ERK activity of daughters relates to the proximity between them. Proximity was calculated by measuring the distance between the positional coordinates of daughters at each time point, and the average distance between each pair was plotted against difference in mean ERK activity (Figures 5.12A-C). A significant correlation between distance and difference in ERK activity of daughters pairs could not be identified using Pearsons correlation coefficient in any of the three experimental replicates (Figures 5.12A-C). Correlations were carried out separately for each replicate as experimental variation can perturb correlation values. As a result analysis was limited to the number of available daughter pairs within each experiment, and correlations of such small number of data points could be precluding a relationship between the distance

and ERK activity levels of daughter pairs. To increase the number of data points that could be evaluated, differences in ERK activity between daughter cells was plotted against the distance between them for each time point (Figure 5.12D-F). Comparison between difference in ERK and distance revealed a weak negative correlation in 2 out of 3 experimental replicates (r=-0.1298 p=$1.04\times10^{-05}$ and r=-0.0877 p=$9.31\times10^{-06}$ for replicates 1 and 3 respectively), implying that ERK activity levels of daughters becomes more similar as the distance between them increases (Figure 5.12D-F). However, the correlation between distance and difference in ERK activity of daughter cells that I have observed are very weak and this relationship could not be identified in all three experimental replicates. Overall these data suggest the degree of similarity in the ERK activity behaviour of daughters is not strongly related to intercellular distance.

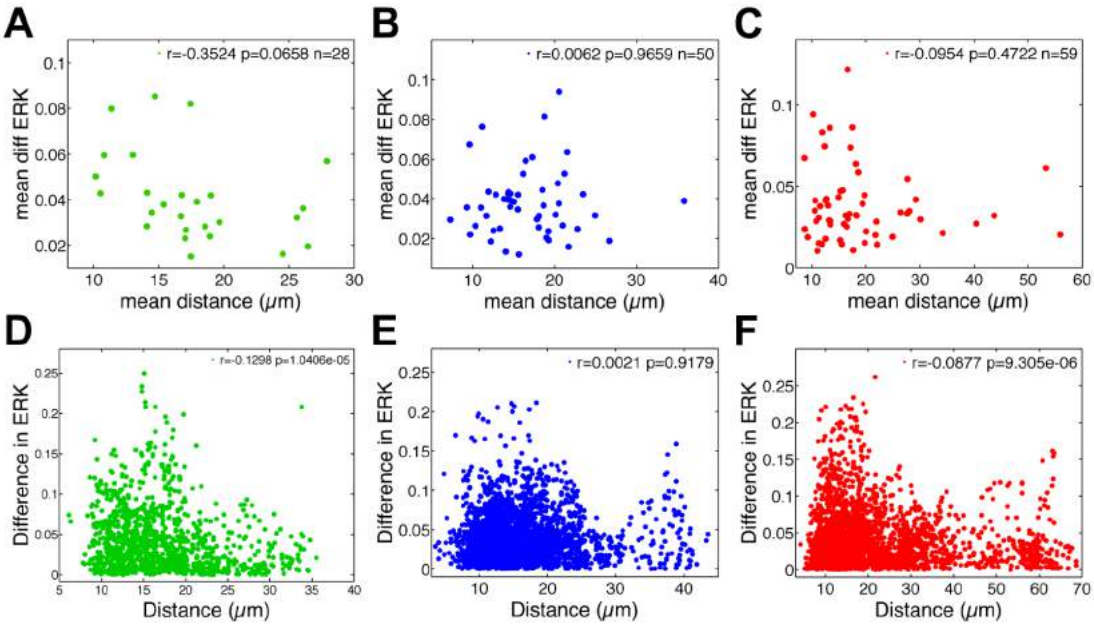


**Figure 5.12: Comparison of intercellular distance and difference in ERK activity of daughters.** (A-C) Scatter plots of mean distance and difference in mean ERK activity between daughter pairs of (a) experiment 1 (green), (b) experiment 2 (blue), and (c) experiment 3 (red). (D-F) Scatter plots of difference in ERK activity and distance between daughters at every time-point of (d) experiment 1, (e) experiment 2, and (f) experiment 3. Pearson's correlation coefficient value of each experiment are shown on the corresponding scatter plot

## 5.7 Summary

In this chapter I have shown how our method for monitoring the ERK activity of individual cells can be used to examine the spatial regulation of ERK activity within an ES cell colony. Using the positional coordinates generated during tracking I have investigated the effects of environmental factors, such as density and neighbouring interactions, on ERK activity levels. The findings shown here would imply that differences in the density of the local environment of a cell could act as a determinant for ERK activity dynamics (Figures 5.3 and 5.4). I have demonstrated a general trend of cells in the centre of colonies, where density is higher, to display lower levels of ERK activity compared to cells at the edge less densely populated regions (Figure 5.2). In contrast, I have also identified a positive correlation between Nanog expression and cell density; high density resulted in enhanced Nanog expression compared to areas of low density (Figure 5.5). By comparing the ERK activity of neighbouring cells, using correlation and bootstrapping approaches, I have found cells of close proximity to display more similar ERK activity kinetics (Figures 5.8 and 5.9). Collectively, these data would support the idea that local environmental influences are able to modulate ERK activity and Nanog expression within an ES cell colony.

Examination of the ERK activity of daughter cells showed cells of the same inheritance to exhibit more similar ERK activity behaviours (Figure 5.10). Previous work by Cannon et al. (2015) showed similarities in between daughters, in terms of Nanog expression, remained the same regardless of the distance between them. The data I have shown, for ERK dynamics, is in accordance with this finding as I was unable to identify a clear correlation between differences in the ERK activity of daughters and the overall distance between them (Figure 5.12). These findings suggest closely related cells display similar ERK activity behaviours and similarities in the ERK activity of daughters is likely to be the result of inheritance rather than environmental regulation. Conversely, I have also shown cells in close proximity of one another to exhibit more similar ERK activity levels, arguing the case for

local environment induced similarities in ERK signalling. As cell motility within ES cell colonies is relatively limited during these early stages of differentiation, it is possible that the neighbours being correlated descend from the same lineage and are likely to be more similar to one another as a result.

Here I have shown novel approaches that can be applied to the quantitative single-cell study of activity dynamics in ES cell colonies, and have provided a detailed analysis of how environmental factors influence ERK activity. These approaches will facilitate our understanding of how differences in the spatial organisation of ERK signalling regulates the transition from naïve pluripotency towards lineage commitment.

# Chapter 6

# Discussion

## 6.1 Summary of Results

This work presents a new quantitative single cell study of ERK activity in ES cells, which has begun to elucidate a potential role for ERK dynamics in governing the pluripotent state. A protocol was established for using the FRET based biosensor, EKAREV, to monitor the dynamics of ERK at the single cell resolution. Ratiometric FRET imaging was carried out using a wide-field system, and images were processed in imageJ and quantitatively analysed using a MATLAB curated single cell tracking approach. ERK activity dynamics of each cell were compared to its corresponding pluripotent state 16h after the induction of differentiation, using Nanog expression as a inverse read-out of the extent of differentiation. Quantitative analysis of this data was unable to find a strong correlation between mean ERK activity and Nanog intensity at the single level. Data driven clustering of dynamic ERK profiles revealed two distinct responses of transient and sustained activity that were robustly found across multiple experiments. However, a consistent relationship between these distinct patterns of behaviour and the expression levels of Nanog could not be identified.

Additional analysis tools were applied to quantify the local cell density environment of each cell and to compare the ERK activity behaviour of neighbouring cells. These data identified ERK activity levels to be influenced by local cell density, with cells in densely population areas of a colony exhibiting reduced levels of ERK activity compared to cells in low density areas. Density was also found to influence the initial kinetics of the ERK activity response following the induction of differentiation, shown by differing basal levels and amplitude in activity reached. In addition to a cell density affect, the neighbours of a cell were found to display a more similar ERK activity response in relation to the rest of the population, indicating a potential local environment signalling affect. Extraction and analysis of the ERK activity dynamics of daughter cells also identified an increased similarity in activity between daughter pairs, with similarity between daughters being independent of the portion of the time series, experimental day, and FOV in which they appeared. Similarities in the ERK activity behaviour of daughters appeared to be largely independent of the proximity between them, implying that similarities between neighbours could arise from inheritance rather than increased proximity. Overall, these data suggest a strong cell autonomous contribution to the strength of ERK signalling.

## 6.2 ERK activity as a regulator of Nanog expression

Advancements in single cell technology and use of fluorescent reporters have highlighted the potentially dynamic nature of the pluripotent state, in which cells display varying levels of pluripotency factors, influencing their ability to respond to differentiation cues. The pluripotency factor Nanog could be considered to be the 'poster child' of this metastable pluripotent state, due to its heterogeneous expression under serum/LIF culture conditions, and ability to revert cells between a high expressing state of increased self-renewal capacity and low expression state that primes cells for differentiation (Chambers et al., 2007). The timescale of these fluctuations is now established as occurring over several days, which questions the biological relevance of the changing expression levels- for example

in the blastocyst, where Nanog is only expressed for around 2 days. However, the discovery of these fluctuating states has led to a desire to understand the mechanisms driving this switch between states. The FGF4/ERK signalling pathway is often proposed to be a key component of the heterogeneous expression pattern of Nanog, as inhibition of this pathway results in a more uniform expression (Ying et al., 2008). ERK activity has been shown to negatively regulate the expression of Nanog, with Nanog levels decreasing with increasing levels of ERK activity (Hamazaki et al., 2006; Santostefano et al., 2012). However, a robust correlation between ERK activity levels and Nanog expression could not be identified at the single cell level (Figures 3.1 and 4.6). This may relate to a recent report that was unable to distinguish a relationship between the levels of Nanog and a transcriptional reporter for Sprouty, which was used as read out of ERK activity, within individual cells under serum/LIF conditions at a single snapshot in time (Morgani et al., 2018b).

This, however, leads into the question of what are the reasons for this weak relationship in Nanog expression and ERK activity levels within individual cells? One possibility, which I shall discuss in more depth shortly, is that dynamics rather than absolute levels of ERK, play a more important role in regulating the pluripotent state of an individual cell. Alternatively, if we think of ERK activity acting as a threshold between a self-renewing and lineage primed state (Yang et al., 2012; Hamilton et al., 2013), ERK activity may only be related to extreme scenarios of Nanog expression. In this view, cells expressing intermediate levels of Nanog will be poorly correlated with ERK activity and their inclusion in correlation calculations of ERK activity and Nanog expression could be perturbing the identification of a relationship between these two variables. In addition, the maintenance of ERK activity above the threshold required to induce the low Nanog expressing lineage primed state may be dependent on the level of flux through the ERK signalling pathway. Borrowing ideas from metabolism (Azeloglu and Iyengar, 2015), flux represents the rate of turnover of molecules within a pathway and measurements of the active state of ERK may not necessarily be comparable

to the rate of flux through the ERK signalling pathway. Consequently, although a cell is exhibiting a high level of ERK activity, demonstrated by increased pERK levels, the rate of flux may be too low to maintain ERK activity above the required threshold preventing a transition into the lineage primed state. Following the ERK activity kinetics of individual ES cells under serum/LIF conditions in relation to the changing expression of Nanog could further elucidate how ERK activity is able to regulate this dynamic heterogeneity.

In terms of dynamic variation in ERK activity, I was particularly interested in the activation profile of ERK during exit from the naïve state and subsequent entry into lineage commitment. In agreement with previous reports (Yang et al., 2012; Nett et al., 2018), a pulse in ERK activity was identified following the induction of differentiation by the removal of 2i/LIF (Figure 4.5). Monitoring of the ERK activity dynamics of individual cells showed a large amount of cell-cell variation in the kinetics of this initial response. However, distinct features of this pulse such as amplitude, initial base level, and time to reach half-maximal, were all found to be weak predictors of the Nanog expression levels detected 16h post 2i/LIF withdrawal. Clustering of dynamic profiles of ERK revealed two distinct responses of transient or sustained activity following 2i/LIF removal, with cells of the sustained cluster exhibiting an overall reduced expression in Nanog. However, it is of note that the relationship between these two dynamic profiles and Nanog expression constitutes a weak affect and was not reproducible across all three experimental replicates.

Understanding the weak coupling between differentiation rate and ERK activity is informed by a recent study on RSK, a negative regulator of ERK (Nett et al., 2018). In the absence of RSK, ESCs have elevated levels of ERK phosphorylation and precociously exit pluripotency and differentiate, in population level measurements. Our findings, in single cells, of weak coupling between ERK activity and the rate of differentiation are compatible with the RSK study. Our approach is to monitor the normal dynamic range of ERK signaling, with the regulation governing ERK

activity levels, such as by RSK, intact. We propose that the strong effects of RSK depletion on the differentiation response, compared to the weak effects we observe, occur because this perturbation takes cells out of the normal dynamic range

Further clustering of later stages of the time series suggested differences in the expression of Nanog could be mediated by ERK activation kinetics after the initial pulse response (Figure 4.13). Although, dynamics within this pulse have previously been shown to be of importance in the regulation of cell fate choices (Yang et al., 2012), it has recently emerged that a second pulse in ERK activity may also be of relevance in controlling the exit from the naïve sate (Nett et al., 2018). This second pulse in ERK activity becomes apparent around 15-16h post 2i removal, and is therefore likely to have been excluded from our dataset due to the imaging time course used. Longer time-scale monitoring of ERK activity could potentially indicate additional heterogeneity within this second pulse that may be more correlated with Nanog expression levels. However, is must be stated that we see strong Nanog down-regulation by 16h, even without a second peak in ERK, suggesting any effects of a second peak might be minor, at least as far as Nanog is concerned. FRET time-lapse imaging of cells over 16h causes a loss in cell vitality and an increased occurrence of photobleaching, perturbing the possibility of extending the experimental time course in order to factor in this second peak. A potential alternative would be to begin imaging after the initial induction of differentiation, following this initial pulse response that has already been examined in depth, and investigating the relationship between ERK activity and Nanog expression at a later stages of the differentiation time course.

Another important thing to consider in the work I have shown here, is that at present I have only compared ERK activity dynamics to the expression of Nanog. However, the experimental system I have created can also be applied to study of additional markers involved in the exit from the naïve state. For example, recent work has shown ERK activity to be a key mechanism in the down regulation kinetics of the pluripotency factor Klf4, which in turn is able to down-regulate the expression of

Nanog and subsequent exit from the naïve state (Dhaliwal et al., 2018). As well as factors of the naïve pluripotency network, ERK activity has also been associated with the lineage priming factor Tcf15, which when activated rapidly induces the down-regulation of Nanog (Davies et al., 2013). Thus, imaging of additional factors, that act upstream of Nanog, using the method I have described, could facilitate our understanding of how FGF4/ERK signalling is able to regulate the molecular changes involved in the transition from the naïve state.

## 6.3 ERK activity and the microenvironment of ES cells

Having measured the ERK activity dynamics of cells following the onset of differentiation, I was next interested to see how these dynamics related to the spatial arrangement of ES cells within a colony. Quantification of the density of the environment surrounding each cell identified ERK activity to be negatively correlated with increasing density, with cells in densely populated areas exhibiting overall reduced levels of ERK activity than cells in lower density areas (i.e. at the colony edge) (Figure 5.2). In contrast, Nanog expression was found to be positively correlated to cell density, with cells in a high density environment demonstrating an increased expression in Nanog (Figure 5.5).

Localised differences in cell density have previously been shown to influence the expression levels of Nanog (Cannon et al., 2015). Furthermore, an overall decrease in Nanog expression, and its downstream target Rex1, towards the colony edge has also been identified, providing further indication of a possible cell density dependent effect (Hamazaki et al., 2006; Herberg et al., 2015). It is currently unclear how the spatial patterning of these pluripotency markers arise. A possibility, from the findings I have shown here, is the spatial distribution in Nanog expression is the consequence of cell density dependent differences in ERK activity, although the apparent inverse coupling between ERK activity and density was not completely penetrant in all replicas. A cell density dependent affect on ERK activity has

been seen in NRK cells, with ERK activity decreasing with increasing density, thus in agreement with the cell density dependent relationship our data suggests, albeit weakly (Aoki et al., 2013). At this stage it remains unclear the mechanisms driving this density dependent effect in ERK activity. It is possible the increased compaction of cells in highly dense areas of the colony could cause a reduction in the number of available receptors limiting the ability to respond to autocrine and paracrine released FGF. Alternatively, contact regulated inhibition or reduced endocytosis may also be potential mechanisms of cell density mediated control and further experiments would be needed to examine these possibilities.

Local differences in the stem cell microenvironment, such as the make up of surrounding cells and the local density have been shown to mediate the differentiation potential of ES cells (Lorincz, 2006; White et al., 2013). From the data I have shown it appears both these features may contribute to regulating the ERK activity behaviour of ES cells (Figures 5.2 and 5.8), consistent with previous reports demonstrating levels of secreted endogenous factors to be related to the density and local cell organisation within an ES cell colony (Peerani et al., 2009; Moledina et al., 2012). Thus the environmentally controlled differences in ERK activity I have observed could be mediating the spatial patterning associated with the loss of pluripotency. Indeed, a recent mathematical model showed the rate of transition between pluripotent states to be highly dependent on changes in a cell's local environment, such as density and position within a colony (Strasser et al., 2015). Furthermore, an additional model has shown negative FGF4/ERK signalling between adjacent cells to be a key intercellular regulator of pluripotency in ES cells (Herberg et al., 2015). Taken together these findings suggest that the spatial heterogeneity of the signalling environment, as well as temporal variation in response, is likely to be an important feature of regulation in controlling the stem cell fate.

## 6.4 Understanding potential causes of local similarity in the ERK signalling dynamics of ES cells

From the data I had collected I was also able to extract information on the behaviour of daughter cells in regards to their ERK activity and their positional relationship to one another over the course of time. Examination of the ERK activity of daughters, using a bootstrapping approach, showed daughter pairs to display similar ERK activity behaviours (Figure 5.10). Comparisons of ERK activity between neighbouring cells implied cells of a closer proximity displayed a more similar activity profile of ERK (Figures 5.8 and 5.9) . However, similarities in the ERK activity of daughters was unrelated to the distance between them (Figure 5.12), bringing into question whether similarities in ERK activity based upon proximity result from either 1) Proximity dependent local environment influences or rather 2) Inheritance of regulators that are able to modulate the output levels of ERK.

From the study of differences in ERK activity between daughters in relation to their distance, it appears that similarities in activity are more likely to be the consequence of inheritance rather than proximity. However, it is important to take into account that without visualising cell membranes we are unable to determine the degree of contact between daughter and neighbouring cells. Consequently, the distances calculated could be providing a distorted view of proximity, making it difficult to establish a correlation between distance and similarities in the kinetic behaviour of ERK activity. Although proximity was found not to influence the degree of similarity between daughter cells, local environmental influences within a colony could still be mediating the overall increased comparability in the ERK activity behaviour of daughters and neighbouring cells. For example, local cell density differences may be causing comparable responses in ERK activity of neighbours by mediating the degree of contact between cells. Comparing the density of a cells environment to its level of correlation with its neighbours could potentially identify a link between these two effects. In addition, understanding whether cell-cell contact is a requirement of these observed similarities, for example by inhibiting

the function of E-cadherins, which have a known role in maintaining the pluripotent state (Redmer et al., 2011), could also help elucidate the importance of proximity in regulating the ERK activity behaviour of neighbouring and daughters cells.

Inheritance, however, could still be the principle cause of similarity in the ERK activity dynamics between neighbouring and daughter cells. Similarities in the ERK activity of behaviour of daughters was found to be independent of their colony context, with daughter cells exhibiting a greater degree of similarity to one another than other daughter cells within the same colony. This finding, taken together with the observation that similarities between daughters are largely independent of proximity, supports the idea that inheritance rather than location is a more important regulator of similarity between daughter and neighbouring cells. A retained memory of protein state across generations has previously been proposed to influence the behaviour of individual cells, with proteins from the same pathway being more correlated to one another than proteins from different pathways (Sigal et al., 2006). As the FGF4/ERK pathway is not involved in cell cycle progression of ES cells (Burdon et al., 2002), it is possible that regulatory mechanisms within the ERK pathway continue to remain, even once a cell has divided. Thus the shared similarity in the behaviour of daughters could arise from the inheritance of molecules involved in the regulation of the ERK activity. For example, phosphatase inhibitors are known to negatively regulate ERK activity over a period of hours following transcription (Patterson et al., 2009), and equal inheritance of these factors between daughters could lead to an initial similarity in ERK dynamics. Measuring the differences in the levels of known negative regulators of the ERK signalling pathways, such as DUSP1/6 and RSK1, in dividing cells and subsequent daughter pairs could further inform these ideas.

## 6.5 Future Directions

Two emerging themes from this thesis stand further investigation. Firstly, we observed only a weak correlation between ERK activity and rate of exit from

pluripotency. This suggests that the decision to exit pluripotency is distributed over more of the signalling network of the cell. It would therefore be useful to gain a more comprehensive assessment of the dynamics of the signalling network, by combining an ERK biosensor with sensors for other pathways. As the FRET sensor is difficult to combine with multiple fluorophores, it would make more sense here to use a localisation reporter for ERK activity such as ERK-KTR (Regot et al., 2014). Other local parts of the network to consider in this analysis would be WNT/GSK3/Akt/-catenin hub and the LIF-JAK-STAT3 pathway. These pathways could be monitored using a STAT3 localisation reporter (Cimica et al., 2011) and a transcriptional reporter to Wnt/-catenin signalling (Ferrer-Vaquer et al., 2010). As well as imaging other sensors of signalling pathways, application of the ERK-KTR reporter would allow for simultaneous imaging of live single cell reporters for Nanog (Xenopoulos et al., 2015; Ochiai et al., 2014b), and other pluripotency factors. Monitoring of the dynamic behaviour of Nanog in relation to changing dynamics in ERK could potentially infer a much stronger correlation.

In addition to alternative reporters for monitoring ERK activity, optogenetics has also emerged as alternative tool for investigating how ERK activity dynamics regulate specific cellular outcomes (Toettcher et al., 2013). As aforementioned, I showed clustering to identify two distinct patterns of ERK activity, which could potentially be influencing the expression of Nanog and the rate of exit from the naïve state (Figure 4.11). Optogenetics allows for the direct manipulation of the temporal pattern of ERK activity, through a light inducible Ras (Toettcher et al., 2013), and could be used to mimic these distinct dynamic profiles and determine their functional significance in modulating the ES cell pluripotent state. Although other pathways activated by Ras, such as PI 3-kinase, would also need to be accounted for.

Secondly, I observed environmental effects on ERK and similarities in the ERK activity between daughter cells. These data may reflect the potential of cells and their sensitivity to extracellular influences in normal development. So it would

be obvious to apply our ERK FRET approach in a more realistic developmental context. Initially, this could involve monitoring the ERK activity of ES cells during later stages of development. For example monitoring ERK activity in EpiSCs, which have the capacity to develop into multiple cell types *in vitro*. Monitoring of ERK activity could then be compared against markers of different fates - such as neural (Sox1) (Pevny et al., 1998), mesoderm (Foxa2) (Burtscher and Lickert, 2009), or cardiomycocyte (Cer1) (Liu et al., 2014). The final destination of this line of work would ultimately be the embryo itself. How do ERK dynamics relate to the TE/ICM and PrE/EPI cell fate decisions in the pre-implantation mouse embryo? The FGF/ERK signalling pathway is a known to be essential for formation of the PrE in early embryos and down-regulation of Nanog and other naive factors during EPI maturation (Silva et al., 2009). Could the environmental affects I have observed in terms of density and increased similarity between neighbours be of relevance in the fate choices of the embryo? Indeed, changing the position and environment of a cell in the embryo has been shown to influence its fate, and its possible that this may be concurrent with the spatial regulation of ERK (Grabarek et al., 2012).

A convenient in vitro way-point to the embryo-proper would be to image FRET dynamics in embryoid bodies (EBs) that mimic the structure of the morphogenetic micro-environment of the early embryo (Itskovitz-Eldor et al., 2000; Bratt-Leal et al., 2009). Cells within these EBs are able to spontaneously differentiate in response to their engineered 3D micro-environment and the monitoring ERK activity dynamics within these structures, could be a possible strategy for investigating the relationship between spatial patterning of the embryo and environmentally controlled differences in ERK activity.

In this work I have provided an analytical framework for studying the ERK activation kinetics of ES cells at a single cell resolution, in relation to the pluripotent state and in the context of the spatially diverse environment of an ES cell colony. To my knowledge, many of the approaches I have shown here have not previously been applied to the study of ERK activity in ES cells providing a new perspective

on how ERK is temporally and spatially regulated within an ES cell colony. Overall our observations point to the insights that can be gained by following biochemistry inside living single cells over time during differentiation, and application of this system to additional developmental contexts could provide further insights into the mechanisms contributing to cell decision-making.

# Bibliography

Abranches, E., Guedes, A. M. V., Moravec, M., Maamar, H., Svoboda, P., Raj, A., and Henrique, D., (2014), Stochastic NANOG fluctuations allow mouse embryonic stem cells to explore pluripotency. *Development (Cambridge, England)*, 141(14):2770–9.

Acampora, D., Di Giovannantonio, L. G., and Simeone, A., (2013), Otx2 is an intrinsic determinant of the embryonic stem cell state and is required for transition to a stable epiblast stem cell condition. *Development (Cambridge, England)*, 140(1):43–55.

Ahmed, S., Grant, K. G., Edwards, L. E., Rahman, a., Cirit, M., Goshe, M. B., and Haugh, J. M., (2014), Data-driven modeling reconciles kinetics of ERK phosphorylation, localization, and activity states. *Molecular Systems Biology*, 10(1):718–718.

Albeck, J. G., Mills, G. B., and Brugge, J. S., (2013), Frequency-modulated pulses of ERK activity transmit quantitative proliferation signals. *Molecular cell*, 49(2): 249–61.

Antolović, V., Miermont, A., Corrigan, A. M., and Chubb, J. R., (2017), Generation of Single-Cell Transcript Variability by Repression. *Current Biology*, 27(12): 1811–1817.e3.

Aoki, K. and Matsuda, M., (2009), Visualization of small GTPase activity with

fluorescence resonance energy transfer-based biosensors. *Nature protocols*, 4 (11):1623–1631.

Aoki, K., Komatsu, N., Hirata, E., Kamioka, Y., and Matsuda, M., (2012), Stable expression of FRET biosensors: A new light in cancer research. *Cancer Science*, 103(4):614–619.

Aoki, K., Kumagai, Y., Sakurai, A., Komatsu, N., Fujita, Y., Shionyu, C., and Matsuda, M., (2013), Stochastic ERK activation induced by noise and cell-to-cell propagation regulates cell density-dependent proliferation. *Molecular cell*, 52(4): 529–40.

Avilion, A. A., Nicolis, S. K., Pevny, L. H., Perez, L., Vivian, N., and Lovell-Badge, R., (2003), Multipotent cell lineages in early mouse development depend on SOX2 function. *Genes and Development*, 17(1):126–140.

Azeloglu, E. U. and Iyengar, R., (2015), Signaling networks: Information flow, computation, and decision making. *Cold Spring Harbor Perspectives in Biology*, 7(4):a005934.

Balázsi, G., Van Oudenaarden, A., and Collins, J. J. Cellular decision making and biological noise: From microbes to mammals, (2011). OPTIISSN 00928674.

Bao, S., Tang, F., Li, X., Hayashi, K., Gillich, A., Lao, K., and Surani, M. A., (2009), Epigenetic reversion of post-implantation epiblast to pluripotent embryonic stem cells. *Nature*, 461(7268):1292–1295.

Becker, W., Bergmann, A., Biskup, C., Zimmer, T., Klöcker, N., Benndorf, K., Ii, P., Jena, D., Karls, E., Tübingen, U., Ii, P., and Tübingen, D. Multi-wavelength TCSPC lifetime imaging. In Periasamy, A. and So, P. T. C., editors, *SPIE BiOS*, volume 4620, pages 79–84. International Society for Optics and Photonics, (2002). doi: 10.1117/12.470679.

Bernstein, B. E., Mikkelsen, T. S., Xie, X., Kamal, M., Huebert, D. J., Cuff, J.,

Fry, B., Meissner, A., Wernig, M., Plath, K., Jaenisch, R., Wagschal, A., Feil, R., Schreiber, S. L., and Lander, E. S., (2006), A Bivalent Chromatin Structure Marks Key Developmental Genes in Embryonic Stem Cells. *Cell*, 125(2):315–326.

Bessonnard, S., De Mot, L., Gonze, D., Barriol, M., Dennis, C., Goldbeter, A., Dupont, G., and Chazaud, C., (2014), Gata6, Nanog and Erk signaling control cell fate in the inner cell mass through a tristable regulatory network. *Development*, 141(19):3637–3648.

Betschinger, J., Nichols, J., Dietmann, S., Corrin, P. D., Paddison, P. J., and Smith, A., (2013), Exit from pluripotency is gated by intracellular redistribution of the bHLH transcription factor Tfe3. *Cell*, 153(2):335–347.

Birtwistle, M. R., von Kriegsheim, A., Kida, K., Schwarz, J. P., Anderson, K. I., and Kolch, W., (2011), Linear approaches to intramolecular Förster resonance energy transfer probe measurements for quantitative modeling. *PloS one*, 6(11):e27823.

Boroviak, T. and Nichols, J., (2014), The birth of embryonic pluripotency. *Philosophical Transactions of the Royal Society B: Biological Sciences*, 369 (1657):20130541.

Boroviak, T., Loos, R., Lombard, P., Okahara, J., Behr, R., Sasaki, E., Nichols, J., Smith, A., and Bertone, P., (2015), Lineage-Specific Profiling Delineates the Emergence and Progression of Naive Pluripotency in Mammalian Embryogenesis. *Developmental Cell*, 35(3):366–382.

Bourillot, P. Y., Aksoy, I., Schreiber, V., Wianny, F., Schulz, H., Hummel, O., Hubner, N., and Savatier, P., (2009), Novel STAT3 target genes exert distinct roles in the inhibition of mesoderm and endoderm differentiation in cooperation with Nanog. *Stem Cells*, 27(8):1760–1771.

Bradley, A., Evans, M., Kaufman, M. H., and Robertson, E., (1984), Formation of germ-line chimaeras from embryo-derived teratocarcinoma cell lines. *Nature*, 309(5965):255–256.

Bratt-Leal, A. M., Carpenedo, R. L., and McDevitt, T. C., (2009), Engineering the embryoid body microenvironment to direct embryonic stem cell differentiation. *Biotechnology Progress*, 25(1):43–51.

Brons, I. G. M., Smithers, L. E., Trotter, M. W., Rugg-Gunn, P., Sun, B., Chuva De Sousa Lopes, S. M., Howlett, S. K., Clarkson, A., Ahrlund-Richter, L., Pedersen, R. A., and Vallier, L., (2007), Derivation of pluripotent epiblast stem cells from mammalian embryos. *Nature*, 448(7150):191–195.

Brummer, T., Naegele, H., Reth, M., and Misawa, Y., (2003), Identification of novel ERK-mediated feedback phosphorylation sites at the C-terminus of B-Raf. *Oncogene*, 22(55):8823–8834.

Buehr, M. and Smith, A., (2003), Genesis of embryonic stem cells. *Philosophical transactions of the Royal Society of London. Series B, Biological sciences*, 358 (1436):1397–402; discussion 1402.

Buehr, M., Meek, S., Blair, K., Yang, J., Ure, J., Silva, J., McLay, R., Hall, J., Ying, Q. L., and Smith, A., (2008), Capture of Authentic Embryonic Stem Cells from Rat Blastocysts. *Cell*, 135(7):1287–1298.

Burdon, T., Smith, A., and Savatier, P., (2002), Signalling, cell cycle and pluripotency in embryonic stem cells. *Trends in Cell Biology*, 12(9):432–438.

Burtscher, I. and Lickert, H., (2009), Foxa2 regulates polarity and epithelialization in the endoderm germ layer of the mouse embryo. *Development*, 136(6): 1029–1038.

Cadiñanos, J. and Bradley, A., (2007), Generation of an inducible and optimized piggyBac transposon systemy. *Nucleic Acids Research*, 35(12).

Canham, M. A., Sharov, A. A., Ko, M. S., and Brickman, J. M., (2010), Functional heterogeneity of embryonic stem cells revealed through translational amplification of an early endodermal transcript. *PLoS Biology*, 8(5):e1000379.

Cannon, D., Corrigan, A. M., Miermont, A., McDonel, P., and Chubb, J. R., (2015), Multiple cell and population-level interactions with mouse embryonic stem cell heterogeneity. *Development*, 142(16):2840–2849.

Chambers, I., Colby, D., Robertson, M., Nichols, J., Lee, S., Tweedie, S., and Smith, A., (2003), Functional expression cloning of Nanog, a pluripotency sustaining factor in embryonic stem cells. *Cell*, 113(5):643–655.

Chambers, I., Silva, J., Colby, D., Nichols, J., Nijmeijer, B., Robertson, M., Vrana, J., Jones, K., Grotewold, L., and Smith, A., (2007), Nanog safeguards pluripotency and mediates germline development. *Nature*, 450(7173):1230–4.

Chazaud, C., Yamanaka, Y., Pawson, T., and Rossant, J., (2006), Early Lineage Segregation between Epiblast and Primitive Endoderm in Mouse Blastocysts through the Grb2-MAPK Pathway. *Developmental Cell*, 10(5):615–624.

Chen, J. Y., Lin, J. R., Cimprich, K. A., and Meyer, T., (2012), A Two-Dimensional ERK-AKT Signaling Code for an NGF-Triggered Cell-Fate Decision. *Molecular Cell*, 45(2):196–209.

Cheng, A. M., Tracy, Saxton, M., Sakai, R., Kulkarni, S., Mbamalu, G., Vogel, W., Tortorice, C. G., Cardiff, R. D., Cross, J. C., Muller, W. J., Pawson, T., and Research, S. L., (1998), Mammalian Grb2 Regulates Multiple Steps in Embryonic Development and Malignant Transformation. *Cell*, 95:63110.

Cimica, V., Chen, H. C., Iyer, J. K., and Reich, N. C., (2011), Dynamics of the STAT3 transcription factor: Nuclear import dependent on ran and importin-$\beta$1. *PLoS ONE*, 6(5):e20188.

Cohen-Saidon, C., Cohen, A. A., Sigal, A., Liron, Y., and Alon, U., (2009), Dynamics and Variability of ERK2 Response to EGF in Individual Living Cells. *Molecular Cell*, 36(5):885–893.

Corrigan, A. M. and Chubb, J. R., (2014), Regulation of transcriptional bursting by

a naturally oscillating signal. *Current Biology*, 24(2):205–211.

Cowley, S., Paterson, H., Kemp, P., and Marshall, C. J., (1994), Activation of MAP kinase kinase is necessary and sufficient for PC12 differentiation and for transformation of NIH 3T3 cells. *Cell*, 77(6):841–852.

Davies, O. R., Lin, C. Y., Radzisheuskaya, A., Zhou, X., Taube, J., Blin, G., Waterhouse, A., Smith, A. J., and Lowell, S., (2013), Tcf15 Primes Pluripotent Cells for Differentiation. *Cell Reports*, 3(2):472–484.

de la Cova, C., Townley, R., Regot, S., and Greenwald, I., (2017), A Real-Time Biosensor for ERK Activity Reveals Signaling Dynamics during C. elegans Cell Fate Specification. *Developmental Cell*, 42(5):542–553.e4.

Dessauges, C. and Pertz, O. Developmental ERK Signaling Goes Digital, (2017). OPTIISSN 18781551.

Dhaliwal, N. K., Miri, K., Davidson, S., Tamim El Jarkass, H., and Mitchell, J. A., (2018), KLF4 Nuclear Export Requires ERK Activation and Initiates Exit from Naive Pluripotency. *Stem cell reports*, 10(4):1308–1323.

Dietrich, J.-E. and Hiiragi, T., (2007), Stochastic patterning in the mouse pre-implantation embryo. *Development*, 134(23):4219–4231.

Duncan, R. R., Bergmann, A., Cousin, M. A., Apps, D. K., and Shipston, M. J., (2004), Multi-dimensional time-correlated single photon counting (TCSPC) fluorescence lifetime imaging microscopy (FLIM) to detect FRET in cells. *Journal of Microscopy*, 215(1):1–12.

Dunn, S.-J., Martello, G., Yordanov, B., Emmott, S., and Smith, a. G., (2014), Defining an essential transcription factor program for naïve pluripotency. *Science (New York, N.Y.)*, 344(6188):1156–60.

Eldar, A. and Elowitz, M. B., (2010), Functional roles for noise in genetic circuits. *Nature*, 467(7312):167–173.

Elowitz, M. B., Levine, A. J., Siggia, E. D., and Swain, P. S., (2002), Stochastic gene expression in a single cell. *Science (New York, N.Y.)*, 297(5584):1183–6.

Enver, T., Pera, M., Peterson, C., and Andrews, P. W., (2009), Stem Cell States, Fates, and the Rules of Attraction. *Cell Stem Cell*, 4(5):387–397.

Evans, M. J. and Kaufman, M. H., (1981), Establishment in culture of pluripotential cells from mouse embryos. *Nature*, 292:154–156.

Faddah, D. A., Wang, H., Cheng, A. W., Katz, Y., Buganim, Y., and Jaenisch, R., (2013), Single-cell analysis reveals that expression of nanog is biallelic and equally variable as that of other pluripotency factors in mouse escs. *Cell Stem Cell*, 13(1):23–29.

Feldman, B., Poueymirou, W., Papaioannou, V., DeChiara, T., and Goldfarb, M., (1995), Requirement of FGF-4 for postimplantation mouse development. *Science*, 267(5195):246–249.

Fernandes, T. G., Fernandes-Platzgummer, A. M., da Silva, C. L., Diogo, M. M., and Cabral, J. M. S., (2010), Kinetic and metabolic analysis of mouse embryonic stem cell expansion under serum-free conditions. *Biotechnology Letters*, 32(1): 171–179.

Ferrer-Vaquer, A., Piliszek, A., Tian, G., Aho, R. J., Dufort, D., and Hadjantonakis, A. K., (2010), A sensitive and bright single-cell resolution live imaging reporter of Wnt/-catenin signaling in the mouse. *BMC Developmental Biology*, 10(1):121.

Ficz, G., Hore, T. A., Santos, F., Lee, H. J., Dean, W., Arand, J., Krueger, F., Oxley, D., Paul, Y. L., Walter, J., Cook, S. J., Andrews, S., Branco, M. R., and Reik, W., (2013), FGF signaling inhibition in ESCs drives rapid genome-wide demethylation to the epigenetic ground state of pluripotency. *Cell Stem Cell*, 13 (3):351–359.

Filipczyk, A., Gkatzis, K., Fu, J., Hoppe, P., Lickert, H., Anastassiadis, K.,

and Schroeder, T., (2013), Biallelic Expression of Nanog Protein in Mouse Embryonic Stem Cells. *Cell Stem Cell*, 13(1):12–13.

Findlay, G. M., Smith, M. J., Lanner, F., Hsiung, M. S., Gish, G. D., Petsalaki, E., Cockburn, K., Kaneko, T., Huang, H., Bagshaw, R. D., Ketela, T., Tucholska, M., Taylor, L., Bowtell, D. D., Moffat, J., Ikura, M., Li, S. S., Sidhu, S. S., Rossant, J., and Pawson, T., (2013), Interaction domains of Sos1/Grb2 are finely tuned for cooperative control of embryonic stem cell fate. *Cell*, 152(5):1008–1020.

Fuchs, E., Tumbar, T., and Guasch, G. Socializing with the neighbors: Stem cells and their niche, (2004). OPTIISSN 00928674.

Goolam, M., Scialdone, A., Graham, S. J., MacAulay, I. C., Jedrusik, A., Hupalowska, A., Voet, T., Marioni, J. C., and Zernicka-Goetz, M., (2016), Heterogeneity in Oct4 and Sox2 Targets Biases Cell Fate in 4-Cell Mouse Embryos. *Cell*, 165(1):61–74.

Grabarek, J. B., Zyzyńska, K., Saiz, N., Piliszek, A., Frankenberg, S., Nichols, J., Hadjantonakis, A.-K., and Plusa, B., (2012), Differential plasticity of epiblast and primitive endoderm precursors within the ICM of the early mouse embryo. *Development (Cambridge, England)*, 139(1):129–39.

Graf, T. and Stadtfeld, M., (2008), Heterogeneity of Embryonic and Adult Stem Cells. *Cell Stem Cell*, 3(5):480–483.

Guo, G., Huss, M., Tong, G. Q., Wang, C., Li Sun, L., Clarke, N. D., and Robson, P., (2010), Resolution of Cell Fate Decisions Revealed by Single-Cell Gene Expression Analysis from Zygote to Blastocyst. *Developmental Cell*, 18(4): 675–685.

Habibi, E., Brinkman, A. B., Arand, J., Kroeze, L. I., Kerstens, H. H., Matarese, F., Lepikhov, K., Gut, M., Brun-Heath, I., Hubner, N. C., Benedetti, R., Altucci, L., Jansen, J. H., Walter, J., Gut, I. G., Marks, H., and Stunnenberg, H. G.,

(2013), Whole-genome bisulfite sequencing of two distinct interconvertible DNA methylomes of mouse embryonic stem cells. *Cell Stem Cell*, 13(3):360–369.

Hall, J., Guo, G., Wray, J., Eyres, I., Nichols, J., Grotewold, L., Morfopoulou, S., Humphreys, P., Mansfield, W., Walker, R., Tomlinson, S., and Smith, A., (2009), Oct4 and LIF/Stat3 Additively Induce Krüppel Factors to Sustain Embryonic Stem Cell Self-Renewal. *Cell Stem Cell*, 5(6):597–609.

Hamazaki, T., Kehoe, S. M., Nakano, T., and Terada, N., (2006), The Grb2/Mek Pathway Represses Nanog in Murine Embryonic Stem Cells. *Molecular and Cellular Biology*, 26(20):7539–7549.

Hamilton, W. B., Kaji, K., and Kunath, T., (2013), ERK2 Suppresses Self-Renewal Capacity of Embryonic Stem Cells, but Is Not Required for Multi-Lineage Commitment. *PLoS ONE*, 8(4).

Hanafusa, H., Torii, S., Yasunaga, T., and Nishida, E., (2002), Sprouty1 and Sprouty2 provide a control mechanism for the Ras/MAPK signalling pathway. *Nature Cell Biology*, 4(11):850–858.

Hansen, C. H. and van Oudenaarden, A., (2013), Allele-specific detection of single mRNA molecules in situ. *Nature methods*, 10(august):1–5.

Hao, N. and O'Shea, E. K., (2012), Signal-dependent dynamics of transcription factor translocation controls gene expression. *Nature structural & molecular biology*, 19(1):31–9.

Harvey, C. D., Ehrhardt, A. G., Cellurale, C., Zhong, H., Yasuda, R., Davis, R. J., and Svoboda, K., (2008), A genetically encoded fluorescent sensor of ERK activity. *Proceedings of the National Academy of Sciences of the United States of America*, 105(49):19264–9.

Hayashi, K. and Surani, M. A., (2009), Self-renewing epiblast stem cells exhibit

continual delineation of germ cells with epigenetic reprogramming in vitro. *Development*, 136(21):3549–3556.

Hayashi, K., Lopes, S. M. C. d. S., Tang, F., and Surani, M. A., (2008), Dynamic Equilibrium and Heterogeneity of Mouse Pluripotent Stem Cells with Distinct Functional and Epigenetic States. *Cell Stem Cell*, 3(4):391–401.

Hayashi, K., Ohta, H., Kurimoto, K., Aramaki, S., and Saitou, M., (2011), Reconstitution of the mouse germ cell specification pathway in culture by pluripotent stem cells. *Cell*, 146(4):519–532.

Herberg, M., Kalkan, T., Glauche, I., Smith, A., and Roeder, I., (2014), A model-based analysis of culture-dependent phenotypes of mESCs. *PloS one*, 9 (3):e92496.

Herberg, M., Zerjatke, T., de Back, W., Glauche, I., and Roeder, I., (2015), Image-based quantification and mathematical modeling of spatial heterogeneity in ESC colonies. *Cytometry Part A*, 87(6):481–490.

Higgs, H. N. and Peterson, K. J., (2005), Phylogenetic analysis of the formin homology 2 domain. *Molecular biology of the cell*, 16(1):1–13.

Hirate, Y., Cockburn, K., Rossant, J., and Sasaki, H., (2012), Tead4 is constitutively nuclear, while nuclear vs. cytoplasmic Yap distribution is regulated in preimplantation mouse embryos. *Proceedings of the National Academy of Sciences*, 109(50):E3389–E3390.

Hiratsuka, T., Fujita, Y., Naoki, H., Aoki, K., Kamioka, Y., and Matsuda, M., (2014), Intercellular propagation of extracellular signal-regulated kinase activation revealed by in vivo imaging of mouse skin. *eLife*, 4:e05178.

Hu, M., Krause, D., Sharkies, S., Dexter, M., Heyworth, C., and Enver, T., (1997), Multilineage gene expression preceded commitment in the hemopoietic system. *Genes and Development*, 11:774–785.

Huang, Y. Z., Zang, M., Xiong, W. C., Luo, Z., and Mei, L., (2003), Erbin suppresses the MAP kinase pathway. *Journal of Biological Chemistry*, 278(2): 1108–1114.

Hum, J. M., Siegel, A. P., Pavalko, F. M., and Day, R. N. Monitoring biosensor activity in living cells with fluorescence lifetime imaging microscopy, (2012). OPTIISSN 14220067.

Itskovitz-Eldor, J., Schuldiner, M., Karsenti, D., Eden, A., Yanuka, O., Amit, M., Soreq, H., and Benvenisty, N., (2000), Differentiation of human embryonic stem cells into embryoid bodies compromising the three embryonic germ layers. *Molecular medicine (Cambridge, Mass.)*, 6(2):88–95.

Ivanova, N., Dobrin, R., Lu, R., Kotenko, I., Levorse, J., DeCoste, C., Schafer, X., Lun, Y., and Lemischka, I. R., (2006), Dissecting self-renewal in stem cells with RNA interference. *Nature*, 442(7102):533–538.

Ivics, Z., Li, M. A., Mátés, L., Boeke, J. D., Nagy, A., Bradley, A., and Izsvák, Z., (2009), Transposon-mediated genome manipulation in vertebrates. *Nature Methods*, 6(6):415–422.

Jares-Erijman, E. A. and Jovin, T. M., (2003), FRET imaging. *Nature biotechnology*, 21(11):1387–95.

Johnson, H. E., Goyal, Y., Pannucci, N. L., Schüpbach, T., Shvartsman, S. Y., and Toettcher, J. E., (2017), The Spatiotemporal Limits of Developmental Erk Signaling. *Developmental Cell*, 40(2):185–192.

Johnson, M. H. and McConnell, J. M., (2004), Lineage allocation and cell polarity during mouse embryogenesis. *Seminars in Cell and Developmental Biology*, 15 (5):583–597.

Johnson, M. H. and Ziomek, C. A., (1981), The foundation of two distinct cell lineages within the mouse morula. *Cell*, 24(1):71–80.

Kalkan, T. and Smith, A., (2014), Mapping the route from naive pluripotency to lineage specification. *Philosophical transactions of the Royal Society of London. Series B, Biological sciences*, 369(1657):20130540–.

Kalkan, T., Olova, N., Roode, M., Mulas, C., Lee, H. J., Nett, I., Marks, H., Walker, R., Stunnenberg, H. G., Lilley, K. S., Nichols, J., Reik, W., Bertone, P., and Smith, A., (2017), Tracking the embryonic stem cell transition from ground state pluripotency. *Development*, 144(7):1221–1234.

Kalmar, T., Lim, C., Hayward, P., Mu??oz-Descalzo, S., Nichols, J., Garcia-Ojalvo, J., and Arias, A. M., (2009), Regulated fluctuations in Nanog expression mediate cell fate decisions in embryonic stem cells. *PLoS Biology*, 7(7).

Kholodenko, B. N., Kiyatkin, A., Bruggeman, F. J., Sontag, E., Westerhoff, H. V., and Hoek, J. B., (2002), Untangling the wires: A strategy to trace functional interactions in signaling and gene networks. *Proceedings of the National Academy of Sciences*, 99(20):12841–12846.

Kobayashi, T., Mizuno, H., Imayoshi, I., Furusawa, C., Shirahige, K., and Kageyama, R., (2009), The cyclic gene Hes1 contributes to diverse differentiation responses of embryonic stem cells. *Genes and Development*, 23(16):1870–1875.

Koch, W. J., Hawes, B. E., Allen, L. F., and Lefkowitz, R. J., (1994), Direct evidence that Gi-coupled receptor stimulation of mitogen-activated protein kinase is mediated by G beta gamma activation of p21ras. *Proceedings of the National Academy of Sciences of the United States of America*, 91(26):12706–10.

Komatsu, N., Aoki, K., Yamada, M., Yukinaga, H., Fujita, Y., Kamioka, Y., and Matsuda, M., (2011), Development of an optimized backbone of FRET biosensors for kinases and GTPases. *Molecular biology of the cell*, 22(23): 4647–56.

Kopp, J. L., Ormsbee, B. D., Desler, M., and Rizzino, A., (2008), Small Increases

in the Level of Sox2 Trigger the Differentiation of Mouse Embryonic Stem Cells. *Stem Cells*, 26(4):903–911.

Krawchuk, D., Honma-Yamanaka, N., Anani, S., and Yamanaka, Y., (2013), FGF4 is a limiting factor controlling the proportions of primitive endoderm and epiblast in the ICM of the mouse blastocyst. *Developmental Biology*, 384(1):65–71.

Kumar, R. M., Cahan, P., Shalek, A. K., Satija, R., Keyser, A. D., Li, H., Zhang, J., Pardee, K., Gennert, D., Trombetta, J. J., Ferrante, T. C., Regev, A., Daley, G. Q., and Collins, J. J., (2014), Deconstructing transcriptional heterogeneity in pluripotent stem cells. *Nature*, 516(729):56–61.

Kunath, T., Saba-El-Leil, M. K., Almousailleakh, M., Wray, J., Meloche, S., and Smith, A., (2007), FGF stimulation of the Erk1/2 signalling cascade triggers transition of pluripotent embryonic stem cells from self-renewal to lineage commitment. *Development (Cambridge, England)*, 134(16):2895–2902.

Langlois, W. J., Sasaoka, T., Saltiel, A. R., and Olefsky, J. M., (1995), Negative feedback regulation and desensitization of insulin- and epidermal growth factor-stimulated p21ras activation. *Journal of Biological Chemistry*, 270(43): 25320–25323.

Lanner, F. and Rossant, J., (2010), The role of FGF/Erk signaling in pluripotent cells. *Development (Cambridge, England)*, 137:3351–3360.

Lee, R., Walker, S., Savery, K., Frank, D., and Gaudet, S., (2014), Fold Change of Nuclear NF-$\kappa$B Determines TNF-Induced Transcription in Single Cells. *Molecular Cell*, 53(6):867–879.

Leeb, M., Dietmann, S., Paramor, M., Niwa, H., and Smith, A., (2014), Genetic exploration of the exit from self-renewal using haploid embryonic stem cells. *Cell Stem Cell*, 14(3):385–393.

Leitch, H. G., McEwen, K. R., Turp, A., Encheva, V., Carroll, T., Grabole,

N., Mansfield, W., Nashun, B., Knezovich, J. G., Smith, A., Surani, M. A., and Hajkova, P., (2013), Naive pluripotency is associated with global DNA hypomethylation. *Nature Structural & Molecular Biology*, 20(3):311–316.

Levine, J. H., Lin, Y., and Elowitz, M. B., (2013), Functional roles of pulsing in genetic circuits. *Science*, 342(6163):1193–1200.

Li, P., Tong, C., Mehrian-Shai, R., Jia, L., Wu, N., Yan, Y., Maxson, R. E., Schulze, E. N., Song, H., Hsieh, C. L., Pera, M. F., and Ying, Q. L., (2008), Germline Competent Embryonic Stem Cells Derived from Rat Blastocysts. *Cell*, 135(7): 1299–1310.

Liu, Y., Kaneda, R., Leja, T. W., Subkhankulova, T., Tolmachov, O., Minchiotti, G., Schwartz, R. J., Barahona, M., and Schneider, M. D., (2014), Hhex and cer1 mediate the Sox17 pathway for cardiac mesoderm formation in embryonic stem cells. *Stem Cells*, 32(6):1515–1526.

Loh, K. M. and Lim, B., (2011), A precarious balance: Pluripotency factors as lineage specifiers. *Cell Stem Cell*, 8(4):363–369.

Loh, Y. H., Wu, Q., Chew, J. L., Vega, V. B., Zhang, W., Chen, X., Bourque, G., George, J., Leong, B., Liu, J., Wong, K. Y., Sung, K. W., Lee, C. W., Zhao, X. D., Chiu, K. P., Lipovich, L., Kuznetsov, V. A., Robson, P., Stanton, L. W., Wei, C. L., Ruan, Y., Lim, B., and Ng, H. H., (2006), The Oct4 and Nanog transcription network regulates pluripotency in mouse embryonic stem cells. *Nature Genetics*, 38(4):431–440.

Lorincz, M. T., (2006), Optimized neuronal differentiation of murine embryonic stem cells: role of cell density. *Methods in molecular biology (Clifton, N.J.)*, 330:55–69.

Maamar, H., Raj, A., and Dubnau, D., (2007), Noise in Gene Expression Determines Cell Fate in Bacillus subtilis. *Science*, 317(5837):526 LP – 529.

Maître, J. L., Turlier, H., Illukkumbura, R., Eismann, B., Niwayama, R., Nédélec, F., and Hiiragi, T., (2016), Asymmetric division of contractile domains couples cell positioning and fate specification. *Nature*, 536(7616):344–348.

Marchetti, S., Gimond, C., Chambard, J.-C., Touboul, T., Roux, D., Pouyssegur, J., and Pages, G., (2005), Extracellular Signal-Regulated Kinases Phosphorylate Mitogen-Activated Protein Kinase Phosphatase 3/DUSP6 at Serines 159 and 197, Two Sites Critical for Its Proteasomal Degradation. *Molecular and Cellular Biology*, 25(2):854–864.

Marks, H., Kalkan, T., Menafra, R., Denissov, S., Jones, K., Hofemeister, H., Nichols, J., Kranz, A., Francis Stewart, A., Smith, A., and Stunnenberg, H. G., (2012), The transcriptional and epigenomic foundations of ground state pluripotency. *Cell*, 149(3):590–604.

Marshall, C., (1995), Specificity of receptor tyrosine kinase signaling: Transient versus sustained extracellular signal-regulated kinase activation. *Cell*, 80(2): 179–185.

Martello, G., Bertone, P., and Smith, A., (2013), Identification of the missing pluripotency mediator downstream of leukaemia inhibitory factor. *The EMBO journal*, 32(19):2561–74.

Martinez Arias, A. and Brickman, J. M., (2011), Gene expression heterogeneities in embryonic stem cell populations: origin and function. *Current opinion in cell biology*, 23(6):650–6.

Martinez Arias, A., Nichols, J., and Schröter, C., (2013), A molecular basis for developmental plasticity in early mammalian embryos. *Development (Cambridge, England)*, 140(17):3499–510.

Maryu, G., Miura, H., Uda, Y., T. Komatsubara, A., Matsuda, M., and Aoki, K., (2018), Live-cell imaging with genetically encoded protein kinase activity reporters. *Cell Structure and Function*, 43(1):61–74.

Matsuda, T., Nakamura, T., Nakao, K., Arai, T., Katsuki, M., Heike, T., and Yokota, T., (1999), STAT3 activation is sufficient to maintain an undifferentiated state of mouse embryonic stem cells. *EMBO Journal*, 18(15):4261–4269.

McKay, M. M. and Morrison, D. K., (2007), Integrating signals from RTKs to ERK/MAPK. *Oncogene*, 26(22):3113–3121.

Meissner, A., Mikkelsen, T. S., Gu, H., Wernig, M., Hanna, J., Sivachenko, A., Zhang, X., Bernstein, B. E., Nusbaum, C., Jaffe, D. B., Gnirke, A., Jaenisch, R., and Lander, E. S., (2008), Genome-scale DNA methylation maps of pluripotent and differentiated cells. *Nature*, 454(7205):766–770.

Miyanari, Y. and Torres-Padilla, M.-E., (2012), Control of ground-state pluripotency by allelic regulation of Nanog. *Nature*, 483(7390):470–3.

Moledina, F., Clarke, G., Oskooei, A., Onishi, K., Gunther, A., and Zandstra, P. W., (2012), Predictive microfluidic control of regulatory ligand trajectories in individual pluripotent cells. *Proceedings of the National Academy of Sciences*, 109(9):3264–3269.

Molotkov, A., Mazot, P., Brewer, J. R., Cinalli, R. M., and Soriano, P., (2017), Distinct Requirements for FGFR1 and FGFR2 in Primitive Endoderm Development and Exit from Pluripotency. *Developmental Cell*, 41(5): 511–526.e4.

Morgani, S., Nichols, J., and Hadjantonakis, A. K., (2017), The many faces of Pluripotency: In vitro adaptations of a continuum of in vivo states. *BMC Developmental Biology*, 17(1):7.

Morgani, S. M., Metzger, J. J., Nichols, J., Siggia, E. D., and Hadjantonakis, A. K., (2018), Micropattern differentiation of mouse pluripotent stem cells recapitulates embryo regionalized cell fate patterning. *eLife*, 7.

Morgani, S. M., Saiz, N., Garg, V., Raina, D., Simon, C. S., Kang, M., Arias, A. M.,

Nichols, J., Schröter, C., and Hadjantonakis, A. K., (2018), A Sprouty4 reporter to monitor FGF/ERK signaling activity in ESCs and mice. *Developmental Biology*, 441(1):104–126.

Murphy, L. O., Smith, S., Chen, R. H., Fingar, D. C., and Blenis, J., (2002), Molecular, interpretation of ERK signal duration by immediate early gene products. *Nature Cell Biology*, 4(8):556–564.

Murray, P., Prewitz, M., Hopp, I., Wells, N., Zhang, H., Cooper, A., Parry, K. L., Short, R., Antoine, D. J., and Edgar, D., (2013), The self-renewal of mouse embryonic stem cells is regulated by cell-substratum adhesion and cell spreading. *International Journal of Biochemistry and Cell Biology*, 45(11):2698–2705.

Najm, F. J., Chenoweth, J. G., Anderson, P. D., Nadeau, J. H., Redline, R. W., McKay, R. D., and Tesar, P. J., (2011), Isolation of epiblast stem cells from preimplantation mouse embryos. *Cell Stem Cell*, 8(3):318–325.

Navarro, P., Festuccia, N., Colby, D., Gagliardi, A., Mullin, N. P., Zhang, W., Karwacki-Neisius, V., Osorno, R., Kelly, D., Robertson, M., and Chambers, I., (2012), OCT4/SOX2-independent Nanog autorepression modulates heterogeneous Nanog gene expression in mouse ES cells. *EMBO J*, 31(24):4547–4562.

Nett, I. R., Mulas, C., Gatto, L., Lilley, K. S., and Smith, A., (2018), Negative feedback via RSK modulates Erkdependent progression from naïve pluripotency. *EMBO reports*, page e45642.

Nichols, J. and Smith, A., (2009), Naive and Primed Pluripotent States. *Cell Stem Cell*, 4(6):487–492.

Nichols, J., Evans, E. P., and Smith, A. G., (1990), Establishment of germ-line-competent embryonic stem (ES) cells using differentiation inhibiting activity. *Development (Cambridge, England)*, 110(4):1341–1348.

Nichols, J., Zevnik, B., Anastassiadis, K., Niwa, H., Klewe-Nebenius, D., Chambers, I., Scholer, H., and Smith, A., (1998), Formation of pluripotent stem cells in the mammalian embryo dependes on the POU transcription factor Oct4. *Cell*, 95(3):379–391.

Nichols, J., Silva, J., Roode, M., and Smith, A., (2009), Suppression of Erk signalling promotes ground state pluripotency in the mouse embryo. *Development (Cambridge, England)*, 136:3215–3222.

Nishioka, N., ichi Inoue, K., Adachi, K., Kiyonari, H., Ota, M., Ralston, A., Yabuta, N., Hirahara, S., Stephenson, R. O., Ogonuki, N., Makita, R., Kurihara, H., Morin-Kensicki, E. M., Nojima, H., Rossant, J., Nakao, K., Niwa, H., and Sasaki, H., (2009), The Hippo Signaling Pathway Components Lats and Yap Pattern Tead4 Activity to Distinguish Mouse Trophectoderm from Inner Cell Mass. *Developmental Cell*, 16(3):398–410.

Nissen, S. B., Perera, M., Gonzalez, J. M., Morgani, S. M., Jensen, M. H., Sneppen, K., Brickman, J. M., and Trusina, A., (2017), Four simple rules that are sufficient to generate the mammalian blastocyst. *PLoS Biology*, 15(7):e2000737.

Niwa, H., (2007), How is pluripotency determined and maintained? *Development (Cambridge, England)*, 134(4):635–46.

Niwa, H., Burdon, T., Chambers, I., and Smith, A., (1998), Self-renewal of pluripotent embryonic stem cells is mediated via activation of STAT3. *Genes & development*, 12(13):2048–60.

Niwa, H., Miyazaki, J. I., and Smith, A. G., (2000), Quantitative expression of Oct-3/4 defines differentiation, dedifferentiation or self-renewal of ES cells. *Nature Genetics*, 24(4):372–376.

Niwa, H., Toyooka, Y., Shimosato, D., Strumpf, D., Takahashi, K., Yagi, R., and Rossant, J., (2005), Interaction between Oct3/4 and Cdx2 determines trophectoderm differentiation. *Cell*, 123(5):917–929.

Niwa, H., Ogawa, K., Shimosato, D., and Adachi, K., (2009), A parallel circuit of LIF signalling pathways maintains pluripotency of mouse ES cells. *Nature*, 460 (7251):118–122.

Ochiai, H., Sugawara, T., Sakuma, T., and Yamamoto, T., (2014), Stochastic promoter activation affects Nanog expression variability in mouse embryonic stem cells. *Scientific reports*, 4:7125.

Ochiai, H., Sugawara, T., Sakuma, T., and Yamamoto, T., (2014), Stochastic promoter activation affects Nanog expression variability in mouse embryonic stem cells. pages 1–9.

Ohnishi, Y., Huber, W., Tsumura, A., Kang, M., Kurimoto, K., Oleś, A. K., and Araúzo-bravo, M. J., (2014), Cell-to-cell expression variability followed by signal reinforcement progressively segregates early mouse lineages. *Nat Cell Biol*, 16(1):27–37.

Osorno, R., Tsakiridis, A., Wong, F., Cambray, N., Economou, C., Wilkie, R., Blin, G., Scotting, P. J., Chambers, I., and Wilson, V., (2012), The developmental dismantling of pluripotency is reversed by ectopic Oct4 expression. *Development*, 139(13):2288–2298.

Ozbudak, E. M., Thattai, M., Kurtser, I., Grossman, A. D., and Van Oudenaarden, A., (2002), Regulation of noise in the expression of a single gene. *Nature Genetics*, 31(1):69–73.

Pages, G., Brunet, A., L 'allemain, G., Pouyssegur, J., Pagès, G., Brunet, A., L'Allemain, G., and Pouysségur, J., (1994), Constitutive mutant and putative regulatory serine phosphorylation site of mammalian MAP kinase kinase (MEK1). *The EMBO journal*, 13(13):3003–10.

Papatsenko, D., Darr, H., Kulakovskiy, I. V., Waghray, A., Makeev, V. J., Macarthur, B. D., and Lemischka, I. R., (2015), Single-Cell Analyses of ESCs Reveal

Alternative Pluripotent Cell States and Molecular Mechanisms that Control Self-Renewal. *Stem Cell Reports*, 5(2):207–220.

Patterson, K. I., Brummer, T., O'brien, P. M., and Daly, R. J., (2009), Dual-specificity phosphatases: critical regulators with diverse cellular targets. *Biochemical Journal*, 418(3):475–489.

Peerani, R., Onishi, K., Mahdavi, A., Kumacheva, E., and Zandstra, P. W., (2009), Manipulation of signaling thresholds in "engineered stem cell niches" identifies design criteria for pluripotent stem cell screens. *PLoS ONE*, 4(7):e6438.

Pevny, L. H., Sockanathan, S., Placzek, M., and Lovell-Badge, R., (1998), A role for SOX1 in neural determination. *Development*, 125(10):1967–1978.

Pietraszewska-Bogiel, A. and Gadella, T. W., (2011), FRET microscopy: From principle to routine technology in cell biology. *Journal of Microscopy*, 241(2): 111–118.

Plusa, B., Piliszek, A., Frankenberg, S., Artus, J., and Hadjantonakis, A.-K., (2008), Distinct sequential cell behaviours direct primitive endoderm formation in the mouse blastocyst. *Development*, 135(18):3081–91.

Purvis, J. E. and Lahav, G., (2013), Encoding and decoding cellular information through signaling dynamics. *Cell*, 152(5):945–56.

Raj, A., Peskin, C. S., Tranchina, D., Vargas, D. Y., and Tyagi, S., (2006), Stochastic mRNA synthesis in mammalian cells. *PLoS Biology*, 4(10):1707–1719.

Raj, A., Rifkin, S. A., Andersen, E., and Van Oudenaarden, A., (2010), Variability in gene expression underlies incomplete penetrance. *Nature*, 463(7283):913–918.

Redmer, T., Diecke, S., Grigoryan, T., Quiroga-Negreira, A., Birchmeier, W., and Besser, D., (2011), E-cadherin is crucial for embryonic stem cell pluripotency and can replace OCT4 during somatic cell reprogramming. *EMBO Reports*, 12 (7):720–726.

Regot, S., Hughey, J. J., Bajar, B. T., Carrasco, S., and Covert, M. W., (2014), High-sensitivity measurements of multiple kinase activities in live single cells. *Cell*, 157(7):1724–1734.

Rousseeuw, P. J., (1987), Silhouettes: A graphical aid to the interpretation and validation of cluster analysis. *Journal of Computational and Applied Mathematics*, 20(C):53–65.

Ryu, H., Chung, M., Dobrzynski, M., Fey, D., Blum, Y., Lee, S. S., Peter, M., Kholodenko, B. N., Jeon, N. L., and Pertz, O., (2015), Frequency modulation of ERK activation dynamics rewires cell fate. *Molecular Systems Biology*, 11(11): 838–838.

Sanderson, M. J., Smith, I., Parker, I., and Bootman, M. D., (2014), Fluorescence microscopy. *Cold Spring Harbor Protocols*, 2014(10):1042–1065.

Santos, S. D. M., Verveer, P. J., and Bastiaens, P. I. H., (2007), Growth factor-induced MAPK network topology shapes Erk response determining PC-12 cell fate. *Nature Cell Biology*, 9(3):324–330.

Santostefano, K. E., Hamazaki, T., Pardo, C. E., Kladde, M. P., and Terada, N., (2012), Fibroblast growth factor receptor 2 homodimerization rapidly reduces transcription of the pluripotency gene Nanog without dissociation of activating transcription factors. *Journal of Biological Chemistry*, 287(36):30507–30517.

Sasagawa, S., Ozaki, Y. I., Fujita, K., and Kuroda, S., (2005), Prediction and validation of the distinct dynamics of transient and sustained ERK activation. *Nature Cell Biology*, 7(4):365–373.

Sasaki, A., Taketomi, T., Kato, R., Saeki, K., Nonami, A., Sasaki, M., Kuriyama, M., Saito, N., Shibuya, M., and Yoshimura, A., (2003), Mammalian Sprouty4 suppresses Ras-independent ERK activation by binding to Raf1. *Nature Cell Biology*, 5(5):427–432.

Schmid, T. and Hajnal, A. Signal transduction during C. elegans vulval development: A NeverEnding story, (2015). OPTIISSN 18790380.

Schröter, C., Rué, P., Mackenzie, J. P., and Martinez Arias, A., (2015), FGF/MAPK signaling sets the switching threshold of a bistable circuit controlling cell fate decisions in embryonic stem cells. *Development*, 142(24):4205–16.

Selwood, L. and Johnson, M. H. Trophoblast and hypoblast in the monotreme, marsupial and eutherian mammal: Evolution and origins, (2006). OPTIISSN 02659247.

Semrau, S., Goldmann, J. E., Soumillon, M., Mikkelsen, T. S., Jaenisch, R., and Van Oudenaarden, A., (2017), Dynamics of lineage commitment revealed by single-cell transcriptomics of differentiating embryonic stem cells. *Nature Communications*, 8(1):1096.

Shin, S.-Y., Rath, O., Choo, S.-M., Fee, F., McFerran, B., Kolch, W., and Cho, K.-H., (2009), Positive- and negative-feedback regulations coordinate the dynamic behavior of the Ras-Raf-MEK-ERK signal transduction pathway. *Journal of Cell Science*, 122(3):425–435.

Sigal, A., Milo, R., Cohen, A., Geva-Zatorsky, N., Klein, Y., Liron, Y., Rosenfeld, N., Danon, T., Perzov, N., and Alon, U., (2006), Variability and memory of protein levels in human cells. *Nature*, 444(7119):643–646.

Silva, J. and Smith, A., (2008), Capturing Pluripotency. *Cell*, 132(4):532–536.

Silva, J., Nichols, J., Theunissen, T. W., Guo, G., van Oosten, A. L., Barrandon, O., Wray, J., Yamanaka, S., Chambers, I., and Smith, A., (2009), Nanog Is the Gateway to the Pluripotent Ground State. *Cell*, 138(4):722–737.

Singer, Z. S., Yong, J., Tischler, J., Hackett, J. A., Altinok, A., Surani, M. A., Cai, L., and Elowitz, M. B., (2014), Dynamic Heterogeneity and DNA Methylation in Embryonic Stem Cells. *Molecular Cell*, 55(2):319–331.

Singh, A. M., Hamazaki, T., Hankowski, K. E., and Terada, N., (2007), A Heterogeneous Expression Pattern for Nanog in Embryonic Stem Cells. *Stem Cells*, 25(10):2534–2542.

Smith, A. G., Heath, J. K., Donaldson, D. D., Wong, G. G., Moreau, J., Stahl, M., and Rogers, D., (1988), Inhibition of pluripotential embryonic stem cell differentiation by purified polypeptides. *Nature*, 336(6200):688–690.

Smith, A., (2013), Nanog Heterogeneity: Tilting at Windmills? *Cell Stem Cell*, 13 (1):6–7.

Smith, A., (2017), Formative pluripotency: the executive phase in a developmental continuum. *Development*, 144(3):365–373.

Smith, A. G., (2001), Embryo-derived stem cell: Of Mice and Men. *Annual Review of Cell and Developmental Biology*, 17(1):435–462.

Sparta, B., Pargett, M., Minguet, M., Distor, K., Bell, G., and Albeck, J. G., (2015), Receptor level mechanisms are required for epidermal growth factor (EGF)-stimulated extracellular signal-regulated kinase (ERK) activity pulses. *Journal of Biological Chemistry*, 290(41):24784–24792.

Spiering, D., Bravo-Cordero, J. J., Moshfegh, Y., Miskolci, V., and Hodgson, L., (2013), Quantitative ratiometric imaging of FRET-biosensors in living cells. *Methods in Cell Biology*, 114:593–609.

Stavridis, M. P., Lunn, J. S., Collins, B. J., and Storey, K. G., (2007), A discrete period of FGF-induced Erk1/2 signalling is required for vertebrate neural specification. *Development (Cambridge, England)*, 134(16):2889–2894.

Strasser, M. K., Feigelman, J., Theis, F. J., and Marr, C., (2015), Inference of spatiotemporal effects on cellular state transitions from time-lapse microscopy. *BMC Systems Biology*, 9(1):61.

Strumpf, D., (2005), Cdx2 is required for correct cell fate specification and

differentiation of trophectoderm in the mouse blastocyst. *Development*, 132(9): 2093–2102.

Süel, G. M., Kulkarni, R. P., Dworkin, J., Garcia-Ojalvo, J., and Elowitz, M. B., (2007), Tunability and noise dependence in differentiation dynamics. *Science (New York, N.Y.)*, 315(5819):1716–9.

Swift, S. R. and Trinkle-Mulcahy, L., (2004), Basic principles of FRAP , FLIM and FRET. *Proceedings of the Royal Microscopical Society*, 39:3–10.

Symmons, O. and Raj, A., (2016), What's Luck Got to Do with It: Single Cells, Multiple Fates, and Biological Nondeterminism. *Molecular Cell*, 62(5):788–802.

Taleahmad, S., Mirzaei, M., Samadian, A., Hassani, S. N., Haynes, P. A., Salekdeh, G. H., and Baharvand, H., (2017), Low focal adhesion signaling promotes ground state pluripotency of mouse embryonic stem cells. *Journal of Proteome Research*, 16(10):3585–3595.

Tarkowski, A. K. and Wróblewska, J., (1967), Development of blastomeres of mouse eggs isolated at the 4- and 8-cell stage. *Journal of Embryology and Experimental Morphology*, 18(1):155–180.

Tay, S., Hughey, J. J., Lee, T. K., Lipniacki, T., Quake, S. R., and Covert, M. W., (2010), Single-cell NF-B dynamics reveal digital activation and analogue information processing. *Nature*, 466(7303):267–271.

Tee, W. W., Shen, S. S., Oksuz, O., Narendra, V., and Reinberg, D., (2014), Erk1/2 activity promotes chromatin features and RNAPII phosphorylation at developmental promoters in mouse ESCs. *Cell*, 156(4):678–690.

Tesar, P. J., Chenoweth, J. G., Brook, F. A., Davies, T. J., Evans, E. P., Mack, D. L., Gardner, R. L., and McKay, R. D., (2007), New cell lines from mouse epiblast share defining features with human embryonic stem cells. *Nature*, 448(7150): 196–199.

Thomson, M., Liu, S. J., Zou, L. N., Smith, Z., Meissner, A., and Ramanathan, S., (2011), Pluripotency factors in embryonic stem cells regulate differentiation into germ layers. *Cell*, 145(6):875–889.

Toettcher, J. E., Weiner, O. D., and Lim, W. A., (2013), Using optogenetics to interrogate the dynamic control of signal transmission by the Ras/Erk module. *Cell*, 155(6):1422–1434.

Toyooka, Y., Shimosato, D., Murakami, K., Takahashi, K., and Niwa, H., (2008), Identification and characterization of subpopulations in undifferentiated ES cell culture. *Development (Cambridge, England)*, 135:909–918.

van den Berg, D. L. C., Zhang, W., Yates, A., Engelen, E., Takacs, K., Bezstarosti, K., Demmers, J., Chambers, I., and Poot, R. A., (2008), Estrogen-Related Receptor Beta Interacts with Oct4 To Positively Regulate Nanog Gene Expression. *Molecular and Cellular Biology*, 28(19):5986–5995.

Warmflash, A., Sorre, B., Etoc, F., Siggia, E. D., and Brivanlou, A. H., (2014), A method to recapitulate early embryonic spatial patterning in human embryonic stem cells. *Nature Methods*, 11(8):847–854.

White, D. E., Kinney, M. A., McDevitt, T. C., and Kemp, M. L., (2013), Spatial Pattern Dynamics of 3D Stem Cell Loss of Pluripotency via Rules-Based Computational Modeling. *PLoS Computational Biology*, 9(3):e1002952.

Wilson, M. Z., Ravindran, P. T., Lim, W. A., and Toettcher, J. E., (2017), Tracing Information Flow from Erk to Target Gene Induction Reveals Mechanisms of Dynamic and Combinatorial Control. *Molecular Cell*, 67(5):757–769.e5.

Wray, J., Kalkan, T., and Smith, A. G., (2010), The ground state of pluripotency. *Biochemical Society Transactions*, 38(4):1027–1032.

Wray, J., Kalkan, T., Gomez-Lopez, S., Eckardt, D., Cook, A., Kemler, R., and Smith, A., (2011), Inhibition of glycogen synthase kinase-3 alleviates

Tcf3 repression of the pluripotency network and increases embryonic stem cell resistance to differentiation. *Nature Cell Biology*, 13(7):838–845.

Xenopoulos, P., Kang, M., Puliafito, A., DiTalia, S., and Hadjantonakis, A. K., (2015), Heterogeneities in nanog expression drive stable commitment to pluripotency in the mouse blastocyst. *Cell Reports*, 10(9):1508–01520.

Yamaguchi, S., Kimura, H., Tada, M., Nakatsuji, N., and Tada, T., (2005), Nanog expression in mouse germ cell development. *Gene Expr Patterns*, 5(5):639–646.

Yamanaka, Y., Lanner, F., and Rossant, J., (2010), FGF signal-dependent segregation of primitive endoderm and epiblast in the mouse blastocyst. *Development*, 137(5):715–724.

Yang, S.-H., Kalkan, T., Morrisroe, C., Smith, A., and Sharrocks, A. D., (2012), A genome-wide RNAi screen reveals MAP kinase phosphatases as key ERK pathway regulators during embryonic stem cell differentiation. *PLoS genetics*, 8(12):e1003112.

Yeo, J. C., Jiang, J., Tan, Z. Y., Yim, G. R., Ng, J. H., Göke, J., Kraus, P., Liang, H., Gonzales, K. A. U., Chong, H. C., Tan, C. P., Lim, Y. S., Tan, N. S., Lufkin, T., and Ng, H. H., (2014), Klf2 is an essential factor that sustains ground state pluripotency. *Cell Stem Cell*, 14(6):864–872.

Ying, Q. L., Nichols, J., Chambers, I., and Smith, A., (2003), BMP induction of Id proteins suppresses differentiation and sustains embryonic stem cell self-renewal in collaboration with STAT3. *Cell*, 115(3):281–292.

Ying, Q.-L., Wray, J., Nichols, J., Batlle-Morera, L., Doble, B., Woodgett, J., Cohen, P., and Smith, A., (2008), The ground state of embryonic stem cell self-renewal. *Nature*, 453(7194):519–523.

Yuan, H., Corbi, N., Basilico, C., and Dailey, L., (1995), Developmental-specific

activity of the FGF-4 enhancer requires the synergistic action of Sox2 and Oct-3. *Genes and Development*, 9(21):2635–2645.

Zhang, X., Zhang, J., Wang, T., Esteban, M. A., and Pei, D., (2008), Esrrb activates Oct4 transcription and sustains self-renewal and pluripotency in embryonic stem cells. *Journal of Biological Chemistry*, 283(51):35825–35833.